Abstract

Loss of bone mass and structure is one of the most prominent risk factors associated with manned spaceflight. The main objective of this multifaceted project was therefore to establish a precise diagnostic method for quantifying alterations in the structural composition of human trabecular bone. Tools based on evaluation of 2D Computed Tomography (CT) and 3D micro-CT (μCT) images by measures of complexity were developed. These tools quantify different aspects of spatial bone architecture. The measures, methods, and results were validated by comparison with conventional histomorphometry and biomechanical testing. In order to visualize the obtained μCT data, special tools had to be developed, which are able to handle huge amounts of data. Additionally, bone models were designed to simulate and predict bone loss, provide test objects for the new structural measures, and gain insight into the effects of mechanical loading on bone structural alterations. A novel ultrasonic methodology for bone structure assessment is in development utilizing the results of experiments about skeletal discordance and new insights in ultrasound technology. The outcome of this comprehensive project will have an impact on health care for space-flying personnel as well as for patients with bone diseases on Earth.

Table of Contents

Foreword

This Final Report represents the achievements of the Second Phase of the Research Project "2D and 3D Quantification of Bone Structure and its Changes in Microgravity Condition by Measures of Complexity". The short form of the project title is "Bone3D".

The Second Phase of the project started at the end of Phase 1 in January 2003. The reporting time span is two years and nine months from 1 January 2003 to 30 September 2005. The project is an ESA project under MAP AO-99-030. The ESTEC contract number is 14592/00/NL/SH, CCN 001, CCN 002, and CPA002.

The website of the project http://bone3D.zib.de contains information that cannot be reproduced in print. The visitor will be able to see additional materials including large 3D vertebral data sets visualization and movies showing 3D data of human bone biopsies acquired by micro-computed tomography.

A list of publications is provided in this report. The full texts of the papers are available to the interested reader by contacting the author, a library, or the journal. More publications are in preparation at this point of time (October/November 2005).

Acknowledgements

The project was funded partly by the European Space Agency; Siemens AG (Germany); Scanco Medical AG (Switzerland); and F. Hoffmann-La Roche Ltd, Pharmaceuticals Division (Roche Pharmaceuticals) (Switzerland), the Center of Muscle and Bone Research at the Charité–University Medicine Berlin, Campus Benjamin Franklin (Germany), the University of Potsdam (Germany), the Konrad Zuse Institute Berlin (Germany), and the University of Aarhus (Denmark).

The scientific team members are grateful for the financial support they received. In addition to the financial involvement of the industrial partners Siemens AG and Scanco Medical AG, the industrial support received was outstanding and made this project successful. Dr. Andres Laib and Markus Burkhart, Scanco Medical AG, Switzerland, are acknowledged for their excellent and meticulous μCT scanning of the bone samples. The project team acknowledges Mercury Computer Systems GmbH, Germany for providing licenses for the Amira software.

The personal involvement of Dr. Roger Binot (technical officer) from ESTEC, as well as from the administrative officer Mrs. Viviane Janssens, is greatly acknowledged and brought the communication between ESA and the project partners to a comfortable level of mutual understanding.

We would like to thank Professor Gottfried Bogusch, Institute of Cell Biology and Neurobiology, Center for Anatomy, Charité Berlin, Germany and Professor Renate Graf, Institute of Vegetative Anatomy (former Anatomical Institute of Free University Berlin), Center for Anatomy, Charité Berlin who provided the human bone material essential for the project. The team is very thankful for the support, without it this basic research project would not have achieved its goals. The assistance in technical matters by Prof. Bogusch and the help of the anatomical lab technicians were invaluable for the project.

Professor Boris V. Morukov, Institute of Biomedical Problems (IMBP), Moscow, Russia, Dr. Laurence Vico and Professor Christian Alexandre, Laboratoire de Biologie du Tissu Osseux, Faculté de Médecine, Saint-Etienne, France, are gratefully acknowledged for scientific co-operation and for providing and preparing the histological sections of the iliac bone specimens from the 370 day bedrest study.

The team thanks the radiological technicians Erika May, Martina Kratzsch, and Frank Touby at the Center of Muscle and Bone Research, Charité–University Medicine Berlin, Campus Benjamin Franklin (Germany) for their work.

Inger Vang Magnussen, Institute of Anatomy, University of Aarhus, is gratefully acknowledged for her skilled assistance in preparing the histological sections.

We are grateful to Markus Hartman, Max Planck Institute of Colloids and Interfaces, Potsdam, Germany for computational work on simulation of bone remodelling.

The involvement of Hewlett-Packard (Germany) in the initial stage of the project in the basic configuration, set-up, and linkage of several new electronic components was thankfully received by the team members in Berlin and Potsdam.

The technical department at the Campus Benjamin Franklin, Charité–University Medicine Berlin, (Mr. Forster and Mr. Bräuer) helped always in time to solve technical problems with laboratory equipment and the set-up requirements for radiological examinations.

Project Team

Technical Officer	ESA/ESTEC	Noordwijk	The Netherlands	Dr. R. Binot
Project Coordinator	MPICI / CBF	Berlin	Germany	Dr. P. Saparin Dr. W. Gowin (till 07/2004)
Academic Partners	MPICI (since 10/2004)	Potsdam	Germany	Dr. P. Saparin Prof. Dr. P. Fratzl Dr. R. Weinkamer
	CBF	Berlin	Germany	Dr. W. Gowin (till 09/2003) Dr. P. Saparin (till 09/2004) Prof. D. Felsenberg G. Beller (since 08/2003)
	UoA	Aarhus	Denmark	Dr. J. S. Thomsen
	UoP	Potsdam	Germany	Prof. Dr. J. Kurths Dr. N. Marwan
	ZIB	Berlin	Germany	Hon. Prof. H.-C. Hege S. Prohaska, M.S.
	RTU (since 03/2005)	Riga	Latvia	Dr. A. Tatarinov
Industrial Partners	Siemens	Forchheim	Germany	C. Asbeck, Dipl. Eng.
	Scanco	Zürich	Switzerland	Dr. B. Koller
	Mercury	Berlin	Germany	Dr. M. Westerhoff
Project User Group	Roche Pharmaceuticals	Basel	Switzerland	
	Hewlett-Packard	Hamburg	Germany	

Abbreviations used for the Project Teams

MPICI	Max Planck Institute of Colloids and Interfaces, Department of Biomaterials
CBF	Center of Muscle and Bone Research, Charité–University Medicine Berlin, Campus Benjamin Franklin (former Free University Berlin, University Hospital Benjamin Franklin)
UoA	University of Aarhus, Institute of Anatomy, Department of Connective Tissue Biology
UoP	University of Potsdam, Institute of Physics, Nonlinear Dynamics
ZIB	Zuse Institute Berlin, Department of Scientific Visualization
RTU	Riga Technical University / Kamri Sia
Scanco	Scanco Medical AG
Siemens	Siemens AG, Siemens Medical Solutions
Mercury	Mercury Computer Systems GmbH

Project Coordinator Contacts

Peter Saparin, Ph.D.

Phone: +49-331-567-9446
Fax: +49-331-567-9402
E-mail: peter.saparin@mpikg.mpg.de

Project Budget

The overall budget for the three years of the Second Phase of the project was € 2.025.025.

ESA funded € 754.598, the Industrial Partners € 298.640, and the Project User Group € 50.000. The remaining sum of € 930.787 was contributed in cash and/or in-kind by the academic partners.

Abbreviations and Glossary

Amira	Software platform for 3Ddata analysis, visualization, and quantification.
ASHI	Averaged Shape Index
BMD	Bone Mineral Density
BUA	Broadband Ultrasonic Attenuation
BV/TV	Histomorphometry measure: Bone volume fraction
CD	Histomorphometry measure: Connectivity Density
CSA	Cross Sectional Area
CT	Computed Tomography
F_{max}	Maximum force = fracture force = ultimate force
H	Mean curvature (3D)
IGE	Index of Global Ensemble (2D complexity measure)
ISH	Shape Entropy (3D complexity measure)
L, V, H, I , C	Symbols used to encode 2D pQCT- or CT-image: Lake, Valley, Highland, Incline, Cliff.
K	Total or Gaussian curvature (3D)
Maximal L-block, Mean L-block	2D complexity measure: size of maximal and mean connected area composed of symbol L
MC, MCC, MCE	Marching Cube, MC Complexity, MC Entropy (3D measures)
MISH	Shape Mutual Information (3D complexity measure)
Nd/Tm	Node-Terminus ratio estimated using node-strut analysis
µCT	Micro-Computed Tomography
pQCT	Peripheral Quantitative Computed Tomography
QCT	Quantitative Computed Tomography
QUS	Quantitative Ultrasound
ROI	Region of Interest
RR, DET, LAM, MDL, TT	Recurrence Rate, Determinism, Laminarity, Mean Diagonal Length, and Trapping Time (recurrence plot measures)
S_a	Entropy of x-ray attenuation distribution (2D measure)
S_n	Normalized 3D Entropy of geometrical location (3D measure)
SCI	Structure Complexity Index (2D complexity measure)
SDI	Structure Disorder Index (2D complexity measure)
SHC, SHE, SHI_{global}	Shape Complexity, Shape Entropy, Global Shape Index (3D)
σ_{max}	Maximum stress = fracture stress = ultimate stress
SoS	Speed of Sound, ultrasonic parameter
Tb.Th, Tb.N, Tb.Sp	Trabecular thickness, trabecular number, and trabecular separation estimated using plate model assumptions
TBPf	Trabecular bone pattern factor
TNI	Trabecular Network Index (2D complexity measure)
$V^*_{m.space}$, $V^*_{b.space}$	Marrow and bone space star volume
VOI	Volume of Interest

1. Project Objectives

Bone loss is the second highest risk factor, after radiation exposure, during long-term spaceflights for the health of space-flying personnel. The project aims at developing tools that are able to assess alterations in the trabecular bone structure and at gaining new quantitative information about the bone metabolism in microgravity condition.

The objectives of the study were to:

- Establish a precise non-invasive diagnostic method for quantification of status and changes in bone structural composition.
- Explore the deterioration of human bone tissue in osteoporosis as a model for bone loss under microgravity conditions.
- Develop tools to evaluate structural loss in bone architecture and provide new quantitative information about the changes in trabecular bone architecture in microgravity condition.

2. Prospects and Scientific Impact

The outcome of the present study can provide the foundation for monitoring, prevention, and treatment of structural changes of bone in microgravity condition. The results of this project have an impact in the following areas:

- Health care for space-flying personnel.
- Health care for patients with bone diseases on Earth.
- Theoretical physics, signal and image analysis, and material science.
- Scientific visualization, interactive visual data analysis, and management of large data sets.

3. Scientific Background and Perspectives

3.1 Osteoporosis. Bone Loss in Microgravity

During an average lifetime bone density declines by more than 50% in women, and more than 30% in men. This decline can decrease below the WHO defined threshold and symptoms of osteoporosis, in particular fractures, can occur. Osteoporosis is characterized by decreased bone mass and a deterioration of the micro-architecture leading to increased skeletal fragility (Marx, 2004). It is a highly prevalent disease, affecting approximately 200 million women worldwide, including one-third of the 60 to 70 years old and two-thirds of those older than 80 years. In the US alone 5 million osteoporotic women have already had osteoporotic fractures. Incidence rates appear to vary sevenfold or more between the European countries, which makes it difficult to cite European epidemiological studies, whereas the variation in rates between different localizations in the US is much less (Ross, 1998). Osteopenia, as a precursor to osteoporosis, may occur for various reasons including immobility, such as bedrest and microgravity.

Since the first manned spaceflights the problem of muscle and bone atrophy has been evident. The largest changes in bone mass after exposure to microgravity have been found at the load-bearing lower extremities (Vico et al., 2000) and in the axial skeleton (LeBlanc et al., 2000). Although no pathological fractures have yet occurred, spaceflight-related bone loss may potentially have serious consequences in long-term spaceflight, especially as the recovery is a long-lasting process, if at all achievable (Zerath et al., 1996, Lafage-Proust et al., 1998).

3.2 Bone Status Assessment and Structural Measures of Complexity

During spaceflight, the body is exposed to microgravity and thereby to skeletal unloading, which results in skeletal atrophy (Lang, et al., 2004; Vico et al., 2000). It has long been recognized, from both clinical and animal studies, that immobilization or skeletal unloading results in a loss of bone mass and bone strength (Allison & Brooks, 1921; Krølner & Toft, 1983; Roux, 1896). It is well known that bone density is a good predictor of compressive bone strength (Bell et al., 1967; Ebbesen, et al., 1999; Mosekilde et al., 1987). However, it has also been suggested that loss of trabecular bone strength and the resulting increased risk of bone fractures depends not only on the loss of trabecular bone density, but also on the loss of structural elements as well as on a loss of connectivity (Kleerekoper et al., 1985; Parfitt, 1987; Mosekilde, 1987). Consequently, it is important when investigating pathological, age-related, treatment-induced, or immobilization-induced changes in trabecular bone to ascertain not only the changes in bone density but also the changes in bone structure.

At present, the only method to evaluate trabecular bone structure *in vivo* is by use of bone biopsies, which is an invasive procedure. The current "gold standard" for investigating trabecular bone structure is histomorphometry applied to histological sections, which is a destructive evaluation method. Recent advances in micro-computed tomography (μCT) and magnetic resonance imaging (MRI) have made it feasible to perform three-dimensional (3D) evaluations non-destructively (Feldkamp et al., 1989; Rüegsegger et al., 1996; Wehrli et al., 2002). However, at present these methods still require an invasive extraction of a bone sample from the individual under examination.

Therefore, the main goal of the present study was to develop a technique or a series of techniques, which are able to evaluate and monitor the trabecular bone structure in a non-invasive and non-destructive manner. The developed methodology shall be applicable to

space-flying personnel so that their skeletal status can be monitored and appropriate countermeasures can be taken if necessary.

Consequently, non-destructive and non-invasive examinations of the human bone status must be performed by use of radiological procedures. Pathological alterations of the bone appear as radiological changes in density and structure. Changes in bone mineral density (BMD) can be detected and quantified by several well established osteodensitometric methods where quantitative computed tomography (QCT) represents the "gold standard". In particular, bones of the lower and upper extremities can be examined with peripheral quantitative computed tomography (pQCT).

In order to assess the trabecular bone structure using CT and μCT images, we propose that the bone structure follows the rule of a complex system. The origin of this complexity is the hierarchical nature of the bone structure (Olson, 1997, Fratzl, 2004). Complexity characterizes a system with many interacting and interrelating components. These various interactions and transactions lead to the emergence of new collective nonlinear properties for the system as a whole (Nature Insight, 2001). The collective behaviour of certain parts of the system implies that this behaviour is a property of the whole system, but not properties of its single parts. Measures of complexity (Zurek, 1990) are needed in order to quantify different aspects of complex nonlinear systems.

The field of nonlinear dynamics develops and applies such measures of complexity, e.g. for quantification of complex spatial structures. Due to the increasing quality of μCT data the focus has recently shifted to the analysis of local curvatures of porous media (Lang et al., 2001, Jinnai et al., 2002).

It has been suggested that fractal dimension increased the ability to predict bone strength (Majumdar et al., 1998) or fracture risk (Benhamou et al., 2001) over that obtained by area BMD alone. However, the merit of fractal dimension is unclear since light microscopy studies have shown that the human trabecular network is not fractal.

Promising techniques proposed for analysis of 1D or 2D data are Moran's index, lacunarity, and recurrence plot based measures. Moran's index describes spatial autocorrelation in a 2D plane, while the lacunarity is a measure of the translational invariance of the structure of the object. Their potential have been shown in applications on general 2D image analysis (Chen et al., 2003) and on investigations of CT or MRI images of bone (Dougherty et al., 2001). Moreover, recent studies of recurrence plot based methods have paved the way for development of new complexity measures for analysis of recurrent structures (Marwan & Kurths, 2005; Romano et al., 2004).

3.3 Visualization of 3D Data

Classical tasks of 3D data visualization are volume rendering and iso-surface rendering. A comprehensive overview of these visualization techniques is provided by Hansen & Johnson (2005). As the spatial resolution of CT equipment continues to improve the need for new techniques for visualization and exploration huge dataset increases too. Thus a decrease in voxel size by a factor of s results in an increase of the resulting amount of (uncompressed) image data by a factor of s^3. Such increase of the data volumes exceeds the technological growth of the capacity of computer main memory (RAM).

Therefore, the resulting data sets typically cannot be loaded completely into the main memory of even specialized graphics workstations. This must be taken into consideration when designing a contemporary visualization system. Such a visualization system should be able to process spatial data of any size, on any size computer with well scaling performance. In

addition, it should allow the user to quickly identify important regions of the data, and then enable focused access to those regions (Law, 1999). External memory algorithms and data structures (Vitter, 2001) provide a general framework for addressing these problems. Recent applications in visualization comprise demand paging (Cox, 1997) and optimized prefetching for visualization (Bergeron, 2005). Massive data sets are often stored centrally, in data repositories; which dictate a need to access and explore the data remotely via the Internet. Distributed visualization (Brodlie, 2004) tries to meet this need. Various strategies for distributing the visualization pipeline may be suitable depending on the size of the data and the applied visualization technique (Luke, 2002). Building a practical system for visualization, remote access and exploration of large data sets is an ongoing research task. In the present project our aim was to build a system which could support research on quantification of trabecular bone structures in 3D.

3.4 Quantitative Ultrasound

Quantitative ultrasound (QUS) is a bone quantification technique without exposure to ionizing radiation (Gregg et al., 1997). The majority of bone QUS devices, which are lightweight and portable, have appeared in the last two decades. The vast majority of these QUS devices was designed for testing calcanei. However, several modalities of axial QUS intended for the long bones, using unilateral access, were also developed (Hans et al., 1999). The two main parameters used in QUS, either independently or in combination, are the ultrasound velocity (Speed of Sound, SoS) and the slope of the attenuation-frequency curve (Broadband Ultrasonic Attenuation, BUA) (Njeh et al., 1999). The main determinant of the SoS is the stiffness of the material, while the BUA is – when measured in trabecular bone – mainly determined by the scattering properties of the trabecular network. Ultrasound attenuation in trabecular bone is not only affected by the bone structure but also depends on the bone density (Njeh et al, 2001). Current axial techniques are limited by the fact that the longitudinal wave velocity is almost exclusively dependent on the material properties of cortical bone, and are therefore not useful for assessment of trabecular bone. Promising new approaches include parameters that are sensitive to bone functional properties and their adaptation at clinically important skeletal sites. Therefore, the aim of our research was to find a novel ultrasonic approach for the characterization of the trabecular structure in the proximal tibia.

4. Results Second Phase

4.1. Collection and Imaging of Bone Specimens and Patients

4.1.1. Set-up of the pQCT-scanner suitable for structural analysis of bone images

Our goal was to find a pQCT scanner that was able to examine the structure of the proximal tibia below the knee joint. It should have a gantry opening of at least 18 cm. However, such a scanner is presently not commercially available. In order to meet our requirements Stratec XCT-3000 (Stratec Medizintechnik GmbH) scanner was rebuild by the manufacture to our specifications. This Stratec pQCT scanner has a gantry opening of 28 cm.

The commercial configuration of the XCT-3000 is limited to BMD measurements and macroscopic measurements like endosteal and periosteal circumferences or moments of inertia. Therefore, it was arranged with Stratec to produce a machine with an individual adapted configuration that is able to acquire an image with a quality suitable for structural analyses. After the device had been assembled, the project team worked together with the manufacturer on adjusting the hardware and image acquisition parameters to fit the requirements. This task has been successfully accomplished and the adapted pQCT-scanner has been installed at the CBF facility in September 2003 (Figure 1). Numerous images were acquired from bone specimens of proximal tibiae and lumbar vertebrae during 2003 and 2004. Furthermore, *in vivo* examinations of the proximal tibiae of test persons started in April 2004. All supportive materials and safety precautions have been applied to the machine in order to scan the proximal tibia of these test persons.

Figure 1. The pQCT-scanner allows *in vivo* imaging and structural analysis of proximal tibia as well as study of bone specimens from different skeletal locations.

4.1.2 Collection of new specimens and their conventional x-ray examination

In addition to the bone specimens harvested during the First Phase of the project (2001–2002), 31 sets of specimens consisting of

- the third lumbar vertebra L3
- the fourth lumbar vertebra L4,
- the proximal tibia,
- the calcaneus (or the whole foot)

were collected from the same side of the donor bodies at the Department of Anatomy, Charité, Campus Mitte, as a result of a collaboration with the head of the department Prof. G. Bogusch. Each single set of bone samples was harvested form one donor. All specimens were stored in formaldehyde solution. All bones underwent an air extracting procedure (see earlier reports) in order to remove artefact generating air bubbles inside the bones. Thereafter, the specimens were packed into plastic bags filled with formaldehyde and stored at approximately 3°C.

All specimens underwent a conventional X-ray examination in order to detect pathologic changes of the bones. Since we planned to perform all further investigations on whole sets of specimens, all sets with fractured third or fourth lumbar vertebral bodies (7 cases) or with other pathologic changes (0 cases as evaluated by x-ray) were excluded.

4.1.3 pQCT imaging of specimens. *In vivo* pQCT examination of healthy subjects

In order to establish the procedures for biomechanical testing of whole vertebral bodies L3 (Section 4.3) and histomorphometry of L4 (Section 4.2.1) we rescanned five L3 and L4 vertebral bodies collected for the first phase of the project with the new XCT 3000 scanner as a pilot study.

Thereafter, the remaining 24 newly collected L3 vertebral bodies were pQCT scanned and the images were visually evaluated. After this evaluation, four more cases showing pathological changes were excluded. However, one specimen with osteolytic and one with osteoblastic changes remained included in the material. Consequently, the material comprised sets of bones from 20 individuals. The fourth lumbar vertebral bodies and the proximal tibiae were also pQCT scanned. The scans at the proximal tibiae were performed 17 mm below the tibial plateau, which is the same location as we used for obtaining trabecular bone biopsies in the first phase of the project.

All scans of vertebral bodies and proximal tibia specimens were performed with the same predefined scan parameters. We performed one 2 mm thick axial slice (tomography) trough the middle of the vertebral body. The aim of the pQCT and CT imaging was to mach the scanned location of both methods (both with 2 mm thick slices) as good as possible. When pQCT imaging was performed before CT imaging, the pQCT imaging was set as our reference that we tried to find again by the CT examination. In the beginning of the investigations, only one scout view was preformed as preparation for the pQCT scan. However, it turned out that this approach was problematic as it was difficult to exactly position the specimens for the CT imaging and it therefore consumed unpredictable amounts of time with repetitions of whole series of CT examinations. Finally, we decided to repeat all previously performed pQCT scans with two perpendicular scout views. We were then able to match the positioning of the specimens for pQCT and CT imaging to an acceptable degree.

After installing additional equipment to fixate the position of the patient's leg (see Figure 1), we were able to perform pQCT of six test subjects. The positioning of the subjects lasts about 30 to 90 minutes. In order to receive high-resolution pQCT-images it is necessary to perform three scans at 20 mm/s. This causes the pQCT scan itself to last approximately 20 minutes.

Therefore, even if the test subjects are fixed in the scanner, in order to reduce moving artifacts, it is very difficult to obtain images that are free from artifacts due to movements.

4.1.4 CT imaging of bone specimens. Definition and optimization of acquisition parameters. *In vivo* CT examination of healthy subjects

The first bone imaging experiments performed at CBF with the Siemens Somatom Sensation 16 high-resolution spiral CT scanner revealed the following problems: 1) the noise level was approximately ten times higher than in the single slice images provided by the Siemens Somatom Plus scanner, which was used during the first phase of the project; and 2) it was not possible to obtain axial slice images at the lumbar vertebrae of test subjects as the gantry of the device cannot be tilted in spiral mode. The last problem was solved by using a Siemens Somatom Sensation 4 helical whole body CT-scanner that is also located at CBF. Using this scanner we were, after several adjustments and test scans with different kernels, collimations and rotation times, and with different modes (spiral CT and single slice technique), able to establish a set of scan parameters suitable for high resolution images of a quality needed for the 2D complexity evaluations.

The 25 L3 and 25 L4 vertebral bodies were scanned before the histomorphometric evaluation and biomechanical tests were performed at the UoA (Section 4.2 and 4.3). All these 50 vertebral bodies were completely scanned in spiral CT mode (axial volumetric acquisition of the entire vertebral body). Furthermore, sequences of axial single slice images were obtained through the middle region of the vertebral body (approximately 1 cm high). The Spiral CT scans delivered volumetric sequences of high-resolution images with 1 and 2 mm slice thicknesses. Additionally, the single slice CT scans delivered high-resolution images with a 4 mm slice thickness.

In addition, 20 proximal tibiae were scanned using single slice CT with slice thicknesses of 1 mm, 2 mm, and 4 mm at the same location that was used for the pQCT scans.

In order to transfer the scan parameter from bone specimen to *in vivo* measurements on test subjects, we started by scanning a body equivalent object, the European Spine Phantom (ESP). The noise level increased to approximately three times of the noise level of the images of the bone specimens. Additional test scans with higher kV and mAs reduced the noise level. However, it was found that even with the increased noise level the image quality was good enough to perform structural analysis. Therefore, it was decided to keep the defined 120 mAs level so as to minimized the effective radiation dose.

Several additional experiments were carried out in order to optimize and verify the acquisition parameters and to estimate the sensitivity of the structural evaluation with respect to the positioning of the specimens. Firstly, the specimens were positioned at different tilt angles. Secondly, several new kernels were tested with a series of different collimations and rotation times. Thirdly, different settings affecting the performance of reconstructions were evaluated.

Next, *in vivo* scans of L3 vertebral bodies as well as *in vivo* scans of proximal tibiae were performed on healthy volunteers. The scans of proximal tibiae were location matched with the pQCT scans performed on the same subjects (Section 4.1.3).

Since the Siemens Somatom Sensation 4 helical CT-scanner that had been used in the project might not be available in the future, the established acquisition parameters were transferred and adapted to a new Siemens Somatom Emotion 6 scanner. Thereby the project team also gained knowledge on how to transfer the imaging and the structural evaluation technique to a different type of CT-machine.

4.1.5 µCT-examination of vertebral bodies and proximal tibia biopsies

During the project, the team acquired a large collection of 3D µCT data sets. The data acquisition was excellently performed by the industrial partner Scanco Medical AG.

During the First Phase of the project proximal tibial bone biopsies were µCT-scanned in a Scanco µCT 40 scanner at a voxel size of 20 µm (Thomsen et al., 2005a). The data were used to developed 3D measures of structural complexity (Section 4.5).

After the procedures for vertebral histomorphometry and biomechanical testing were established during the Second Phase, 25 L3s and 25 L4s were µCT-scanned by Scanco Medical before undergoing biomechanical tests. In addition, all 25 L3s were scanned again after the biomechanical compression tests were performed at UoA. The entire vertebral bodies were µCT-scanned using a Scanco µCT 80 micro-CT machine at a voxel size of 37 µm (0.0371 mm × 0.0371 mm × 0.0370 mm). This corresponds to an average number of slices of approximately 800 and an acquisition time of approximately 2.75 hour. The size of each of the acquired 3D datasets was 2048 × 2048 × 1000 voxels at 2 Bytes, resulting in roughly 8 GB of data per specimen. The 3D datasets from all scanned vertebral bodies have been received and are stored on the project's central data server at ZIB.

4.2 Histomorphometry

At present, static histomorphometry is considered to be the "gold standard" for assessing the architectural composition of trabecular bone. New methods for assessment of the architecture of cancellous bone have to be verified against this "gold standard". However, in contrast to the proposed CT-based methods histomorphometry is a destructive and invasive evaluation procedure.

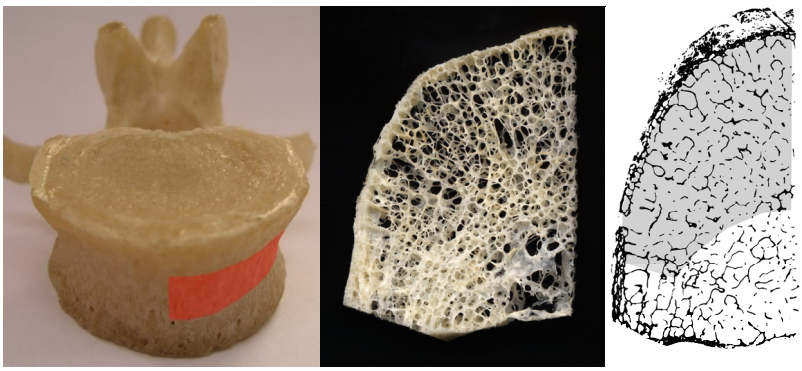

Figure 2. Left: The red marking highlights the region where the 9-mm-thick central bone slice for histomorphometry has been obtained. Center: A photograph showing the 9-mm-thick central bone specimen used for histomorphometry. Right: A 10-µm-thick histological section with the investigated region of interest superimposed in gray.

4.2.1 Vertebral Histomorphometry

In order to perform the best possible comparison between histomorphometry and the CT-based measures, the same vertebral region was evaluated by both techniques (Figure 2). An approximately 9-mm-thick central slice was obtained from one half of each of the vertebral bodies. These bone slices were embedded in methylmetacrylate, cut in 10-µm-thick horizontal sections, stained with aniline blue, and mounted on microscope slides. The bone sections were digitized by scanning them at a high resolution (2,450 dpi which is equivalent to a pixel size of 10 µm) in a flatbed image scanner with an integrated transparency unit. Image artifacts were removed using the GNU Image Manipulation Program (GIMP, http://www.gimp.org). During the interactive editing procedure the digitized images were compared with the original

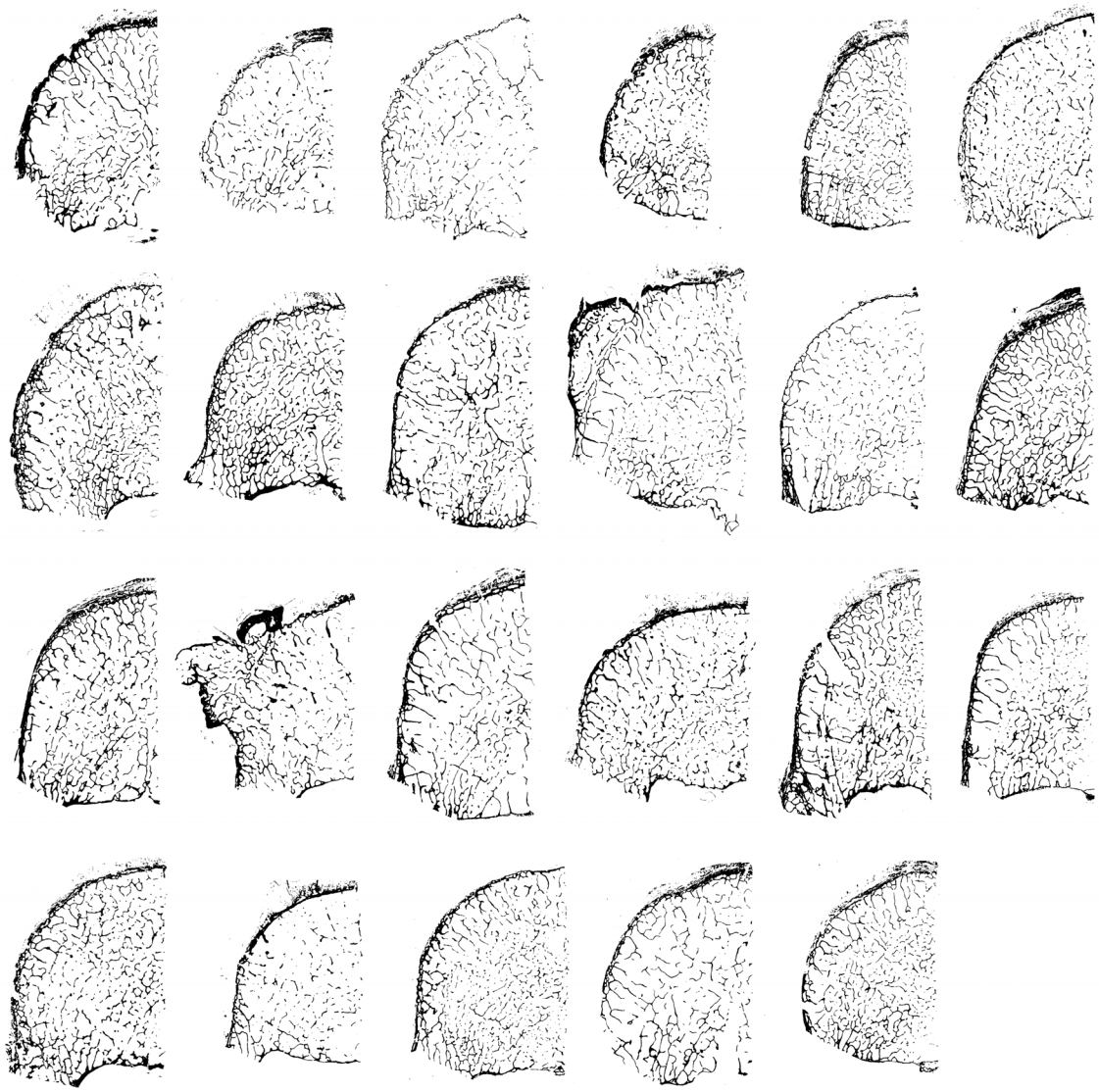

Figure 3. Representative horizontal histological sections from each of the 23 analyzed human lumbar vertebrae. Please note the large diversity of trabecular structure that is represented in the study population. Osteophyte formation is clear in two of the histological sections (row 2, column 4 and row 3, column 2). In addition, the large range of bone volume fractions represented in the population is also directly evident from the sections.

sections using a stereo microscope (Olympus SZ-40, Olympus, Tokyo, Japan). Individual histological sections from each of the vertebral bodies are shown in Figure 3.

The vertebral bone architecture was characterized by histomorphometry based on stereological methods. A custom-made fully automated computer program was used to perform the histomorphometric analyses (Thomsen et al., 2000). The analyzed region of interest (ROI, Figure 2) corresponded to that used for computation of the 2-D pQCT-based measures of complexity (Section 4.4, Figure 11). The histomorphometrical analyses included:

- Bone volume fraction (BV/TV);
- Marrow ($V^*_{\text{m.space}}$) and bone ($V^*_{\text{b.space}}$) space star volume (Vesterby et al., 1991);
- Parallel-plate model (Tb.Th, Tb.N, Tb.Sp) (Parfitt et al., 1983);
- Node-strut analysis (Nd/Tm) (Garrahan et al., 1986);
- Trabecular bone pattern factor (TBPf) (Hahn et al., 1992);
- Connectivity density (CD) (Gundersen et al., 1993).

The computer program used for the histomorphometric analyses is the same as the one used in the first phase of the project for the analysis of biopsies from the proximal tibial metaphysis. Additional descriptions of the workings of the computer program can be found elsewhere (Thomsen et al., 2000; Thomsen et al., 2005a; Thomsen et al., 2005b).

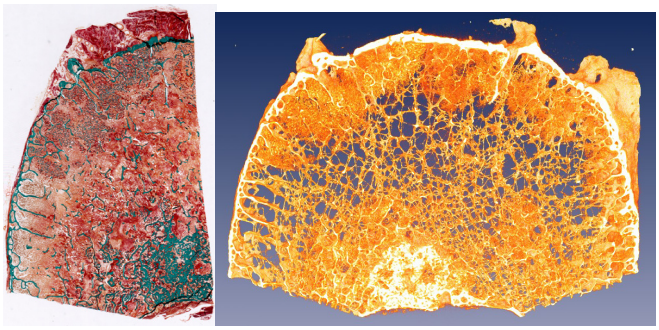

Figure 4. Left: A 10-µm-thick Goldner-trichrome-stained histological section from one of the excluded vertebrae. Bone tissue is stained green. Please note the large formation of bone in the lower right hand corner. Right: 3D reconstruction of an approximately 3-mm-thick section from the same vertebra. Please note the large areas with newly formed bone.

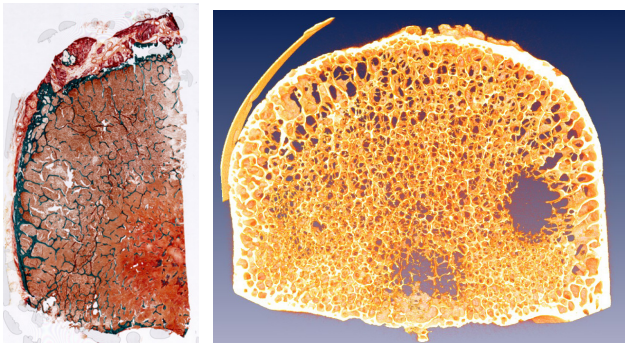

Figure 5. Left: A 10-µm-thick Goldner-trichrome-stained histological section from the other excluded vertebra. Right: µCT-based 3D reconstruction of the same vertebra. Please note the large areas devoid of trabeculae due to aggressive osteoclastic activity.

Two of the 25 vertebral bodies had to be excluded from all subsequent analyses as osteoinductive metastases were found in these vertebral bodies. Figure 4 shows a Goldner-trichrome-stained section (left) and a µCT-based 3D-reconstructed slice (right) from one of the two excluded vertebrae, clearly illustrating the pathological nature of this vertebral body. In the lower right hand corner of the Goldner-trichrome-stained section, there is a massive, almost compact, formation of bone (shown in green). This area can also be found in the lower center of the 3D-reconstructed image as a compact white area. In addition, new woven bone is formed close to the cortical rim. This is seen as either small green areas in the histological section or as orange formations in the 3D-reconstruction. Similarly, Figure 5 shows a Goldner-trichrome-stained section (left) and a 3D-reconstructed slice (right) from the other excluded vertebra. In the 3D-reconstructed image, large areas of the trabecular bone are missing due to aggressive osteoclastic activity. Finally, Figure 6 shows an example of normal osteoclasts (left) and a gigantic osteoclast (right) from one of the two excluded vertebrae. As it is possible to count at least 20–25 nuclei in the 10-µm-thick section, the number of nuclei of this osteoclast can be estimated to approximately 100–200! In comparison, normal osteoclasts have only 5–7 nuclei.

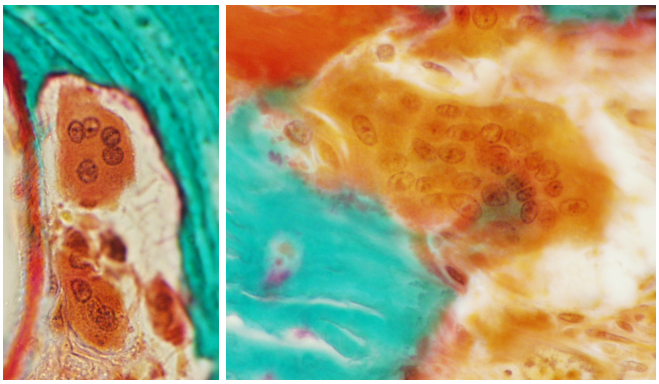

Figure 6. Two Goldner-trichrome-stained sections showing osteoclasts (orange) with multiple nuclei (brown) visible in each cell, mineralized bone (bright green), and osteoid (red). Left: Three normal osteoclasts sitting in a resorption pit. Right: A gigantic osteoclast from one of the excluded vertebrae.

4.2.2 Tibial Histomorphometry

Cylindrical bone samples with a diameter of 7 mm were obtained perpendicular to the length axis of the tibia 17 mm below the tibial plateau at the medial side of the proximal tibial metaphysis from 24 cadavers (Thomsen et al., 2005a). The histological preparation and the histomorphometrical analyses were performed as described for the vertebral bodies.

4.2.3 Iliac Crest Histomorphometry – Influence of Bed Rest on Bone Structure

It is difficult to obtain bone samples from space crews so bed rest studies are used to simulate microgravity in order to study the effects of skeletal unloading on the trabecular architecture. However, undertaking a bed rest study is a major task and is beyond the scope of the present investigation. Instead, the team established a work-relation with the Institute for Biomedical Problems (IMBP) in Russia and gained access to bone sections obtained from test subjects who participated in a 370-day-long bed rest study that was conducted in the 1980s (Grigoriev et al., 1992).The iliac bone biopsies were embedded, sectioned, and stained in St Etienne, France, by Professor Laurence Vico and co-workers.

This 370-day-long bed rest experiment is unique because it is the longest bed rest study ever to be performed. Consequently, these iliac crest bone biopsies gave the team an exceptional opportunity to investigate the bone structural changes that take place during long-term skeletal unloading.

The experiment comprised nine volunteer male subjects 27–42 years of age (mean 35.4 years), which were divided in two study groups, A (n = 4) and B (n = 5), so that the groups were balanced with respect to age, height, and body weight. However, the sections from one of the biopsies from one of the test subjects in group A were mislaid before the team got access to them. Consequently, histomorphometry was available from only three of the four subjects in group A.

During bed rest, the subjects were placed with a 5° head-down tilt. The head-down tilt (antiorthostatic) bed rest is better able to reproduce the physiological responses due to altered fluid distribution experienced by space flying personnel exposed to microgravity than horizontal bed rest (Kakurin et al., 1976a; Kakurin et al., 1976b, Krupina et al., 1976).

The subjects in group A were prophylactically treated with the "first generation" bisphosphonate Xidifon in a dose of 900 mg per day. Concurrent with the bisphosphonate treatment regimen, the subjects in group A underwent an exercise regimen similar to that recommended for prolonged spaceflight (Stepantsov et al., 1985). The exercise regimen was mainly comprised of a treadmill, which was used by the test subjects in a horizontal position. The test subjects were connected to the treadmill by elastic cords attached to a well-fitted vest. The pace of the treadmill was driven solely by the test subject. The treadmill exercise was augumented by a bicycle ergometer, specially designed for spaceflight, which was also pedaled from the horizontal position. The exercise regimen was divided into three 120-day cycles. During each cycle, no exercise took place from day 0 to day 20, whereas exercise was performed for one hour per day from day 21 to day 60 and for two hours per day from day 61 to day 120. However, the final cycle was extended with ten days to a total duration of 130 days. Cylindrical transiliac bone biopsies with a diameter of 8 mm were obtained at the standardized position 2 cm below the iliac crest and 2 cm behind the antero-superior iliac spine (Bordier et al., 1964) at the left ileum before the beginning of the bed rest, and at the

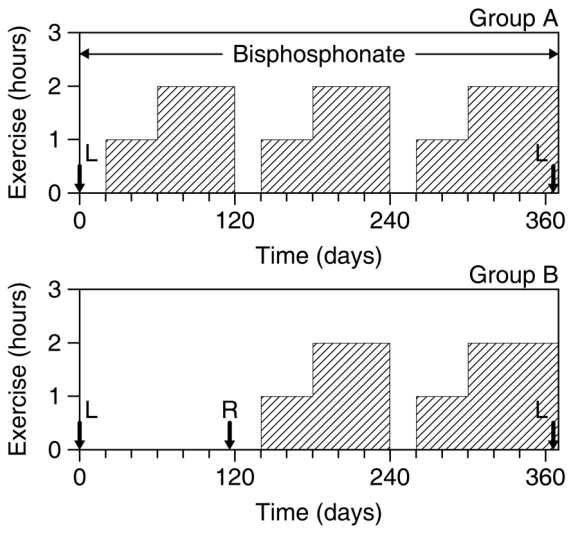

Figure 7. Schematic illustration of the study regimen for groups A and B. The x-axis is the day of the study and the y-axis is the amount of daily exercise. The arrows indicate the time and location (left or right) of the iliac crest bone biopsies.

right ileum at day 366.

The subjects in group B did not, at any point during the study, receive any bisphosphonate treatment. Furthermore, the subjects in group B did not perform any exercise in the first 120-day-cycle, whereas they followed the same exercise regimen as the subjects in group A during the last two cycles (i.e. from day 121 to day 370). Transiliac bone biopsies with a diameter of 8 mm were obtained at the left ileum before the beginning of the bed rest, at the right ileum at day 116, and again at the left ileum at day 366.

Figure 7 demonstrates in detail the study regimen for the two study groups.

The biopsies were infiltrated and embedded in methylmetacrylate and for each biopsy four 7-µm-thick non-consecutive sections were cut. The undecalcified bone sections were stained with modified Goldner trichrome. The stained and mounted sections were placed directly in an image scanner with an integrated transparency scanning unit (Epson Perfection 3200 Photo, Seiko Epson, Nagano, Japan) and digital images were obtained in a resolution of 2,540 dpi (pixel size: 10 µm × 10 µm). The images were interactively edited in order to remove sectioning artifacts and drilling residue and then the images were threshold filtered in order to produce black-and-white images.

The computer program used for the histomorphometrical analyses is the same as that used for the vertebral and tibial analyses (Section 4.2.1). The researcher (JST) was blinded for the group distribution during the histomorphometric measurements in order to obviate measurement bias.

Figure 8 shows the results of the histomorphometric analyses for each test subject. Individual data points are shown with a filled circle. Data points from each test subject have been connected with solid lines, whereas average values for all individuals in the particular group are shown with dashed lines.

The 120 days of bed rest without countermeasures resulted in a significant ($p = 0.046$) decrease of BV/TV (6.3%) and a significant ($p = 0.020$) increase of Tb.Sp (14.7%). This reduction in trabecular bone density corresponds to a loss of 0.37% per week. Furthermore, a decrease of Tb.N (10.2%) was also found, but this was significant at the 0.08 level only. No other significant changes were found for the histomorphometric measures between any of the time points in either of the study groups. Both $V^{*}_{\mathrm{b.space}}$ (20.9%) and Tb.Th (4.1%) were increased after 120 days of bed rest without countermeasures, indicating a larger average trabecular thickness after immobilization. However, neither of these changes was statistically significant. Figures 8 E and F illustrate that the changes of the two 2D bone structural measures Nd/Tm and TBPf exhibit very complex behavior at the different time points for the subjects in group B.

The study has shown that 120 days of 5° head-down tilt bed rest without countermeasures resulted in a significant decrease of BV/TV and a significant increase of Tb.Sp. Furthermore, a decrease of Tb.N was also detected during 120 days of bed rest without countermeasures – but this was significant at the 0.08 level only. No other significant changes were found for the histomorphometric measures between any of the time points in either of the study groups. Finally, the combined treatment with bisphosphonate and exercise was able to prevent significant loss of bone during 370 days of antiorthostatic bed rest.

In contrast to the present study, Vico et al. (1987) found a non-significant decrease of iliac crest BV/TV of 1.2% in subjects exposed to 120 days of 5° head-down tilt bed rest, while Palle et al. (1992) found a non-significant increase of iliac crest BV/TV of 2.8% in subjects undergoing 120 days of 5° head-down tilt bed rest. LeBlanc et al. (1990) did not study the iliac crest *per se*, but found a significant loss of pelvic BMD (0.29% per week), which is

relatively close to what was found in the present study for iliac crest bone biopsies (0.37% per week).

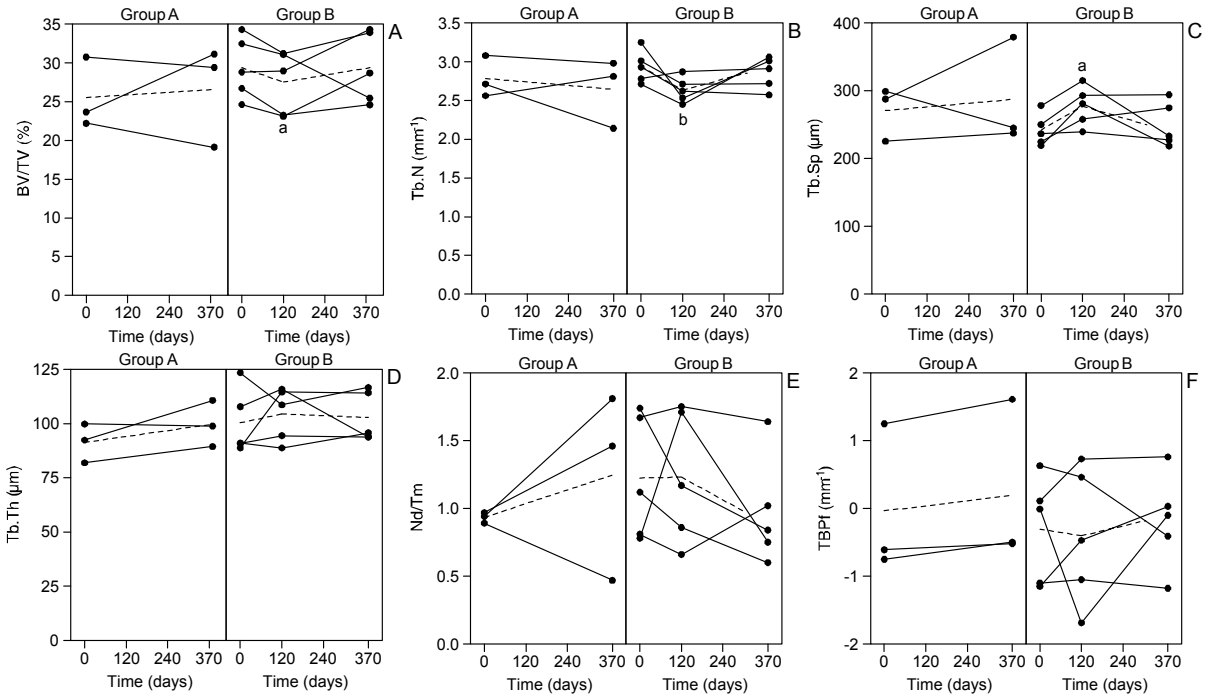

Figure 8. Trabecular bone volume, BV/TV (A); Trabecular number, Tb.N (B); Trabecular separation, Tb.Sp (C); trabecular thickness Tb.Th (D); node terminus ratio, Nd/Tm (E); and trabecular bone pattern factor, TBPf (F) as functions of time for groups A and B. Dashed lines indicate average values for the individuals in the particular group. Key: a: $p < 0.05$ and b: $p < 0.08$.

It is known from clinical studies that immobilization causes a very rapid loss of bone density. Hanson et al. (1975) found a spinal bone loss of 2% loss per week, while Krølner and Toft (1983) found a vertebral bone loss of 0.9% per week. LeBlanc et al. (1987) showed that 5 weeks of bed rest resulted in a spinal BMD loss of 0.21% per week, and in a later study that 17 weeks of horizontal bed rest resulted in a spinal BMD loss of 0.34% per week (LeBlanc et al., 1990). In the present study, the loss of iliac crest bone volume (BV/TV) was 0.37% per week after 120 days of bed rest without countermeasures. Thus, the bone loss is less in healthy subjects exposed to either horizontal or antiorthostatic bed rest than that found in the clinical studies.

Thomsen et al. (1998) have determined the relationship between BV/TV and age at the iliac crest for normal males and females. Using these relationships, the relative age-related loss of BV/TV that takes place for males from 35 years to 36 years of age can be determined to 0.89% per year or 0.017% per week. Thus, in the present study, the rate of bone loss induced by bed rest was 22 times larger than what could be expected for similarly aged males not undergoing bed rest.

We found a very erratic pattern of behavior of the two structural measures Nd/Tm and TBPf during bed rest without countermeasures. This inconsistent behavior of these structural measures is probably due to the inhomogeneous distribution of the trabecular bone structure of the ileum, as the biopsies had to be obtained at different locations at the beginning of the study and at day 116.

The homogeneity of the trabecular bone structure of the iliac crest has previously been investigated (Bordier et al., 1964; Ellis & Peart, 1972; Melsen et al., 1978; Moore et al., 1989). These studies showed that when two iliac crest bone biopsies were simultaneously obtained within a distance of 1–2 cm, reasonably close correlations could be established

between histomorphometric measures derived from those two biopsies. However, if the distance between the biopsies was larger, the relationship between the histomorphometric measures from the two biopsies was substantially weaker. Since the structure of the iliac crest is not homogeneous, observed differences in the bone structure may consequently reflect differences in the sampling site rather than differences between the two time points. Similarly, the lack of an observed difference might also be due to differences in the sampling site combined with the inhomogeneously distributed trabecular bone structure of the ileum. One way to decrease this measurement "noise" is to increase the number of test subjects substantially, which is neither feasible in bed rest studies nor in investigations conducted on space flying personnel. A further complicating factor in such studies is that the test subjects can only be recruited from a limited pool of individuals, which makes it difficult to create evenly balanced study groups.

This indicates that in longitudinal studies where only a few test subjects are available iliac crest bone biopsies is not the ideal tool for obtaining information about changes of the trabecular bone structure. It is probably prudent to consider whether a non-invasive radiological technique applied at a skeletal location, where it is possible to conduct repeated measurements of the same skeletal structure over time, would offer a better assessment of the structural trabecular bone status than iliac crest bone biopsies. In the first part of the project we suggested the proximal tibial metaphysis as such a skeletal location which is well suited for *in vivo* longitudinal assessment of the trabecular bone structure.

In the present study, we found that 120 days of antiorthostatic bed rest induced a loss of Tb.N, which was significant at the 0.08 level. We also found a concurrent non-significant increase in Tb.Th. Palle et al. (1992), who found a significant loss of Tb.N and a concomitant non-significant increase of Tb.Th, made a similar observation. This may indicate that the thinnest trabeculae of the iliac network have been resorbed due to immobilization. When the thinnest trabeculae are removed, the average thickness of the remaining trabeculae will increase, which can explain the simultaneous slight increase in trabecular thickness. However, in order to verify this conjecture a study with substantially more individuals needs to be carried out. Nevertheless, the results obtained in the present study as well as those obtained by Palle et al. (1992) indicate that bed rest-induced bone loss probably functions through a removal of thin trabeculae rather than through an overall thinning of the trabecular network. This is consistent with the recent study by Modlesky et al. (2000), which showed that BV/TV and Tb.N were decreased; Tb.Sp was increased; while Tb.Th was unchanged in spinal cord-injured men compared with normal controls.

In conclusion: Bed rest without countermeasures results in a significant loss of bone density and in a significantly altered bone structure at the iliac crest. There are non-significant indications that the bed rest-induced bone loss involves removal of trabeculae without a general thinning of the trabeculae. A longitudinal series of iliac crest bone biopsies is not the ideal tool for investigating changes of the trabecular bone structure.

An article describing the histomorphometric results of the bed rest study has been published in Aviation, Space, and Environmental Medicine (Thomsen et al., 2005b).

4.3 Biomechanical Testing

In order to evaluate the abilities of the various structural measures to predict bone strength, it is vital to determine the fracture strength of the examined bone. However, as vertebral histomorphometry and biomechanics are both destructive testing methods, more than one vertebral body is required from each individual. Consequently, the third lumbar vertebral

bodies (L3) were used for biomechanical testing, whereas the fourth lumbar vertebral bodies (L4) were used for histomorphometry.

Furthermore, we wanted to be able to compare the trabecular bone structure of the vertebrae before and after they were compression tested. Therefore, it was important that the vertebrae remained intact and no removal of the end plates took place in order to make the bone specimens parallel with the compression machine (Instron 5566, High Wycombe, UK). A putty material used for dental casting was identified (Kneton Lab 80, Erkodent GmbH, Pfalzgrafenweiler, Germany) that have material properties similar to those of intervertebral discs. The putty underwent mechanical testing and Young's modulus was determined to approximately 20 MPa. This elasticity is very close to what have been found experimentally for canine lumbar intervertebral disci (Zimmerman et al., 1992).

The interface material was placed on either side of the vertebral bodies. Before the interface material hardened, the vertebrae were placed in the materials testing machine and a gentle pressure was applied so that the interface material was distributed evenly over the endplates and thus fitted perfectly to the materials testing machine (Figure 9).

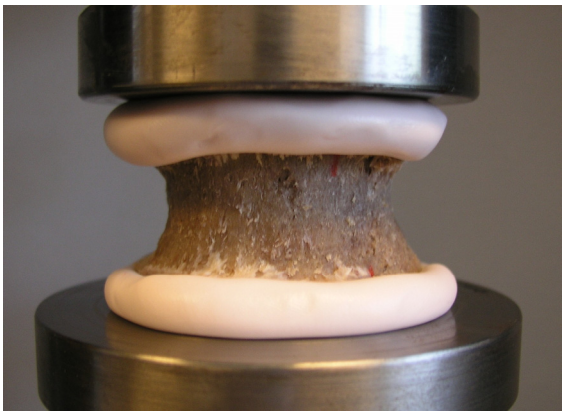

Figure 9. A vertebral body with interface material in the materials testing machine.

After the interface material had hardened, the vertebrae were compressed to failure at a constant deformation rate of 5 mm/min. During compression, force and deformation values were automatically recorded (Figure 10). The failure point is defined as the maximum force applied during the compression. In order to enable a comparison between individuals of different sizes the maximum stress values were computed as the maximum force values divided by the average cross sectional area of the vertebrae.

The average cross-sectional area (CSA) was found by first determine the vertebral volume by use of Archimedes' Principle and then measure the vertebral height with an electronic caliper. The average CSA is then given by the vertebral volume divided by the vertebral height.

During compression the measured failure force is that of the bone, whereas the measured stiffness is a combination of the stiffness of the bone and the interface material. Therefore, in the present study it is not possible to reliably estimate the stiffness of the tested vertebrae.

In addition, it is well know and documented that formalin fixation influence the mechanical properties of bone. Therefore, it will not be possible to compare the biomechanical data with data obtained from vertebrae that have not been fixed with formalin. However, we do believe that the relationships between bone strength and the structural measures are not compromised and that such relationships, reviled by the present investigation, therefore will be valid for non-fixed vertebrae too.

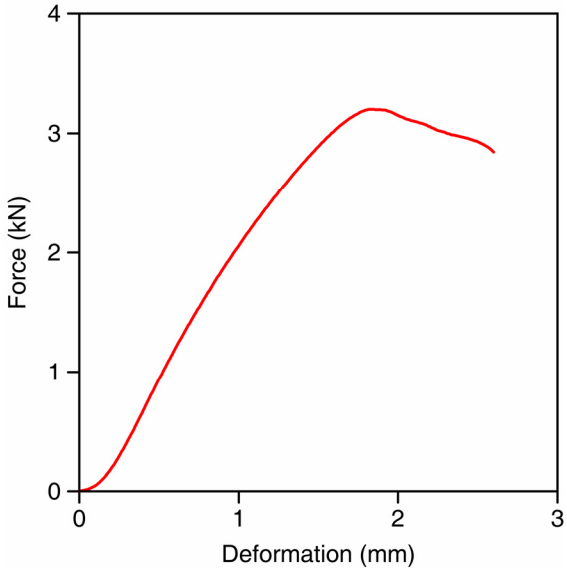

Figure 10. Force-deformation curve originating from the compression testing of one vertebra with interface material attached to both endplates.

4.4 2D Measures of Complexity to Quantify Bone Loss and Estimate Bone Strength from CT- and pQCT images

Images acquired with CT and pQCT from different skeletal sites are used for 2D analysis of loss of bone structure. Normal, osteopenic, and osteoporotic specimens were used as models of bones exposed to microgravity. After development, the procedures were adapted to patient examination and are now ready for examination of space-flying personnel.

4.4.1 Measures of complexity derived from CT images

The method is based on nonlinear and symbolic dynamics of complex systems. The developed technique is especially advantageous when the CT images are unable to resolve individual trabeculae, and the value of each voxel therefore represents contributions from several structural elements.

The very same method was used to analyze the images acquired by pQCT and with whole body CT-scanners. The adaptation of the method to process new class of the images only required an adjustment of control parameters to the expected pixel size, slice thickness, level of noise, and geometrical size of the analyzed bones. The technique consists of three main stages: image preprocessing, image encoding, and quantitative structural assessment.

The image preprocessing includes calibration, standardized segmentation of the ROI (Figure 11, a), and a split of the ROI into entire bone, trabecular bone, and cortical bone (Saparin et al., 2005c).

During image encoding, the attenuation value of each pixel is substituted by one of only five different symbols (Figure 11, b, c). The encoding procedure is based on both the dynamics and the level of X-ray attenuation in the vicinity of an encoded pixel. Finally, the developed set of measures of complexity (extended in comparison to the First Phase of the project) is used for quantification of different aspects of bone architecture in a holistic way (Saparin et al., 2005a, c):

- Structure Complexity Index (SCI) assesses the complexity and homogeneity of the structure as a whole;
- Structure Disorder Index (SDI) measures the degree of order/disorder within the bone;
- Trabecular Network Index (TNI) evaluates richness, orderliness, and homogeneity of the trabecular network;
- Index of Global Ensemble (IGE) assesses the overall dynamics of the structural elements;
- Maximal L-block and Mean L-block quantifies bone tissue replacement by marrow tissue.
- Entropy S_a is the normalized Shannon entropy of x-ray attenuation probability density distribution. In contrast to the above described six measures which based on symbol encoding, the entropy is calculated directly from the attenuation values of the original non-encoded CT-image.

In addition, volumetric BMD was calculated using the same ROI. A detailed description of the method can be found in (Saparin et al., 1998; Gowin et al., 2001; Saparin et al., 2002, 2005c).

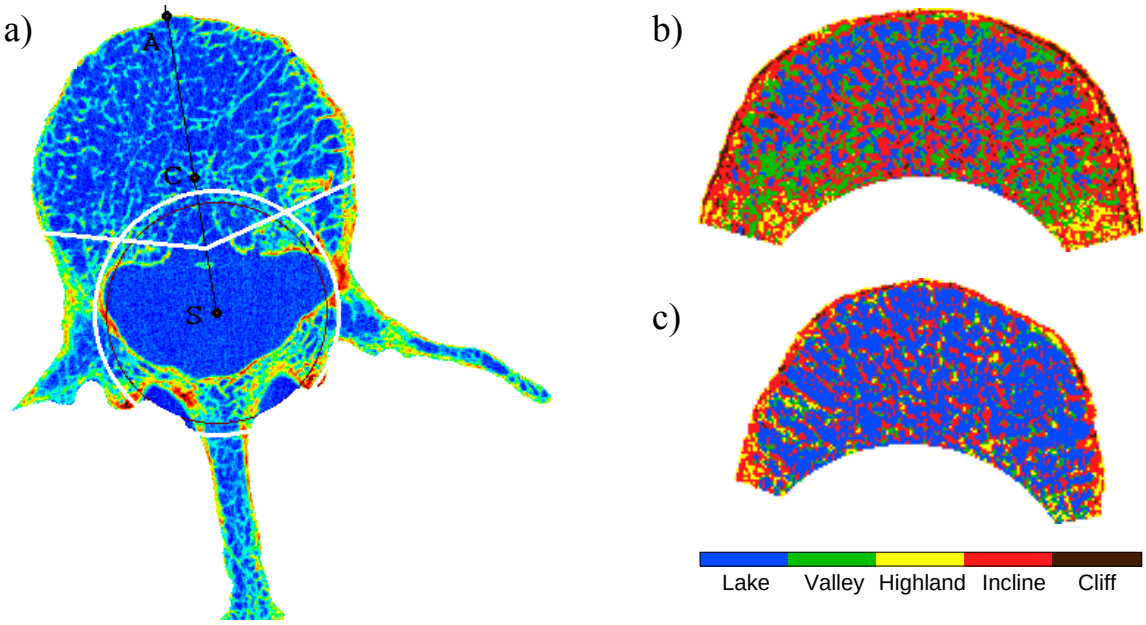

Figure 11. (*a)*: Standardization of vertebral ROI in CT and pQCT-images. Cut off lines (shown in white) remove the posteriors part of the vertebra. SA is the symmetry axis, S is the spine canal center, C is the center of the vertebral body. *(b, c)*: Symbol-encoded ROIs of normal *(b)* and osteoporotic *(c)* vertebrae L4 obtained from mid-axial pQCT slices. Only five different types of symbols are used to represent bone composition.

4.4.2 Relationship between measures of complexity and histomorphometry

The developed structural measures of complexity were compared with histomorphometry using 17 entire L4 vertebral bodies. The population comprised 11 women (aged 75–98 years) and 7 men (aged 57–88 years). All these specimens were selected from population of 23 analyzed in Sections 4.1.1 and 4.2 so that donors with manifestations of diseases that influence the skeleton were excluded. In addition, the population was selected so that the BMD values of the vertebrae were as evenly distributed as possible. The selection was determined before any structure quantification process was initiated. Mid-axial vertebral CT-slices were acquired with a STRATEC XCT-3000 pQCT scanner (STRATEC GmbH, Pforzheim, Germany) at a resolution of 250 µm × 250 µm and a slice thickness of 2 mm.

The Pearson correlation coefficients for the relationships between the measures of complexity and the histomorphometric measures are summarized in Table 1. In some cases logarithmic transformation was applied to the data before calculating the correlation coefficient.

	BV/TV	$V^*_{\mathrm{m.space}}$	$V^*_{\mathrm{b.space}}$	Tb.Th	Tb.N	Tb.Sp	Nd/Tm	TBPf	CD
SCI	0.89	-0.83	…	…	0.84	-0.91	0.72	0.70	0.67
TNI	0.76	-0.84	…	…	0.87	-0.89	…	…	0.89
SDI	0.74	…	…	…	0.71	-0.77	…	-0.66	…
IGE	0.85	-0.78	…	…	0.83	-0.88	0.68	-0.70	…
Max L-bl	-0.84	0.79	…	…	-0.86	0.88	-0.67	0.67	-0.83
Mean L-bl	-0.80	0.81	…	…	-0.86	0.89	…	0.65	-0.76
S_a	0.81	…	…	0.69	0.73	-0.77	0.76	-0.76	…

Table 1. Pearson correlation coefficients between the measures of complexity (rows) and the histomorphometric measures (columns) calculated for the trabecular bone ROI of L4 vertebral bodies. Significance level: $p \leq 0.01$. Coefficients with lower levels of significance have been omitted.

Despite the fact that the measures of complexity were derived from pQCT images with a much lower resolution than the histomorphometric evaluation, very good or excellent correlations were found between the measures of complexity and the appropriate histomorphometric measures (Saparin et al., 2005a, 2005c). The complexity measures can provide information about the bone architecture corresponding to the following histomorphometric parameters: BV/TV, $V^*_{\mathrm{m.space}}$, Tb.N, Tb.Sp, Nd/Tm, TBPf, and CD. In addition, a very good linear correlation, r=0.91, was found between BV/TV and BMD.

Due to the pixel size and the slice thickness the width of a single trabecula cannot be evaluated from 2D CT images. Therefore, at present information provided by the two histomorphometric measures Tb.Th and $V^*_{\mathrm{b.space}}$ cannot be matched by CT-imaging. However, the bedrest study (Section 4.2.3) showed that immobilization, and therefore probably also microgravity, does not have an impact on Tb.Th, whereas BV/TV and Tb.Sp were significantly affected. Therefore, it is safe to say that the technological limitations of the proposed methodology will have no effect on the results when it will be used for the examination of space-flying personnel.

4.4.3 Prediction of bone strength

The ability of the 2D CT-based complexity measures to predict bone strength was investigated by performing pQCT scans and compression tests (Sections 4.1.3 and 4.3) on the same set of 18 human L3 specimens selected as described in Section 4.4.2.

We found that the structural measures obtained from the entire bone (trabecular plus cortical) ROI provided higher correlations with failure stress than structural measures obtained from trabecular bone alone (Saparin et al., 2005a, 2005c). This result reflects that both bone compartment work together and maintain the integrity of the bone. The correlation coefficients for the entire ROI are summarized in Table 2.

	SCI	TNI	SDI	IGE	Max L-bl.	Mean L-bl.	S_a
σ_{max}	0.77	0.70	0.73	0.86	-0.70	-0.61	0.91

Table 2. Pearson correlation coefficients between bone strength σ_{max} and measures of complexity calculated from the entire bone ROI f L3 vertebral bodies. Significance level: $p \leq 0.01$. Coefficients with lower levels of significance have been omitted.

Multiple regression of the bone strength with the measures of complexity resulted in a correlation coefficient of r = 0.96. This indicates that the measures of structural complexity can explain 92% of the variation in vertebral bone strength. Including the BMD into the set of independent variables in the multiple regression analysis did not improve the correlation (Saparin et al., 2005a, 2005c).

4.4.4 Structural complexity at different skeletal sites and optimal location

In order to identify an optimal skeletal location for assessment of the bone structural composition after exposure to microgravity or during osteoporosis, measures of complexity were applied to evaluate seven different skeletal sites: distal radius, humeral midshaft, vertebral body L3, femoral head, femoral neck, proximal tibia, and calcaneus (Saparin et al., 2002, 2005c). Bone samples were obtained from 29 individuals and examined for each of these skeletal sites. The results presented here are obtained in the Phase One of the project but they are crucial for supporting the decision taken for *in vivo* image acquisition and for our recommendation for the bone status assessment in space flying personnel.

It was shown that bones from different skeletal locations have different structural complexities and different degrees of disorder despite having similar BMD values (e.g. SCI vs. BMD, Figure 12). The complexity of the bone architecture is much lower in the distal radius and the femoral neck than in the proximal tibia, calcaneus, or femoral head, although they may have the same BMD value. The normalized slope of the curves in the structure-density diagrams can be used to estimate the relation between the structural differences and the differences in BMD during bone loss. The average normalized slopes for each skeletal location and ROI are summarized in Table 3. The normalized slope for the radius and the femoral neck is two times less than of the femoral head, proximal tibia, calcaneus, and L3. For the same loss in BMD the structural complexity of the femoral head, proximal tibia, calcaneus, and L3 will change twice as fast as at the distal radius and the femoral neck (Figure 12). The humeral mid-diaphysis consists mainly of cortical bone and behaves therefore differently.

Even the most sophisticated cortical-trabecular bone separation procedure is somewhat arbitrary. The cortical bone belongs to the architecture of the bone as much as the trabecular bone. The differences between the slope derived from the entire bone ROI and trabecular bone ROI (see Table 3, last column) estimates the impact of the cortical bone in relation to the density and the complexity of the bone architecture.

Conclusion: the skeletal site most suited for monitoring the bone structural status of space-flying personnel has to be found among: femoral head, proximal tibia, calcaneus, and L3.

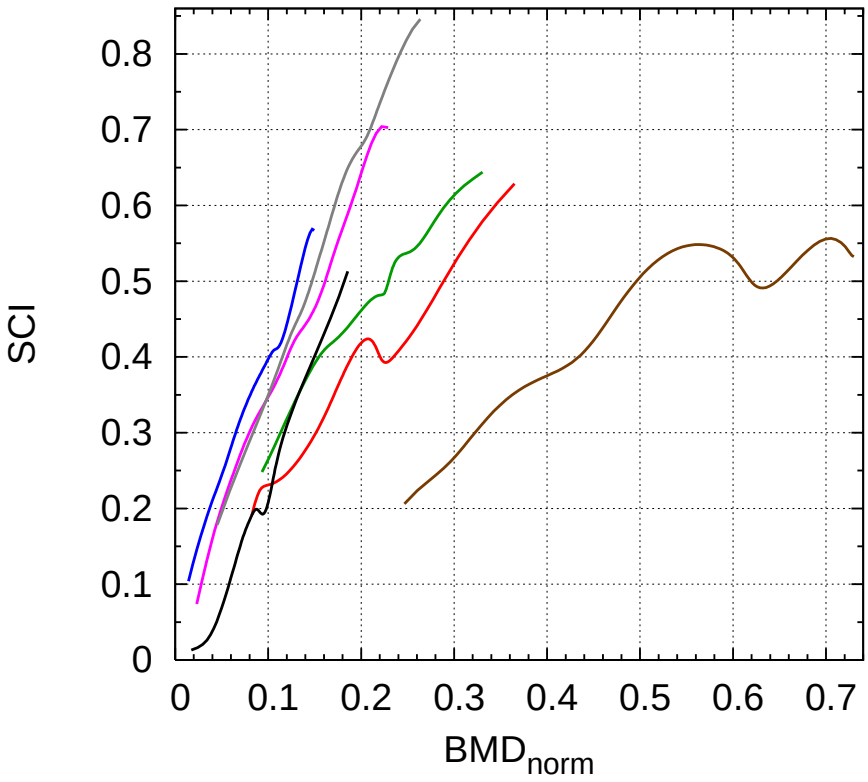

Figure 12. Structure-density diagram for seven different skeletal locations: structure complexity index SCI versus normalized bone mineral density BMD_{norm}. The maximal BMD value encountered in nature (1200 mg/cm^3, Laval-Jeantet, 1983) was used for normalization of the BMD values. The data are approximated by Bezier curves for visualization purposes. For a particular BMD-level, the respective complexity of the bone architecture may differ considerably from one location to another. The curves have different slopes characterizing the different relations between the density and the complexity of the bone architecture at different skeletal locations. Blue: proximal tibia; grey: femoral head; mauve: calcaneus; black: vertebra L3; green: femoral neck; red: distal radius; and brown: humeral mid-shaft.

Skeletal location	Normalized slope		
	Entire ROI	Trabecular ROI	Difference (%)
Femoral head	2.22	2.28	2.7
Proximal tibia	2.17	2.30	6.0
Vertebral body L3	2.16	2.30	6.5
Calcaneus	1.97	2.21	12.2
Femoral neck	1.08	1.45	34.3
Distal radius	1.02	1.29	26.5

Table 3. Normalized slope SCI vs. BMD for different skeletal locations obtained for different ROIs.

4.4.5 *In vivo* examination and quantification of bone structure from vertebral and tibial CT- and pQCT-images

The femoral head cannot be examined physically without the surrounding acetabulum *in vivo*. It excludes this skeletal site for *in vivo* examinations. The calcaneus is a bone with enormous variations in geometry and renders impossible for a standardization process.

With support from the industrial partner Siemens AG the developed method has been implemented for *in vivo* examination of patients or space-flying personnel. This includes CT-imaging of the third lumbar vertebra and CT- or pQCT-imaging of the proximal tibia. The approach to quantify bone structure with the measures of complexity is being adapted to two different kinds of CT-machines capable of obtaining bone images *in vivo*:

- Whole-body CT scanner Siemens Sensation 4 Volume Zoom;
- Peripheral quantitative computer tomography (pQCT) scanner XCT3000, Stratec Medizintechnik GmbH, Pforzheim, Germany.

The devices provide CT-images of distinctive parameters and resolution, but, most importantly, the radiation exposures for a patient are very different. The dose obtained by a patient during the pQCT investigation is 10 times less than the one received during CT-imaging of the lumbar spine region. In addition, the price of the pQCT machine is only a fraction of the cost of the whole-body CT-scanner. A high-resolution and low-radiation pQCT scanner has been specially configured for evaluation of the bone structure in the proximal tibia.

The image analysis program includes BMD measurements and quantification of the architectural composition of the bone regions by 2D measures of complexity.

Six healthy volunteers (no known bone diseases), age range 31 to 52 years, five men and one woman, were selected for the pilot study. CT-images of vertebra L3, CT-images of proximal tibia, and pQCT-images of the proximal tibia were acquired from every person (Figure 13). Slice location in L3 vertebrae: center of vertebral body in the transaxial direction.

The proximal tibia images were acquired 17 mm below the knee joint. Slice thickness of vertebral CT-images is 4 mm, while slice thickness of tibial pQCT images is 2 mm. In order to compare the bones' structure from the tibial CT-images with the structure of the lumbar vertebrae from CT-images, one set of tibial CT-images has been obtained with a slice thickness of 4 mm. Next, in order to perform quantitative comparison of the CT- and pQCT-images of proximal tibiae, another set of tibial CT-images with slice thickness of 2 mm has

been acquired. The entire set of the CT- and pQCT-images obtained *in vivo* from one test person is shown in Figure 13. To the date of the report four test persons were examined on the CT-machine and five volunteers were examined with the pQCT-scanner.

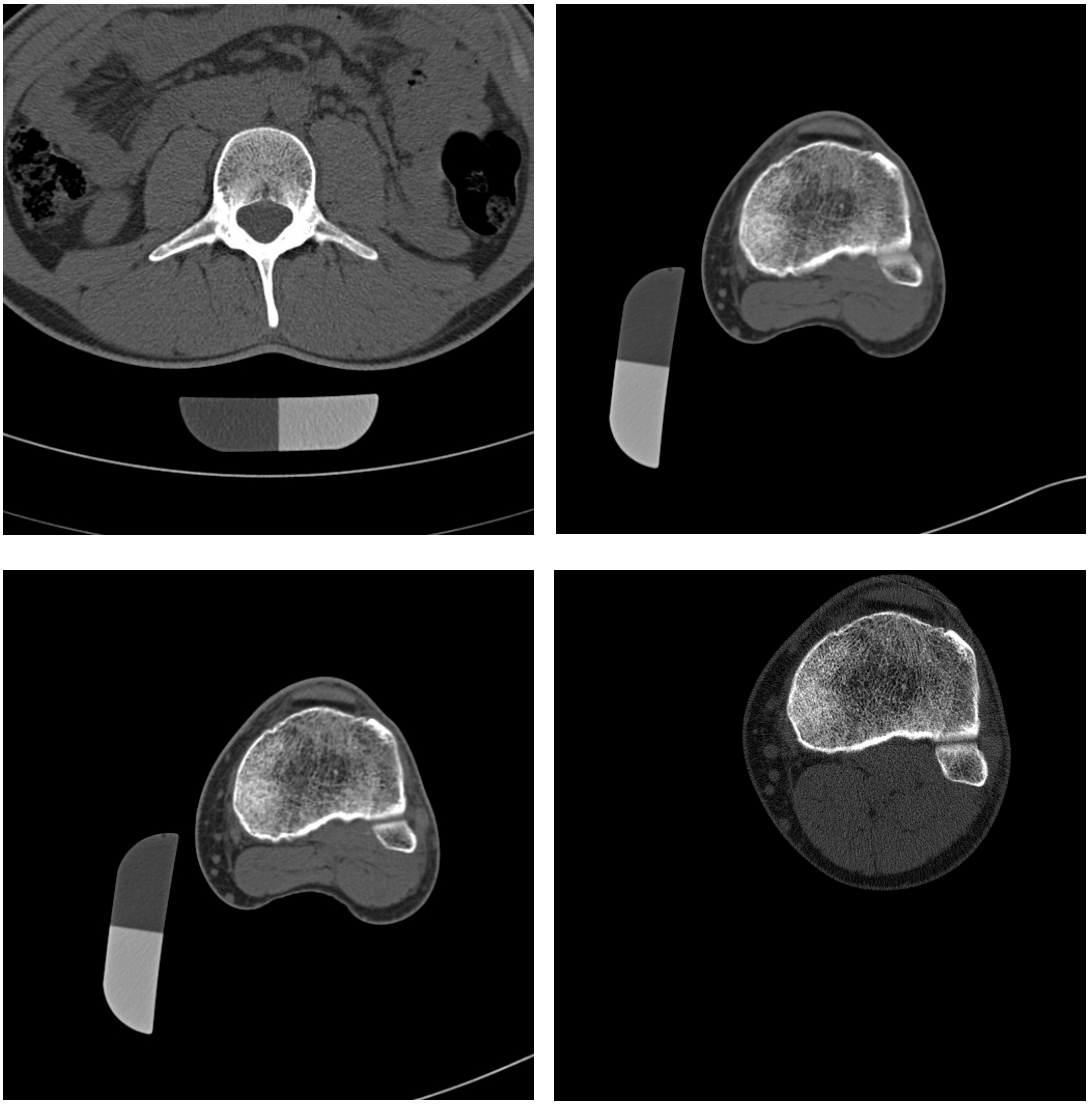

Figure 13. A set of CT- and pQCT-images obtained *in vivo* from the same test person. *Top left:* CT-image of lumbar vertebral L3, slice thickness 4 mm. *Top right:* CT-image of proximal tibia, slice thickness 4 mm. *Bottom left:* CT-image of proximal tibia, slice thickness 2 mm. *Bottom right:* pQCT-slice through the same region of proximal tibia, slice thickness 2 mm.

4.4.5.1 Signal-to-noise ratio in the images acquired *in vivo*

The linear signal-to-noise ratio (SNR) in different regions of different images has been estimated. The SNR in the vertebral CT-images (3.2 in trabecular bone area) is much lower than in the tibial CT-images (9.8 and 8.8 in trabecular bone area of 4 mm and 2 mm thick slices correspondingly) due to the large amount of soft and connective tissue surrounding the vertebrae. The lowest SNR = 2.4 was found in the trabecular bone area of the pQCT images. The pQCT-scanner is a low radiation device, and, as it is known, smaller radiation dose means higher level of noise distortion.

In order to perform analysis of the bone structure from pQCT tibial images acquired *in vivo*, it is necessary to separate the bone architecture from the underlying noise fluctuations. Thus, a noise reduction algorithm must be applied. As we found in the first phase of the project, an

effective noise reduction algorithm for pQCT-images is Adaptive Smoothing Based on Local Statistics (SLS). After the SLS noise reduction is applied, the SNR in pQCT images increases more than two times. All results reported below are obtained after the application of this noise reduction algorithm.

4.4.5.2 Evaluation of complexity of vertebral and tibial bone architecture from CT-images acquired *in vivo*

Analysis of complexity of **vertebral bone architecture** *in vivo* revealed the differences in structural organization of normal bones. The two younger individuals B and C have higher values of their vertebral BMDs; the complexity of their vertebral architectures is 2.6 times higher than the complexity found in the older individual A with a lower BMD. The Maximal L-block, which assesses the area between the trabeculae, has almost the same low value for the two younger volunteers B and C. This measure is 3.3 times higher for test person A. Despite the large differences in complexity, the TNI difference between all test persons is less than 40%. In general, no discordance in the behaviour of the structural measures and BMD was found in the analysis of vertebral CT-images.

The bone structure-bone density diagrams for trabecular bone of **proximal tibia** obtained from the CT-images of slice thickness of 2 mm (pixel size 445 µm) and 4 mm (pixel size 445 µm and 390 µm) reveal very interesting differences in the behaviour of the BMD and the structural measures. For person A, despite a low BMD value, the complexity of the bone architecture is almost as high as the structural complexity of bone D, which has the highest BMD. The SCI is 30% higher than expected for a bone with such a low BMD value. The difference in structural composition of this bone is captured and quantified by all others structural measures: TNI is 20% higher, IGE is 65% higher, and L-block measures are 1.5–3 times lower than expected for the bone of such a low BMD. The degree of disorder (SDI) within the architecture is even smaller than what is found in the bones with higher BMD values. In proximal tibiae the results of the entire bone evaluation confirm all findings we made by analyzing the trabecular bone alone. In particular, despite the low BMD value in the proximal tibia of individual A, the complexity of its architecture is maximal and its degree of disorder is minimal among all analyzed subjects when the entire bone slice is analyzed.

4.4.5.3 Evaluation of bone architecture from pQCT tibial images acquired *in vivo*

The same six healthy volunteers have been measured with the pQCT scanner. The evaluation of the bone structure from pQCT tibial images acquired *in vivo* confirms all the conclusion we made in regards of the special structural properties of the proximal tibia of test person A based in CT-images. Despite the lower BMD value, the structure of this bone is assessed by the structural measures as being close to normal. The pQCT-based structural measures provide the same ranking of the bone architectures as the measures obtained from CT-images. Only L-block based measures derived from pQCT- and CT-image rank the bones with intermediate BMD in a slightly different way. As these measures quantify the organization of inter-trabecular regions, they are the measures that are most affected by the differences in depiction of bone elements by CT- and pQCT-scanners.

4.4.5.3 Summary

Summary of the results obtained by the evaluation of CT- and pQCT-images acquired *in vivo* from healthy volunteers: The developed technique is able to quantify the bone structure from CT- and pQCT-images taken *in vivo*.

- The structural composition of bones images obtained from healthy individuals can be differentiated.

- The evaluation of vertebrae and tibiae results in different ranking of bones by the structural measures and the BMD as well.
- The evaluation of tibial CT-images of different slice thicknesses and pQCT-images provides similar conclusion about bone structure in different individuals.
- The structural measures of complexity and the BMD provide different information about the bone and rank analyzed tibia by their status in a different way. The evaluation of the pQCT tibial images confirms the discordance in the ranking of bones by their structural status found in the appropriate CT-images.

In addition, L3 and proximal tibia of stroke patients (hemiplegic or paraplegic), patients with a fracture of upper or lower limb, and patients with a rupture of a ligament at the lower limb will be investigated in a longitudinal study with the proposed method. CT-scans will be performed at baseline (trauma), and again 3 and 6 months after baseline.

4.4.6 Recommended procedure for bone status assessment for space-flying personnel and for patients on Earth

Based on our investigations we find that the most appropriate procedure for bone status assessment for space-flying personnel and for patients on Earth includes examination of the lumbar spine and the proximal tibia. Examination of the axial skeleton at the lumbar spine by QCT is already the "gold standard" for bone density assessment. Importantly, the developed evaluation of the bone structure uses the same images as the BMD assessment, which therefore does not require additional radiation exposure. By combining the BMD evaluation with an evaluation of the structural composition we achieve the utmost outcome of this non-invasive procedure.

The lower extremities experience the largest changes in bone status during exposure to microgravity (Vico et al., 2000) and it is therefore essential to quantify the skeletal changes. The proximal tibia has a very rich trabecular network which is similar in its behaviour to the vertebral body and is easily accessible. Similar to the lumbar vertebra both the density and the structural composition are to be evaluated at this skeletal site. By comparing the outcome of the axial skeletal examination with the peripheral skeletal examination, we will be able to determine any discordance between these two skeletal sites in their response to microgravity exposure. Such a discrepancy is important for the design and evaluation of individual countermeasures.

Our recommendation for bone status assessment of space-flying personnel is an examination procedure that requires a non-invasive radiological procedure before space flight and after return to Earth. CT-images of the lumbar vertebra L3 and CT- or pQCT-images of the proximal tibia about 17 mm below the knee joint of one leg shall be acquired. The image analysis program includes bone mineral density measurements and the quantification of the architectural composition of the bone regions by measures of complexity. The image acquisition requires keeping certain acquisition parameters constant. The method is standardized.

The team concludes that the proposed method can assess bone status, quantify structural differences in bone architecture, and can be used as a predictor for vertebral bone strength in a non-invasive and non-destructive manner.

4.5 3D Structural Analysis with Measures of Complexity

The rapid improvement in the resolution of 3D μCT scanners has made it possible to perform investigations of the 3D micro-architecture of bone. This have let to an increasing need for measures that are able to quantify the bone structure in 3D data sets obtained with μCT scanners. Initially, the traditional 2D methods were transferred into 3D (Ito et al., 1998), but also a few "true" 3D methods have been suggested (Hildebrand & Rüegsegger 1997a; Hildebrand & Rüegsegger 1997b).

4.5.1 Measures based on symbol-encoding

The symbol-encoding algorithm described in Section 4.4 was modified so that it could be applied to 3D images. Only three different types of symbols representing either soft tissue, internal bone, or surface bone voxels were used to encode the trabecular network. The spatial distributions of local relationships between these symbols within the encoded 3D architecture form the foundation for the structural complexity measures (Saparin et al., 2005b):

- 3D Normalized Entropy S_n of geometrical locations of bone tissue,
- Structure Complexity Index, $SCI_{BV/TV}$, based on bone volume fraction,
- 3D Structure Complexity Index, SCI_{3D},
- Surface Complexity Index (SurfCI) and Surface Index of Global Ensemble (SurfIGE).

Using this method it was shown quantitatively that the complexity of the 3D bone architecture decreases concomitantly with decreasing bone density (Saparin et al., 2005b), which corroborates the findings of the 2D method (Section 4.4). Both the 2D and the 3D approaches confirmed that the complexity of the trabecular bone architecture is higher in proximal tibia than in the lumbar vertebra.

Correlation coefficients for the relationships between the symbol-encoding based 3D structural measures, histomorphometric measures, and bone strength σ_{max} are summarized in Table 4. Furthermore, a multiple regression analysis with bone strength as the dependent variable and the various measures of complexity as independent variables resulted in a correlation coefficient of $r = 0.89$.

	BV/TV	$V^*_{m.space}$	$V^*_{b.space}$	Tb.Th	Tb.N	Tb.Sp	Nd/Tm	TBPf	CD	σ_{max}
SCI_{3D}	0.91	-0.83		0.52	0.93	-0.93	0.74	-0.71	0.62	0.75
$SCI_{BV/TV}$	0.92	-0.87		0.51	0.95	-0.95	0.75	-0.72	0.66	0.73
SurfIGE	-0.76		-0.51	-0.76			-0.75	0.72		
SurfCI	0.78	-0.50		0.57	0.58	-0.72	0.51	-0.55	0.50	0.79
S_n	0.71	-0.87			0.82	-0.83			0.77	0.54

Table 4. Spearman's rank correlation coefficients between the symbol encoding based measures of complexity and histomorphometric measures as well as bone strength σ_{max} for lumbar vertebrae L4. Significance level: $p \leq 0.01$. Coefficients with lower levels of significance have been omitted.

4.5.2 Measures based on precise definition of bone surface and its curvatures

As a novel approach the team introduced a series of tools for analyzing the bone structure based on local evaluations of the 3D shape of the trabeculae. This idea is based on the fact

that different 3D objects of a given volume will have different surface areas, depending on their geometrical shape. For example, a long cylinder (length is much larger than radius) has a larger surface than a cube of the same volume. A sphere is the 3D object that has the smallest possible surface for a given volume. The relationship between the bone surface area and bone volume is locally determined in a small cubic window, which moves through the entire bone. This concept is used for defining several new shape-based structural measures:

- Global Shape Index (SHI_{global}) measures the ratio between entire volume and surface of the whole test object;
- Averaged Shape Index (ASHI) characterizes the mean shape of the trabecular structures. It is able to distinguish rod-like from plate-like structures, and convex from concave structures;
- Shape Complexity (SHC),
- Shape Entropy (SHE) and Shape Mutual Information (MISH) are able to quantify the variety of different shapes.

The most commonly used method for finding the bone volume is to count the bone voxels. However, a more accurate way is to apply an iso-surface algorithm to the 3D bone data, and then determine the bone volume from the iso-surface. The iso-surface algorithm is based on a subset of eight neighbouring voxels, which are arranged at the corners of a cube (Figure 14; Lorensen & Cline, 1987; Marwan et al., 2005). Such a cube is called a marching cube (MC) and forms the backbone of various iso-surface algorithms for visualization/rendering of 3D objects. If two neighbouring voxels of a MC are arranged so that one voxel has a value below and the other above a predefined threshold (i.e. one represents bone and the other marrow), the iso-surface will lie between these voxels. The iso-surface is constructed by a set of triangles, and the surface estimation is given by the sum of the areas of these triangles. The bone volume within the MC is filled with tetrahedrons in such a way, that the resulting surface is identical to the surface formed by the triangles (Figure 14). The sum of the volumes of these tetrahedrons is the estimated bone volume found in the MC.

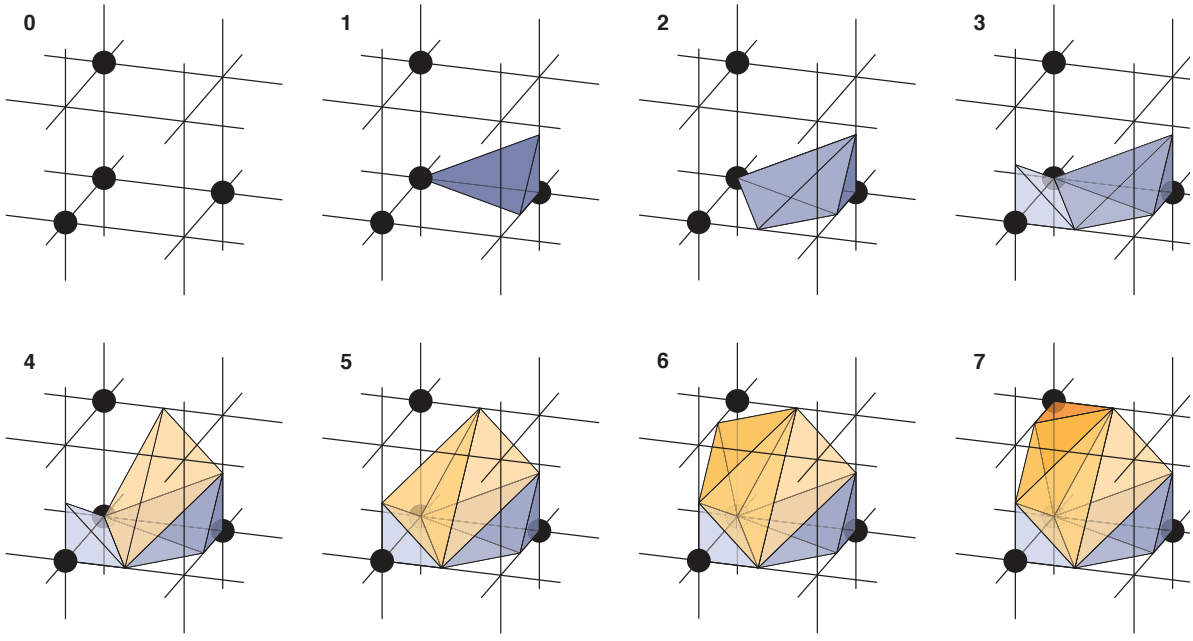

Figure 14. A marching cube consists of eight neighbouring voxels, arranged at the corners of the cube. By filling the MC with tetrahedrons, the volume can be better estimated than by counting bone voxels. Moreover, the distinct MC configurations (see text) were used to introduce a new set of 3-D measures of complexity.

Furthermore, depending on the position of the bone voxels in a MC and by taking rotational symmetry into consideration, there are only 21 unique possible MC cases. Each MC case represents a specific bone surface configuration. Therefore, the distribution of MC cases can be used for defining structural measures of complexity. Consequently, the team developed

- the Marching Cubes Entropy Index (MCE) and
- the Marching Cubes Complexity (MCC), which quantifies the complexity of the bone surface.

All these new measures are used for the assessment of structural differences in 3D trabecular bone architecture of the proximal tibia bone biopsies and the entire vertebrae (Section 4.1.5). Standardized volumes of interest (VOI) were applied to the µCT images for quantification of the 3D architecture.

The VOI for the proximal tibial biopsies was a 10-mm-long cylinder with a diameter of 6 mm and located 5 mm below the cortical shell. The diameter of the tibial VOI was set smaller than the diameter of the biopsy in order to exclude drilling residue left from the coring drill (trephine). The VOIs for the vertebrae were based on the 2D pQCT ROIs calculated for the mid-axial vertebral slices (Figure 2). For each pQCT ROI the symmetry axis and the centre of

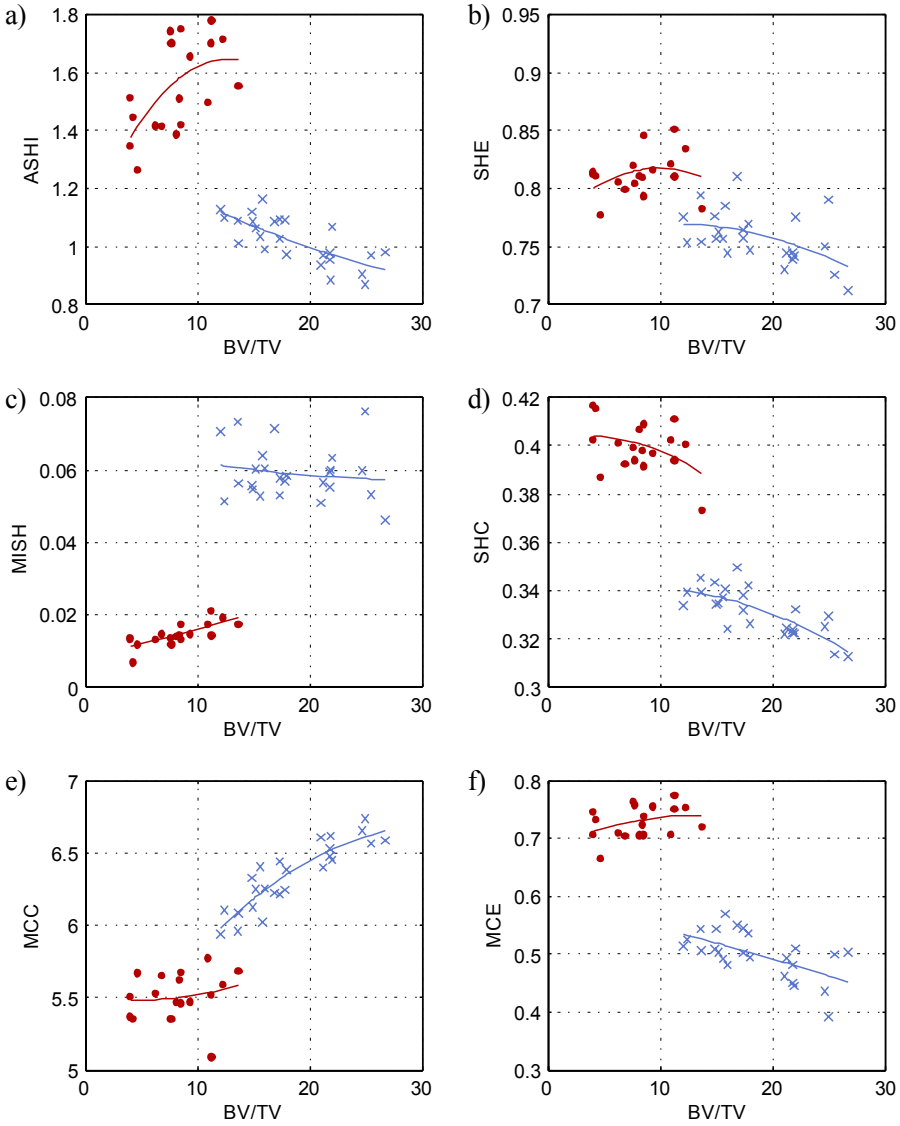

Figure 15. The relation between the 3D complexity measures based MC algorithm and shape index and the bone volume fraction BV/TV calculated for the trabecular bone of the proximal tibiae *(blue)* and the lumbar vertebrae L4 *(red)*: averaged ahape index *(A)*, shape index entropy *(B)*, shape mutual information *(C)*, shape complexity *(D)*, marching cube complexity *(E)*, and marching cube entropy *(F)*. A clear structural difference between the two skeletal sites is due to the occurrence of more concave structures at the proximal tibia.

the vertebra were marked automatically by the 2D segmentation procedure (Saparin et. al., 2005c). The 3D vertebral VOI was a 10 mm high 25 mm × 15 mm cuboid, which was extended in both directions from the central axial slice. The position and the height of the VOI were selected so that it would match the position and slice thickness of a standard QCT-image. The centre of the VOI was located on the left-right symmetry line and the center was shifted 4.5 mm backwards from the centre of the vertebra. The structural measures of complexity based on symbolic dynamics, curvatures, shape, and marching cubes were then computed from these VOIs (Figure 15).

The application of the 3D shape-index-based measures on the two different skeletal sites reveals that the trabecular structure is different at these two sites. The relationship between ASHI and bone volume fraction BV/TV is different at the lumbar vertebra and the proximal tibia (Figure 15A). Moreover, at the proximal tibia there were values of ASHI less than 1.0, which indicate more concave than convex structures. In contrast, at the lumbar vertebra ASHI was greater than 1.4, which indicates more convex than concave structures. In addition it is characteristic that, ASHI decreases with decreasing bone volume fraction for tibial bone, whereas ASHI increases for decreasing bone volume fraction for vertebral bone. This indicates a decreasing of amount of plate-like structures, as plate-like structures have a higher ASHI than rod-like structures. Such differences in the architecture of the two skeletal sites were also seen for most of the other 3D complexity measures (Figure 15).

This result is also confirmed by the calculations of the total curvature K. The total curvature is negative for all tibial biopsies, whereas it is positive for the majority of the lumbar vertebrae (Figure 16). Mean and total curvature reveal similar relationship for tibial and vertebral bone: H and K increased with decreasing BV/TV and Tb.Th (Figure 16). For both the proximal tibia and the lumbar vertebra, mean and total curvature revealed similar relationship: the values of H and K increased with decreasing BV/TV and Tb.Th (Figure 16). It was found that both K and H are less sensitive to the differences in bone architecture than the proposed ASHI.

The shape complexity index SHC and the marching cube complexity MCC exhibit similar behaviors for both skeletal locations (Figure 15 D, E). Moreover, a strong relationship ($r = -0.88$) was found between the MCC and the TBPf. In the first phase of the project we

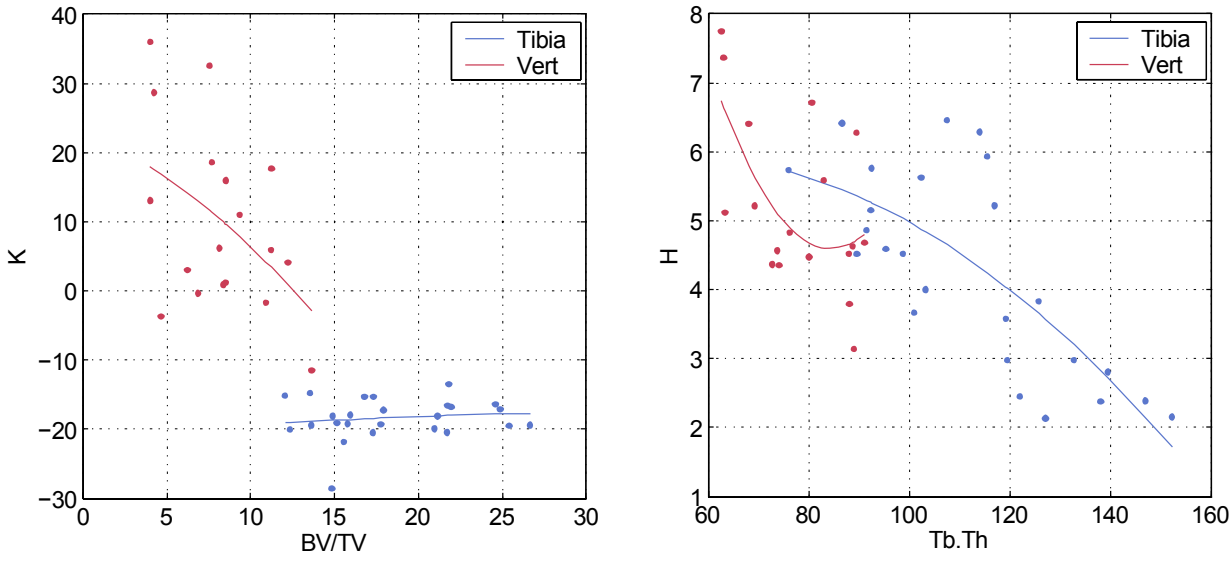

Figure 16. The relation between the total curvature K and BV/TV *(left)* and the mean curvature H and the Tb.Th *(right)* calculated for proximal tibia *(blue)* and lumbar vertebra L4 *(red)*.

showed a very strong relationship between TBPf and structure modeling index (SMI) (Thomsen et al., 2005a). Since SMI quantify the balance between rod-like and plate-like trabeculae, it would be fair to assume that MCC also exhibit such ability.

A comparison of the newly developed measures with histomorphometry reveals good or high correlations between the 3D structural measures and the appropriate histomorphometric measures. The correlations between the 3D complexity measures and the histomorphometric measures are summarized in Tables 5 and 6.

Finally, the 3D measures of complexity of the lumbar vertebrae were compared with the results of the compression tests (Section 4.3). Good correlations were found between compressive bone strength σ_{max} and mean curvature H, MISH, and MCE. A multiple regression analysis with bone strength as the dependent variable and SHI_{global}, ASHI, SHE, MISH, SHC, MCC, H, and K as independent variables revealed a correlation coefficient of

	BV/TV	$V^*_{m.space}$	$V^*_{b.space}$	Tb.Th	Tb.N	Tb.Sp	Nd/Tm	TBPf	CD
SHI_{global}									
ASHI	-0.74		-0.50	-0.74		0.50	-0.68	0.66	
SHE		0.51			-0.50	0.51			
MISH									-0.55
SHC	-0.72	0.60		-0.57	-0.57	0.66	-0.63	0.63	
MCC	0.87	-0.53		0.74		-0.68	0.86	-0.88	
MCE	-0.57			-0.54			-0.70	0.67	
H	-0.89	0.62		-0.72	-0.58	0.74	-0.88	0.90	
K									-0.60

Table 5. Spearman's rank correlation between the MC based measures of complexity and histomorphometric measures obtained for proximal tibia biopsies. Significance level: $p \leq 0.01$. Coefficients with a lower significance level have been omitted.

	BV/TV	$V^*_{m.space}$	$V^*_{b.space}$	Tb.Th	Tb.N	Tb.Sp	Nd/Tm	TBPf	CD	σ_{max}
SHI_{global}	0.50	-0.72			0.65	-0.65				
ASHI	0.50	-0.70			0.62	-0.63			0.67	
SHE										
MISH	0.76	-0.69			0.80	-0.80	0.78	-0.76		0.75
SHC										
MCC										
MCE	0.91	-0.84		0.51	0.92	-0.93	0.74	-0.72		0.71
H	-0.53						-0.52			-0.70
K										-0.58

Table 6. Spearman's rank correlation between the MC based measures of complexity, histomorphometric measures, and bone strength σ_{max} obtained for lumbar vertebrae L4. Significance level: $p \leq 0.01$. Coefficients with a lower significance level have been omitted.

$r = 0.91$. This indicates that these measures of complexity can explain 83% of the variation in vertebral bone strength. It can be inferred that strong bones are in general related with more homogeneous bone, higher complexity of the bone surface, thicker trabeculae, and well connected trabecular bone.

Based on data from the present study we conclude that the 3D structural measures are able to assess different aspects of the bone structure and quantify its architectural differences by evaluation of 3D μCT data sets. They provide a nonlinear holistic quantification of the amount, distribution, shape, connectivity, and structural complexity of trabecular architecture. The developed technique is able to quantify alterations in bone architecture and may help to diagnose and monitor changes in bone structure of patients on Earth as well as of space-flying personnel. It is agreed that the project team will have access to 3D bone imaging data of astronauts at the end of 2005 so that the method can be tested on data from space-flying personnel.

4.5.3 Recurrence Plots

The concept of quantifying recurrences in the trabecular bone structure was also studied in the project. An extension of the recurrence analysis from 1D to 2D and 3D was developed. This analysis enables us to quantify the amount of recurrences and to asses the size of the recurrent structures of spatial data. For this purpose, the following measures were introduced:

- Recurrence Rate (RR), which quantify the amount of spatial recurrences;
- Determinism (DET) and
- Laminarity (LAM), both quantify the amount of extended recurrent structures;
- Mean Diagonals Length (MDL) and
- Trapping Time (TT), both quantify the size of the extended recurrent structures.

The spatial recurrence analysis applied to 25 2D pQCT images of human proximal tibia with trabecular BMD covering the range from 30 to 150 mg/cm^3 (the data are described in Section 4.4.2). The recurrence analysis reveals a clear relationship between the amount of recurrences in 2D pQCT images and the stage of osteoporosis. Strong negative rank correlation ($r = -0.93$) was found between the RR and the BMD. The DET and LAM are related to the BMD (Figure 17) with rank correlation coefficients of $r = -0.66$ and $r = -0.79$, respectively. No significant correlations were found between the MDL, TT, and BMD.

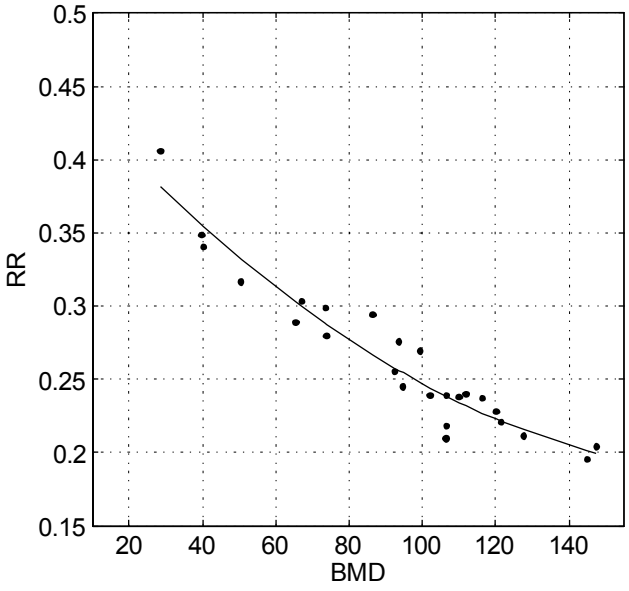

Figure 17. The relationship between the recurrence rate RR and the BMD calculated from pQCT images acquired at the proximal tibiae.

These results indicate that osteoporotic (low BMD) bone contains more recurrent structures than normal (high BMD) bone. The relationship between the recurrence measures and the BMD is non-linear with the curve reaching its highest slop for low BMD values. This finding is in good agreement with the findings reported in Sections 4.4 and 4.5.2 that 2D and 3D complexity decreases with decreasing BMD.

4.5.4 Comparison and synthesis of 2D and 3D results

The results of the analysis of 3D μCT images were compared with the results obtained from the 2D pQCT images. This comparison was preformed for 2D measures of complexity based on symbol encoding and the 3D measures of complexity based on symbol encoding, shape index, and curvatures calculated for proximal tibiae as well as for lumbar vertebrae.

Comparing the measures which evaluate the amount of bone material, a very good linear correlation ($r > 0.9$) was found between the histomorphometric BV/TV, 3D BV/TV, and the BMD for the proximal tibia as well as for the lumbar vertebra. This verify the established standardized procedure for defining ROIs in 2D CT-images, histological sections, and VOIs in 3D data sets.

Structural measures of complexity derived from both 2D and 3D data are in very good agreement and confirm quantitatively that the complexity of the bone architecture decreases with decreasing bone density. The 2D and the 3D approaches both showed that the complexity of the trabecular bone architecture is higher at the proximal tibia than at the lumbar vertebra. The rank correlations coefficients between the appropriate symbol-encoding based 2D and 3D measures are in the $r = 0.75–0.78$ range for proximal tibiae and 0.79–0.86 range for lumbar vertebrae. The reason why the correlations coefficients were lower for the proximal tibiae than for the vertebral bodies may be related to the VOIs used for the 3D analyses (the biopsies) covered a much smaller part of the tibia than the ROIs used for the 2D analyses. Nevertheless, all 2D and 3D approaches exhibit similar relationships between architectural properties and bone density for the investigated specimens.

In contrast, the correlation between the 3D measures based on the MC algorithm and the 2D measures based on symbol encoding is much lower ($|r| = 0.64–0.8$). This is due to the MC algorithm providing a much better defined bone surfaces than the 2D symbol encoded method, which – due to the large pixel size – defines the individual trabecular surfaces so poorly that it is unable to quantify information relating to trabecular thickness (see Section 4.4.2 for details). At the lumbar vertebra the highest correlation coefficients ($|r| \approx 0.7$) were found between ASHI and Mean L-Block, between MISH and SCI, and between MISH and S_a. At the proximal tibia the highest correlations were established between the MCC and SCI, TNI, and S_a ($r = 0.75$, 0.72, and 0.8).

We conclude that the complexity measures based on the MC algorithm and the shape index reveal new structural information in addition that obtained by the 2D measures. The main reason being that information about the thickness, shape, and curvature of the trabeculae cannot be derived from the 2D images. Both the developed 2D and 3D approaches can be used to assess the bone architecture and the differences between the structures of two bone samples. Which technique to use in a given situation depends on a series of considerations including the skeletal location, availability of scanner equipment, acceptable radiation dose, or possibility to extract a bone biopsy.

4.6 3D Visualization and Analysis of Large Data Sets. Fractures and 3D Vertebral Architecture

During the project, the team obtained a large collection of 3D μCT data sets acquired from vertebral bodies. The data acquisition was excellently performed by the industrial partner Scanco Medical AG. Entire vertebral bodies were μCT-scanned before and after compression testing to failure (Section 4.3) at a voxel size of 38 μm. The size of the acquired 3D images was 2048 × 2048 × 1000 voxels at 2 Bytes, resulting in roughly 8 GB of data per vertebral specimen. Nearly 100 of such data sets were acquired and transferred to the project server.

4.6.1 Dealing with large volume data sets

In order to work with such large data sets two fundamental limits have to be dealt with. Firstly, the amount of main computer memory (RAM) available to an application is limited by the number of address bits used by the processor. Until recently, commonly available computer hardware provided only 32 bits addressing. This hardware constrain fundamentally limits the amount of main memory, which is directly accessible by an application, to 4 GB. Therefore, the size of a 3D image data set that could be loaded at once into the computer main memory was limited to approximately $1000^3 = 10^9$ voxels. During the period of the project, computer processors with 64 bit addressing have become commonly available. The 64 bit address space allows allocating up to $1.000.000^3 = 10^{18}$ voxels in RAM as illustrated in Figure 18. In collaboration with our industrial partner Mercury Computer Systems, the visualization system Amira (Stalling et al., 2005) was extended to support 64 bit addressing. The size of image data that can be loaded at once is now (and in the foreseeable future) only limited by the amount of available physical memory.

Secondly, in most cases the data size exceeds the size of available computer RAM. Thus, only subsets of the data can be transferred to the computer main memory; the larger part stays on the hard disk. Algorithms and data structures must be adapted to deal with this situation (Vitter, 2001). In addition, administrative tasks such as data organization and backup become tedious. Thus, it was decided to store the μCT data sets centrally in a data repository at one institution (ZIB) only. A software layer was introduced, which allows handling data at various file formats. The freely available HDF5 (http://hdf.ncsa.uiuc.edu/HDF5) file format was chosen as the optimal storage format for large data sets. Using HDF5 the 3D image data are stored using a hierarchical representation in order to facilitate fast access to low resolution overviews and to provide access at the required level of details. The corresponding high-level software architecture was developed as shown in Figure 19. The visualization methods were extended to allow remote access and handling of data exceeding the size of available computer main memory. The entire vertebral bodies could thereby be visualized, including their trabecular structure (Figure 20). Sub-volumes can be selected interactively for further analysis. The other team institutions have efficient access to the data via the Internet (Prohaska et al., 2004).

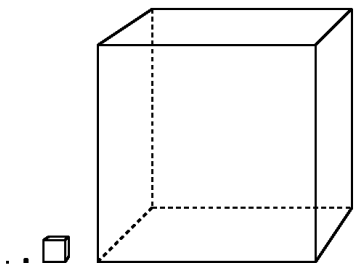

Figure 18. Comparison of 32 bit address space and 64 bit address space. Displayed are four boxes which represent 3D data volumes. The large box to the right is a volume that could be accessed with 64 bits. To the left are three boxes, scaled to 10%, 1% and 0.1% of size. The leftmost, almost invisible dot, illustrates the size of a volume, true to the right scale, that can be allocated with 32 bit addressing.

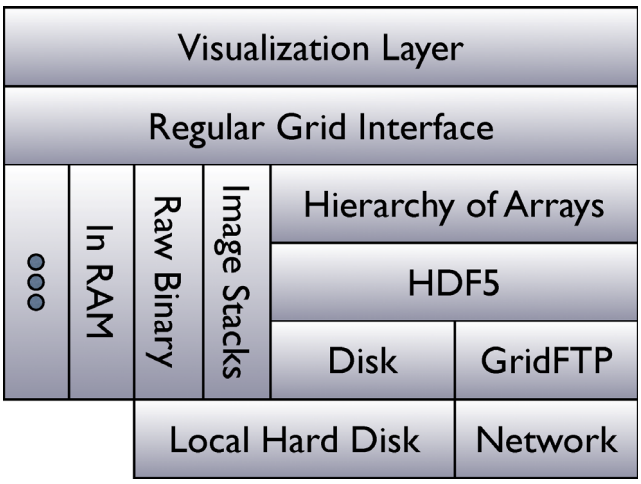

Figure 19. High-level software design. The Visualization Layer accesses data through the Regular Grid Interface. Legacy code (Image Stacks, Raw Binary, in RAM) is wrapped to be accessible through this interface. Newly implemented was a Hierarchy of Arrays stored in HDF5, which uses virtual file drivers, Disk or GridFTP, to access the data on the Local Hard Disk or via a Network.

Figure 20. 3D volume rendering of an entire vertebral body and its trabecular structure (voxel size 38 µm).

4.6.2 Visual analysis of trabecular bone architecture

A major goal of the project was to match and compare images from different sources for validation and to facilitate the development of new assessment methods. Interactive visualization for exploration and identification of sub-volumes for further detailed analysis was considered crucial. An efficient visualization algorithm for central surfaces (skeletons) of the trabecular structure (Prohaska & Hege, 2002) was developed (Figure 21). These facilities are now available as extensions to the commercial version of Amira. The algorithm was extended to allow processing of data exceeding the size of main memory. Therefore, it is now possible to compute skeletons of entire vertebral bodies. However, due to the complexity of the resulting structure, only parts of these skeletons can be loaded and displayed at full resolution. The examples are displayed in Figure 22.

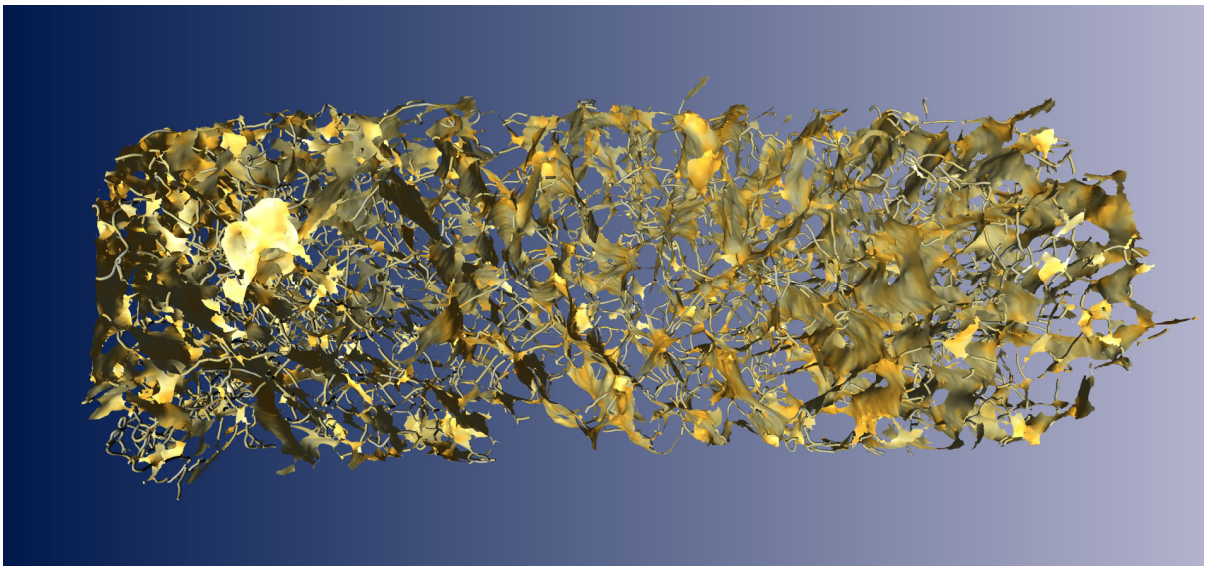

Figure 21. 3D rendering of the skeleton of a proximal tibia biopsy (diameter: 7 mm, length: ≈25 mm). Rod-like structures are rendered as lines, plate-like structures are represented as central surfaces. The thickness of the structure is colour-coded as saturation.

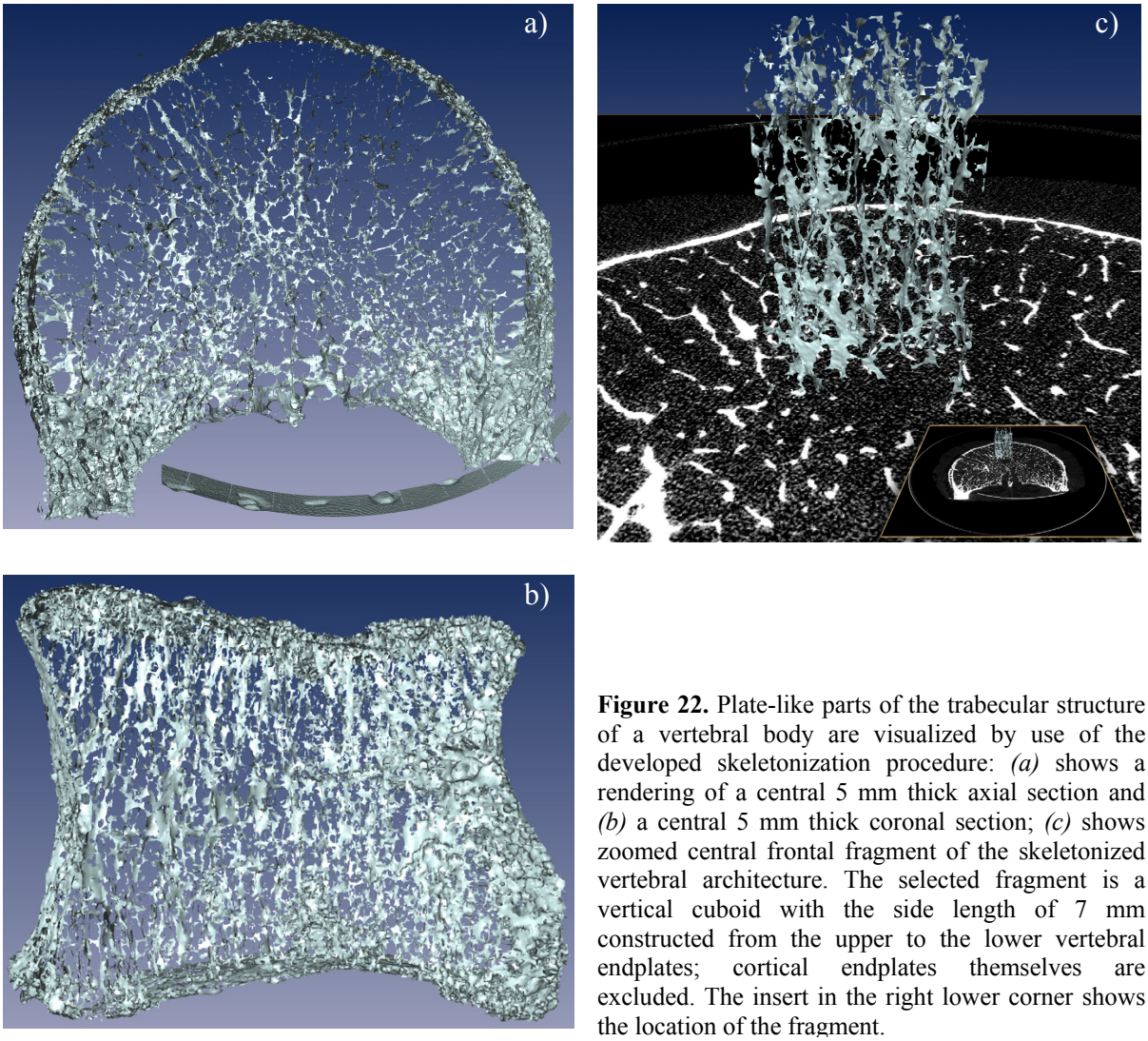

Figure 22. Plate-like parts of the trabecular structure of a vertebral body are visualized by use of the developed skeletonization procedure: *(a)* shows a rendering of a central 5 mm thick axial section and *(b)* a central 5 mm thick coronal section; *(c)* shows zoomed central frontal fragment of the skeletonized vertebral architecture. The selected fragment is a vertical cuboid with the side length of 7 mm constructed from the upper to the lower vertebral endplates; cortical endplates themselves are excluded. The insert in the right lower corner shows the location of the fragment.

4.6.3 Vertebral structure before and after compression tests

Comparison of the trabecular micro-architecture of vertebral bodies before and after compression testing (Section 4.3) is ongoing research undertaken by the project team in addition to the original project proposal. During the project a preliminary manual procedure for performing such comparisons of µCT data sets was established. Matching reference points (landmarks) are selected in the scans and utilized to semi-automatically place the scans in a common coordinate system (Figure 23). The two structures may then be manually compared. Sub-volumes can be selected and any of the visualization techniques available in Amira can be applied including volume rendering, iso-surfaces, or slicing. This comparison is supported through highlighting regions containing changes in the trabecular structure detected by various approaches. The distance between the surfaces of the trabecular structures (Figure 24) and the voxel based difference in the µCT data sets were successfully used by the project team to detect vertebral micro-fractures (Figure 25).

This procedure is the foundation for further research and will be further developed as described in the new MAP proposal (Section 5). Classifying changes in the microscopic structure and deriving a representation summarizing the overall change of the vertebrae are short-term goals. Development of a fully automated procedure is one of our long-term goals as outlined in the next MAP proposal.

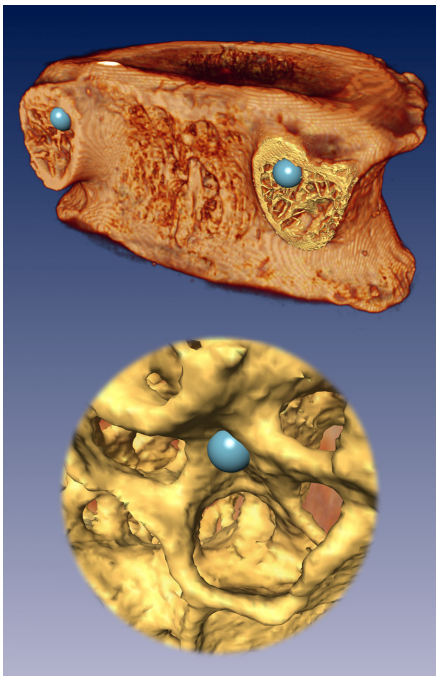

Figure 23. Manually selected reference points are utilized in order to place two µCT-scans in a common coordinate system semi-automatically. The anatomical features of the vertebra or distinctive trabecular formations are used to select the reference points.

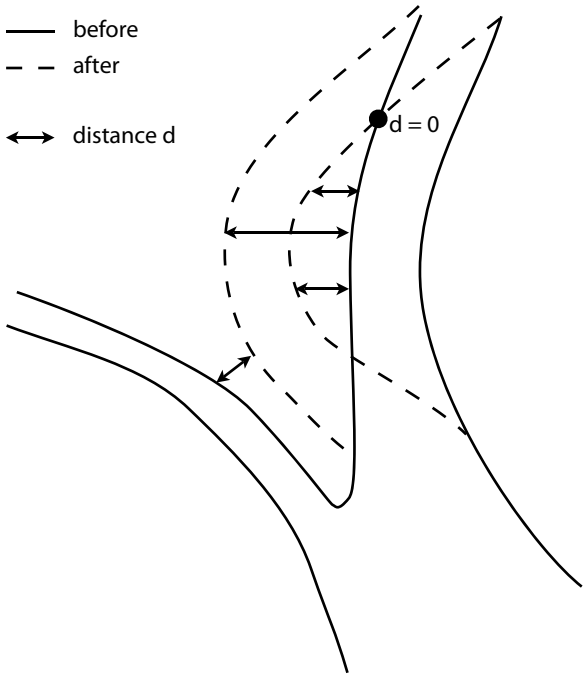

Figure 24. The Euclidian distances *d* between surfaces of the same trabecula before and after compression testing were calculated. Large distances reveal the deformations. Note that the distance measurement may fail at few places if a bone surface moved closer to another non-related surface as indicated by $d = 0$ in the image.

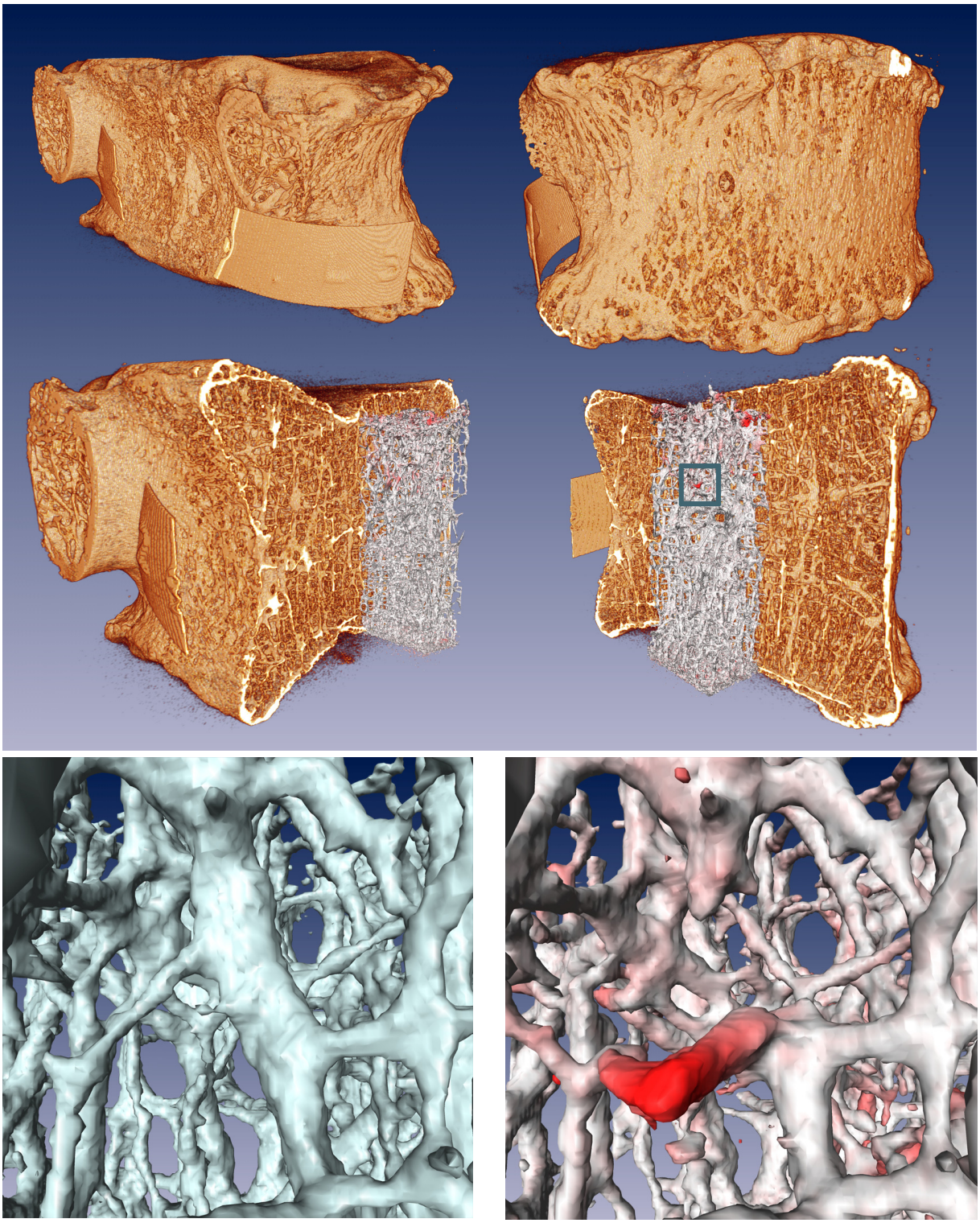

Figure 25. Micro-fracture of the trabecular network in a vertebral body L3 before and after biomechanical compression test. Different views of the entire vertebral volume are displayed at the top. The trabecular structure before *(down, left)* and after *(down, right)* failure load testing is displayed in the bottom row. Structural changes are highlighted in red. A micro-fracture is located in the centre of the right image. The fracture detection procedure is based on the calculation of surface distances.

4.7 Simulation of Bone Remodelling

Living bone is continuously remodelled by specialized cells. The remodelling process is characterized by an intriguing duality concerning the mechanical performance of bone (Heaney, 2003): Bone remodelling has a long term positive effect since it removes microdamages from the bone and fatigue fractures are therefore avoided. On the other hand, the ongoing remodelling process itself is a source of trabecular structural weakness due to the resorption cavities. Not only the bone architecture, but also the turnover rate is thought to play a key role in determining the mechanical quality of bone. This demonstrates the importance of a dynamic view on bone. The dynamics of bone modelling and remodelling is the source for adaptive abilities of the bone tissue to changing loading conditions.

This is further corroborated by the fact that the remodelling process is mechanically controlled, which allows bone to adapt to changes in its loading pattern. The so-called Wolff-Roux law states that bone is removed where mechanically not needed and deposited where the local loading is high (Hart, 2001). This principle is realized by several cellular and biochemical feedback mechanisms. For all the current difficulties of experiments with living animals and human beings and the unclear significance of in vitro experiments, computer models have been successfully used to test and extend our understanding of the remodelling process.

As a first step, we have developed several simplified algorithms to simulate bone loss using 2D (Zaikin et al., 2003, 2005) and 3D CT images (Zaikin et al., 2005). The aim was to extrapolate and predict the bone loss and to provide test objects for the measures of complexity. We developed and tested a threshold algorithm and a virtual slicing algorithm for 2D images. The threshold algorithm simulates bone resorption on the boundary between bone and marrow, representing activity of osteoclasts. The virtual slicing algorithm uses a distribution of the bone material between several virtually created slices to achieve statistically correct results when the bone-marrow transition is not clearly defined. For 3D data, a variation of the threshold algorithm was developed and applied to μCT data. The results of modelling were compared with real CT images using structural measures of complexity in 2D and 3D (Zaikin et al., 2005).

Implementing a specific formulation of the Wolff-Roux law in a computer model and by the use of finite element methods, it was demonstrated that an optimized trabecular architecture emerges, which is maintained and adapts to varying loads (Ruimerman et al., 2005). In our model the trabecular structure inside a human vertebra is mapped on a lattice. The mechanical assessment is performed using a simplified painting algorithm yielding the volume change of each bone element in the structure (Weinkamer et al., 2004). In order to perform changes in the structure, a remodelling rule has to be defined that specifies the probability for depositing or removing a bone element from the bone surface as a function of the local deformation.

Starting the simulations with a homogeneous configuration of a high bone volume fraction, a network-like structure with preferentially vertical and horizontal trabeculae emerged (Figure 26). A general feature of the model is that the bone volume fraction attained a steady-state value. However, the architecture coarsened with a decreasing number of trabeculae, and a concomitant increase in the thickness of the remaining trabeculae (Weinkamer et al., 2004). Small changes in the mechanosensitivity of the cells changed the trabecular structure significantly (Weinkamer et al., 2005) (Figure 26).

In addition, real 3D structural data of human vertebrae obtained by μCT was used as initial condition for the model. A single triaxial loading mode was applied to the system. Under this loading condition the complex trabecular structure rapidly simplified with only a few but thick trabeculae remaining. Apart from the simple mechanical description in our model, the

main reason for this rapid simplification is the uniform loading of the system. Daily activities of a human being lead to a more complex (but unknown) loading pattern of the spine, which presumably plays a role together with the particular biomechanical properties of the intervertebral discs in sustaining the complexity of the vertebral architecture.

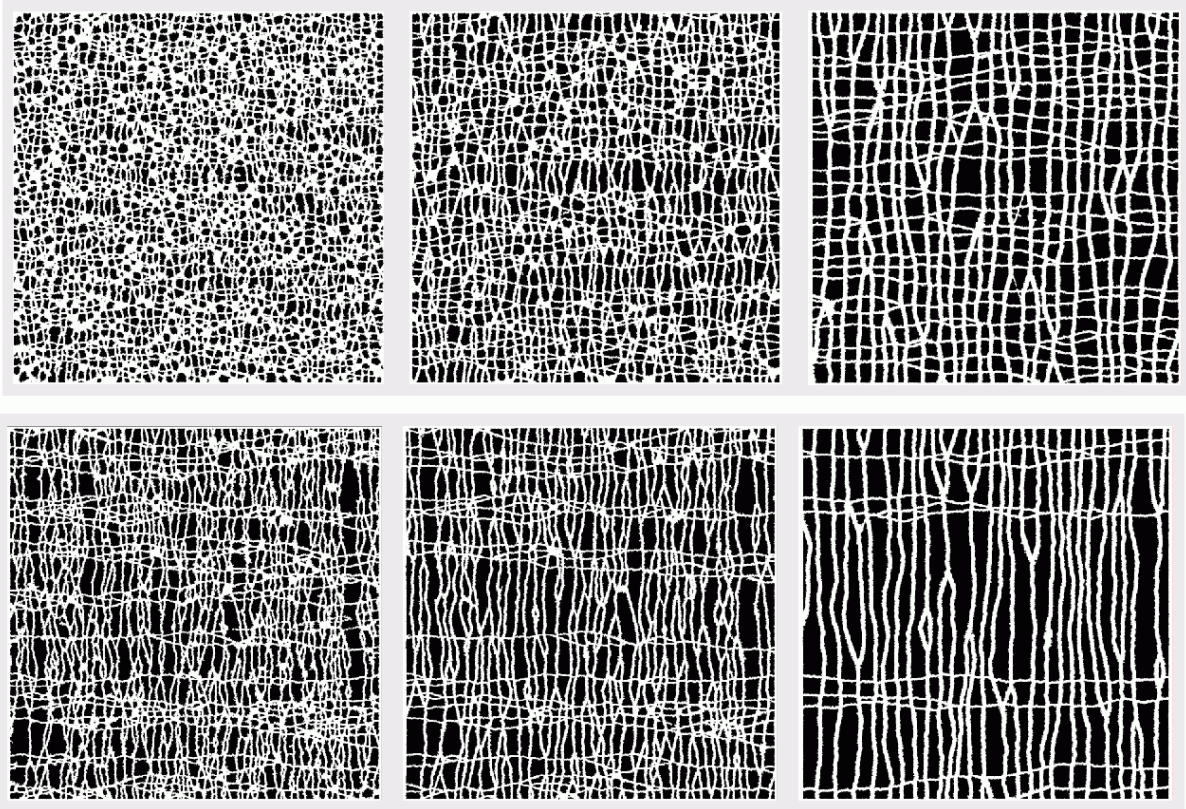

Figure 26. Two different time evolutions of the 2D trabecular bone model. The sensitivity of osteoblasts to the mechanical stimulus is reduced in the bottom row compared to the simulation of the top row. Both simulations begin with a random configuration of high bone volume fraction. Bone matrix is indicated white, marrow black.

Our research now focuses on the interrelation between the control of the remodelling process reflected in the remodelling rule and the resulting architecture (Figure 27). Already very subtle changes in the remodelling rule can change the morphology and the time evolution of the structure. An example is the changes induced to the structure by alterations in how the remodelling rule for the total cell action is distributed to osteoclasts and osteoblasts.

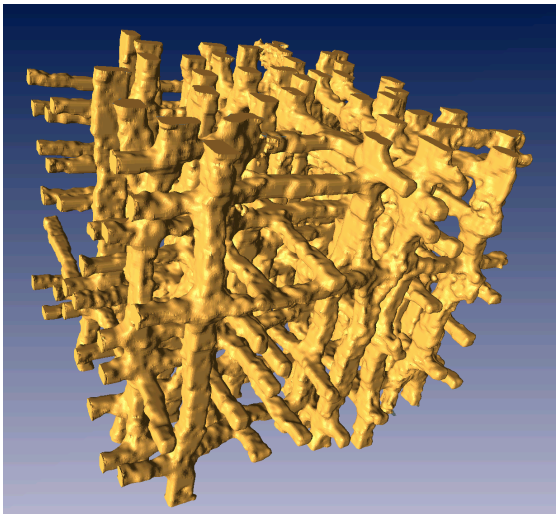

Figure 27. Modelling of evolution of trabecular bone structure in 3D. Shown is a snapshot of the bone architecture that emerged from a random configuration of high bone volume fraction. For the remodelling rule, a step function was assumed that corresponds to an on/off control for the osteoblasts.

4.8 Ultrasound Testing of Proximal Tibia for Quantification of Bone Structure

The project team has proposed the proximal tibial metaphysis as a new site for ultrasonic assessment of the structure of trabecular bone. The advantages of this skeletal site are:

- it is comprised of load-bearing bone, which usually suffer substantial losses during exposure to microgravity (Vico et al., 2000);
- it is mainly composed of trabecular bone and is a highly structured porous medium, where the loss of bone mass is tightly bound with changes of the structure;
- it offers an easy unilateral access to the examination site.

These properties make the proximal tibia an excellent site for examination of osteopenic and osteoporotic patients as well as for space flying personnel. In addition, the method can be extended to other skeletal sites such as the distal tibia or the calcaneus (unilaterally). These sites are mainly composed of trabecular bone surrounded by a thin cortical shell and thin layer of soft connective tissue.

Various ultrasonic methods have been suggested for assessing the bone structure including backscattering (Padilla & Laugier, 2005; Wear & Laib, 2003), broadband velocity dispersion (Chen & Chen, 2005), and guided waves (Muller et. al, 2005). Our approach is different from these methods by creating a measurement technique which utilizes low frequency surface waves applied unilaterally to the proximal tibia. The advantage of this method is that the hardware is compact and does not require a liquid coupling medium. As no acoustic coupling medium is needed the method is well suited for self-examination, which is desirable if the ultrasonic equipment is to be used by space flying personnel. Furthermore, our technique is based on the ultrasonic surface transmission mode and it utilizes spectral derivatives as diagnostic measures for assessing the trabecular bone structure. At present our ultrasonic device is the only available QUS equipment which uses such approach.

4.8.1 Transducers and probes

Different types of ultrasonic transducers were examined in order to establish which transducer type that was best suited for testing proximal tibiae *in vitro* and *in vivo* in surface transmission mode. The transducer types examined were: 1) flat disk-shaped; 2) broadband miniature; 3) point-contact with exponential waveguides; 4) resonant rectangular.

Propagation and spectral parameters were analyzed at propagation lengths (measurement bases) of 20–50 mm. It was revealed that: 1) frequencies in the low kilohertz band are required, in order to obtain responses from subsurface trabecular elements; and 2) *in vivo* readings can be masked significantly by the thin layer of soft tissue that covers the bone. Therefore, low frequency quasi point-contact transducers and adjustable base probes were designed for *in vitro* and *in vivo* ultrasonic measurements at the proximal tibia by surface transmission (Figure 28, a, b).

Propagation signals generated by 0.1 MHz and 0.3 MHz tone-bursts (Tatarinov & Sarvazyan, 2003) and continuous frequency sweeps in the 0.1–0.5 MHz band were acquired and analyzed during transmission of both signal types. A probe with expandable base was designed and manufactured for laboratory measurements (Figure 28 c, d). The probe allows a continuous variation of the distance between the transducer bases of 20–80 mm and adjustment of the angle between the transducers of 0–45º (Tatarinov et al., 2005).

In order to design a probe for standardized *in vivo* measurements, the following considerations were taken into consideration: a) the probes should have a smooth broadband spectral characteristic in order to obtain shorter pulses and in order to be able to perform

frequency sweeps with as little frequency depended distortion as possible; b) it should be possible to place the probes at the test site with a standardized contact pressure; and c) positioning of the probe on the test subject should be standardized.

Transducers with a smooth output frequency characteristic were obtained by placing round acoustic damper-traps on the transducers as shown in Figure 29. These acoustic damper-traps were made of the same piezoelectric material as the sensors. The transducers were implemented in a specially designed probe for *in vivo* application as shown in Figure 30. A double-rigidity spring was used for applying a standardized pressure against the tibia. A probe with a positioning applicator was constructed, which fits the geometry of the proximal tibia and that prevents the probe from moving during measurements. The knee joint slit is used as a reference point for axial positioning of the probe.

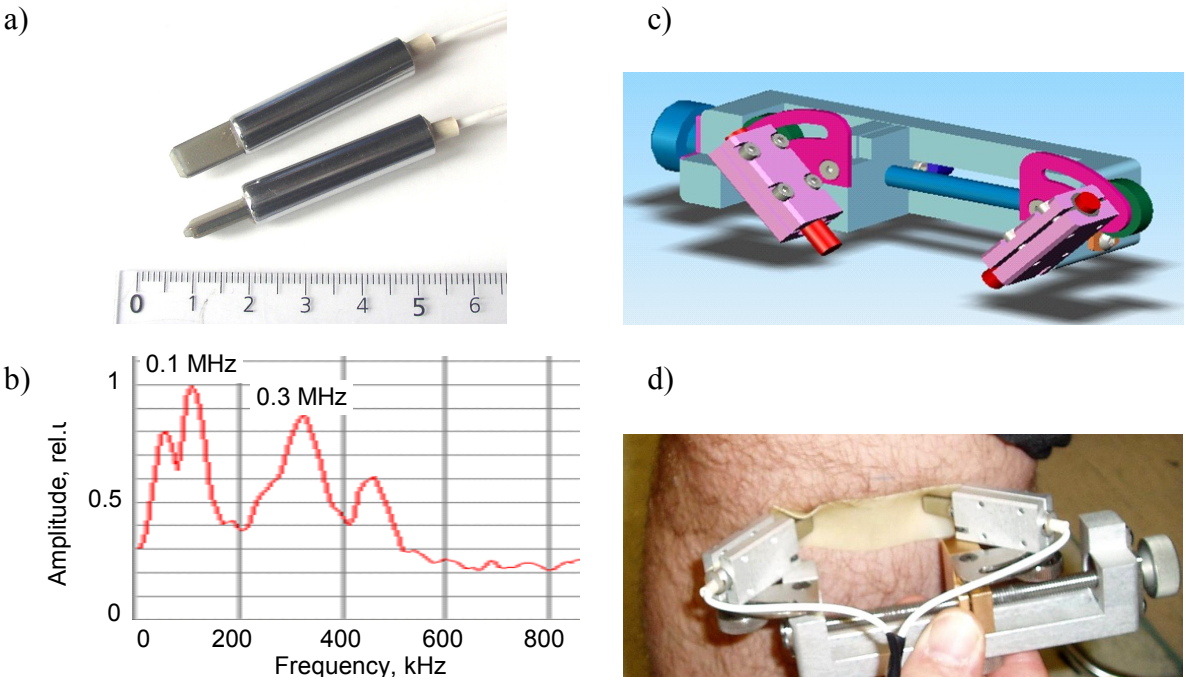

Figure 28. Ultrasonic resonant transducers for laboratory experiments with quasi-point contact *(a)* and their spectrum *(b)* with resonances at 0.1 and 0.3 MHz produced in a bone specimen. Laboratory ultrasonic probe for proximal tibia: design *(c)*; probe positioned on volunteer tibia *(d)*.

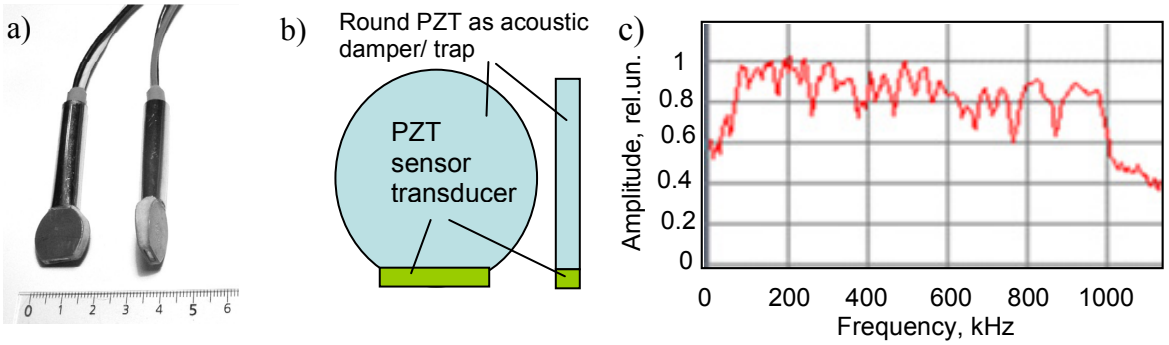

Figure 29. Transducers with broadband characteristics: general view *(a)*; principal structure of the sensor *(b)*; spectral characteristics *(c)*.

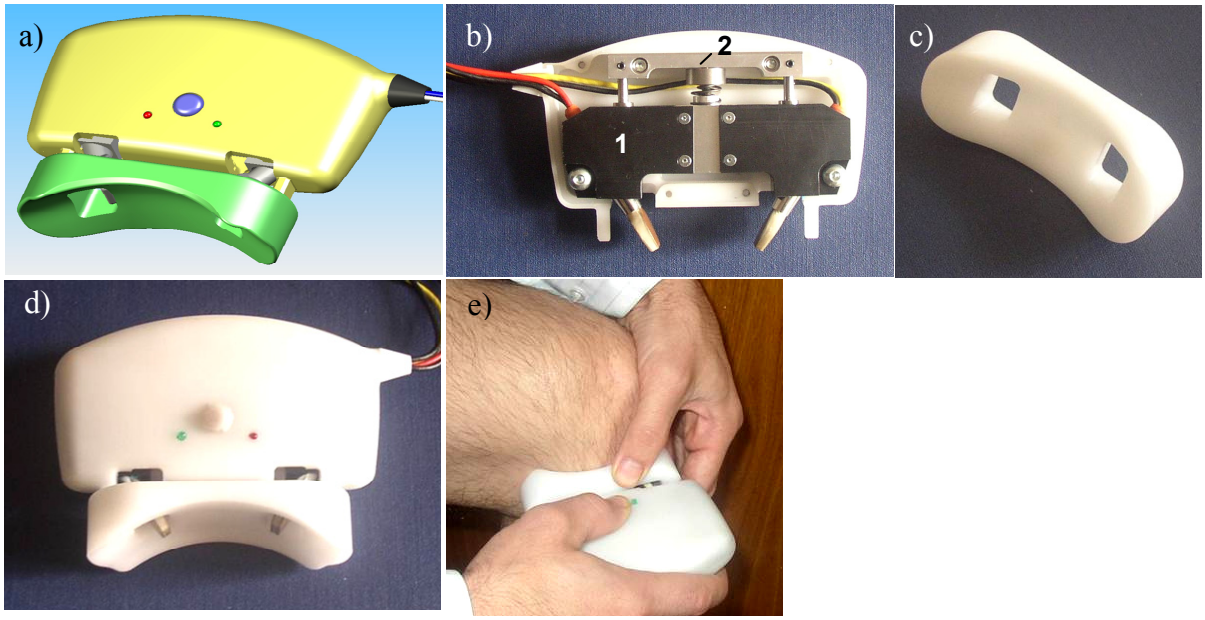

Figure 30. Probe for *in vivo* ultrasonic measurements of proximal tibia. *(a)*: design view; *(b)*: interior showing structure: *1* – holder for the transducers with stiff base and acoustical unbinding sliding along the vertical rails; *2* – immovable frame with springy elements; *(c)*: positioning applicator modelling geometry of the surface of proximal tibia; *(d)*: complete assembly of the probe and the applicator; *(e)*: probe positioned for measurement.

4.8.2 Software for generation of ultrasonic signals, data acquisition and processing

The developed signal generation and data acquisition software included the following features:

- The ability to generate ultrasonic excitation waveforms with the following characteristics: two consecutive sine wave tone-bursts modulated with a Gauss function. The duration of the bursts, their frequencies, and interval between the bursts can be adjusted.
- Real-time views and recordings of the signals which were received after the two described ultrasonic signals had propagated trough the bone.
- Tuning of the signal amplitude and time-base.
- The ability to generate, real-time views and recordings in the time domain of frequency sweeps in the 50–1000 kHz frequency band.
- The ability to present the acquired ultrasonic signals as real views (phase) and as enveloped wave packets (group) after band pass filtration.

The user interface panel used in the laboratory studies is shown in Figure 31.

The signal processing included analysis of temporal, power, and spectral parameters of the propagated signals, measures of velocity, and attenuation and frequency slope of attenuation.

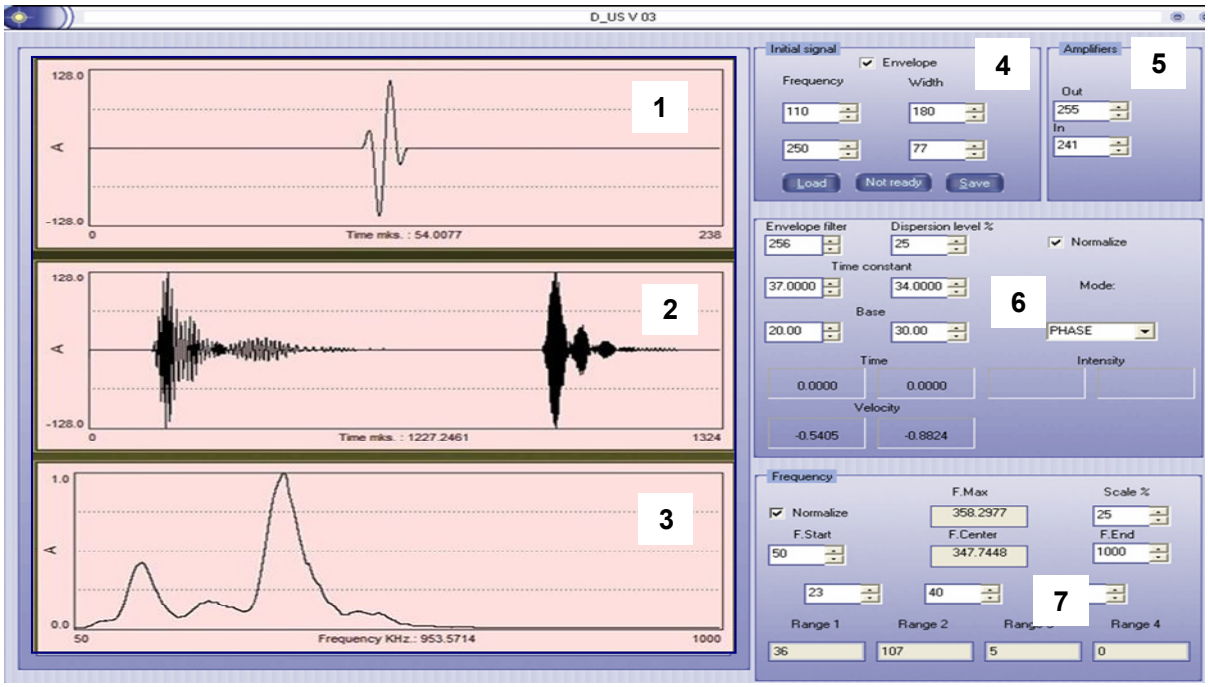

Figure 31. User interface panel: (1) excitation waveform panel; (2) panel for acquired real-time ultrasonic signals; (3) panel for acquired real-time frequency sweeps; (4)–(7) settings for creation of excitation waveforms, input and output amplification, signal processing modes and sweep signals parameters, correspondingly.

4.8.3 Study of artificial media (phantoms)

4.8.3.1 Study of phantoms with different material properties

The aims of these experiments were to test the developed method and hardware, and to investigate the ability of different quantitative ultrasonic parameters to assess the architecture of the bone phantoms. Changes of the scattering properties of the trabecular network with decreasing BMD were modelled by a series of different materials. Several different types of phantoms were investigated (Figure 32):

1. Silicone cuboid-shaped phantoms filled with either large sand particles or gravel, which functioned as acoustic scatterers. Different volumetric concentrations (5% and 10%) and different particle sizes (0.5 mm, 1 mm, and 2 mm) were tested;
2. Composite phantoms consisting of a thin stiff plate of laminate simulating cortical bone and a bulk silicone phantom simulating trabecular bone (as described above). These phantoms were used for testing the ability to assess the structural properties of an porous object placed beneath a thin compact outer layer;
3. Pumice-stones with different pore sizes. Different types of pumice stone with mean pore sizes from 0.5 mm to 3 mm were analyzed. The pores were filled with oil in order to simulate bone marrow.

It was found that it was possible to detect and quantify differences in the internal scatterers obtained from phantoms with similar densities. The results of the phantom studies were that:

– Attenuation of the ultrasound increases with increasing number of scattering elements (filling particles or pores) per unit volume. This means that a complex, interconnected trabecular structure with a high trabecular number will attenuate ultrasound heavier than a sparse structure with fewer interconnections.

- For phantoms with the same density, the number of scatterers affects the distribution of the resulting ultrasonic power spectra. High frequency peaks are dampened much faster than the low frequency components. For phantoms with the same density the difference between the dampening of high and low frequencies increased with increasing number of scattering elements. In the surface transition mode the ultrasonic energy is thus redistributed towards lower frequencies with increasing number of scattering elements.
- The ultrasonic signal is mainly affected by the number of scattering surfaces along the ultrasonic path, whereas the mass of the fillings has a much lower influence on the ultrasonic signals. Therefore, it is to be expected that the bone architecture will affect the transmitted ultrasound signal to a greater extent than the amount of bone material.
- Ultrasonic velocity (phase velocity) is the second most sensitive parameter for detecting structural changes in media with a high porosity. The velocities of wave packets (group velocities) are hard to measures due to the boundary conditions.
- The structure of a material situated beneath a compact plate (simulating cortical bone) can be assessed if the thickness of the plate is much smaller than the wavelength.

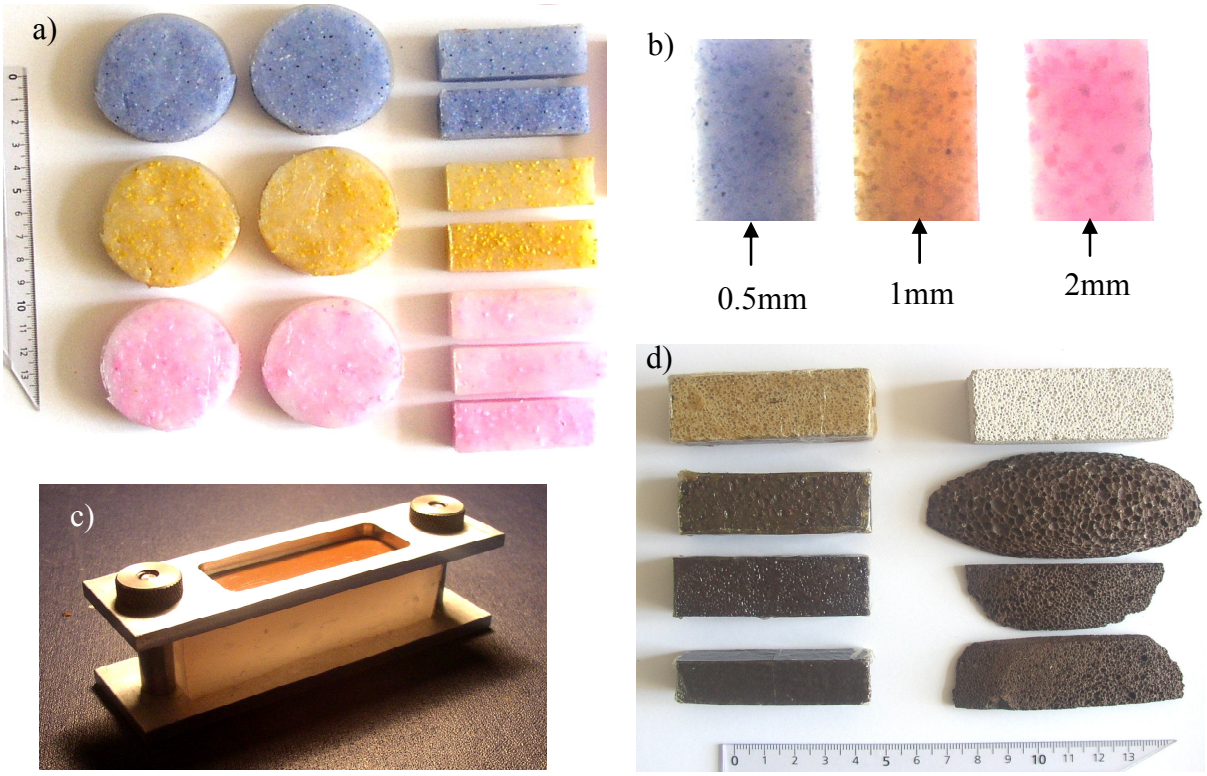

Figure 32. Phantoms simulating scattering properties of the bone: *(a)* round and cuboid silicone phantoms with stony fillings; *(b)* magnified fragments of silicone phantoms; *(c)* combined phantom with changeable cortex and beneath layer; *(d)* pumice-stone specimens

4.8.3.1 Wave penetration depth

In order to estimate how deep the ultrasonic waves propagates into the trabecular structure and in order to investigate which parts of the bones can be evaluated in surface transmission mode, an experiment with pumice-stones was undertaken. In this experiment the velocity of the ultrasound waves was close to the velocity that is used for trabecular bone. The intensity of wave packets with frequencies of 0.1 and 0.3 MHz were measured after cuts with different depths had been sawed in the specimen (Figure 33a).

The obtained intensity curves (Figure 33b) closely resemble the depth profile of vertical particle displacement in Rayleigh surface waves (Viktorov, 1967). This confirms the hypothesis that the main part of the ultrasonic energy is related to surface waves, in which the shear motion component is sensitive to the structural organization of the medium. If it is assumed that the information carrying part of the wave is found for intensities above 30% of the maximum intensity, the informative penetration depths are approximately 15 mm for 0.1 MHz and 5–6 mm for 0.3 MHz packets (Figure 33b).

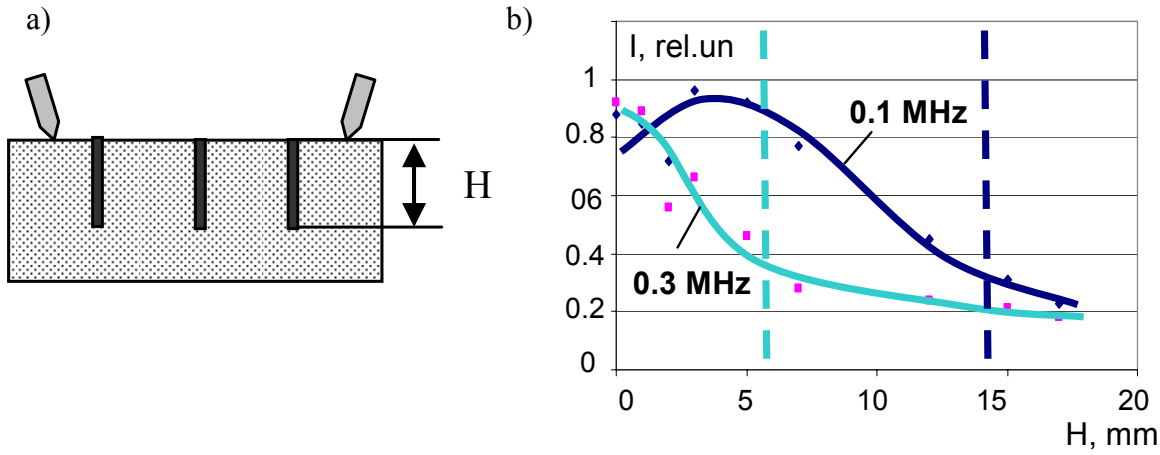

Figure 33. Experiment with wave penetration depth. *(a):* measurement layout; *(b)*: experimental dependence of ultrasound intensity I on depth of slits H.

4.8.4 Results obtained from bone specimens

The method has been developed and validated using 43 proximal tibial specimens including normal, osteopenic, and osteoporotic bone. Resonant 0.1 and 0.3 MHz transducers were used as these transducers can produce and receive powerful ultrasonic responses when no soft tissue is present between the transducers and the bone. Propagation signals generated by short 0.1 MHz and 0.3 MHz tone-bursts and continuous frequency sweeps in the 0.1–0.5 MHz band were acquired during one transmission of the combined signal packet (Tatarinov et al., 2005). These ultrasonic measurements were performed 17 mm below the tibial plateau at an acoustic base (distance) of 40 mm and orientated transversally to the bone axis. The angle between the transducers was adjusted so that the transducers were approximately perpendicular to the bone surface. The measurements were performed in specimens preserved in formaldehyde and packed in plastic bags. Each measurement included three consecutive positioning and data acquisitions followed by an averaging of the results.

In total 19 intact (without bone biopsy holes) tibial specimens and 24 tibial specimens with bone biopsies holes were examined. The same specimens had previously been used for histomorphometry and examination of 2D complexity measures, BMD, and 3D structural measures (Sections 4.2, 4.4, and 4.5). The relationships between the ultrasonic results and the results provided by these measures were investigated.

The following ultrasonic parameters derived from the acquired ultrasonic responses were analyzed (Tatarinov et al., 2005):

1. The ratio of ultrasound intensities at 0.1 and 0.3 MHz, R. This ratio was determined from the area under normalized and enveloped frequency sweep spectra at frequencies around 0.1 MHz ($I_{0.1}$) and 0.3 MHz ($I_{0.3}$) ($R = I_{0.1} / I_{0.3}$). This ratio can be considered as a measure of the frequency slope of attenuation in the 0.1–0.3 MHz band. The range of R was from 0.34 to 2.80 in the bone specimens.

2. The intensity *I* of the entire broadband ultrasonic response in the 0.05–0.5 MHz frequency range. The intensity was determined as the area under normalized and enveloped sweep signal in the 0.05–0.5 MHz band. Under standardized measurement conditions, such intensities can be considered as measures of ultrasonic attenuation. For *I* the normalized range of change was from 5 to 212 in the bone specimens.
3. Intensity *I* normalized by the ratio *R*: *I/R*. The range of *I/R* was 1.3–380.
4. Arrival of wave front. Arrival of propagated signals with frequencies of 0.1 and 0.3 MHz were determined as the moments of crossing of the given amplitude thresholds by the signals processed by a band pass filtering and enveloping. No significant differences between the intervals of wave front arrivals were found when normal and osteoporotic specimens were compared.
5. Arrivals of slow wave packets. Peaks of frequency-filtered and enveloped propagation signals were evaluated as reference points for group velocity of slow wave packets. Different typical propagation peaks were observed; with velocities ranging from 500 to 1500 m/s. While we consider this parameter as potentially informative, more experiments are needed in order to understand the propagation law for such slow waves.

It was found that several of the proposed ultrasonic parameters were able to detect differences between the structural statuses of bones with different BMD (Tatarinov et al., 2005). In particular it was found that high frequencies were prevailing in osteoporotic bones. Sweep responses showed different relative intensities of the 0.1 and 0.3 MHz spectral peaks in bones with either high or low trabecular BMD. A good agreement was thus established between the ratio of these intensities and trabecular bone status assessed by the BMD. A low number of scattering elements – trabeculae – in bones with low trabecular BMD resulted in a weaker attenuation of the ultrasound transmission in the entire frequency band. Additionally, normal and osteoporotic bone could be distinguished by their dispersion of propagating wave packets. At low frequencies (0.1 MHz), at least two different wave modes with different group velocities were recorded. The second (slow type) wave packet propagated faster in normal bone than in osteoporotic bone, whereas no significant difference in propagation velocity of the first wave packets was observed.

Good and very good correlation ($|r|$ = 0.63–0.89) was found between the ultrasonic measures and the CT or μCT-based methods. The Pearson linear correlation coefficients between the ultrasound parameters and 2D measures of complexity, bone densitometry, and 3D morphometric parameters obtained from proximal tibial bone biopsies are summarized in Table 7. In some cases logarithmic transformation was applied to the data before the correlation coefficients were calculated. The highest correlations were found for *R* and *I/R* for the intact specimens, whereas the highest correlations were established for *I/R* for the specimens with a bone biopsy hole.

The highest correlations were obtained for the structural complexity measures that relate to the scattering properties of the trabecular network: SCI, TNI, IGE, and Maximal and Mean L-blocks (Figure 34). A higher number of scattering surfaces along the ultrasonic path, i.e. the complexity of the trabecular network, resulted in a higher attenuation of the ultrasonic intensity in the entire frequency band and caused a shift of the propagation spectrum towards lower frequencies (an increase of *R*). The strength of the relationships with the BMD is comparable to those obtained between the CT-based structural parameters and BMD. This can be explained by a concomitant decrease in bone density and bone structure for decreasing BMD. The correlations with trabecular thickness (Tb.Th) were relatively weak, r = –0.64. This confirms the hypothesis that ultrasound is better related to the bone structure than to the thickness of the trabeculae. This finding is also in good agreement with the established fact

that the scattering, but not the absorption, affects QUS parameters in trabecular bone. The higher correlations coefficients obtained for the intact specimens can be explained by problems with positioning of the ultrasonic probe at specimens with biopsy holes. The positioning was optimal and exactly at the standard location for the intact specimens, whereas the measurement site had to be shifted in order to avoid the biopsy hole in the non-intact specimens. This resulted in an unpredictable influence of the topographical heterogeneity of the tibial surface and trabecular structure.

Technology	Measure	Specimens with a biopsy hole	Specimens without a biopsy hole	
		I/R	*R*	*I/R*
2D Measures of Complexity	Entropy	-0.76	0.70	-0.74
	SCI	-0.79	0.84	-0.78
	TNI	-0.72	0.89	-0.84
	IGE	-0.74	0.88	-0.82
	Max. L-block	0.66	-0.86	0.87
	Mean L-block	0.74	-0.84	0.84
Densitometry	BMD	-0.78	0.86	-0.79
3D Morphometic Measures	SMI	0.68	The 3D measures are biopsy-based and therefore only performed for specimens with a biopsy hole	
	BS/BV	0.63		
	Tb.Th	-0.64		
	Tb.N	-0.63		
	Tb.Sp	0.67		

Table 7. Pearson correlation coefficients between the ultrasonic parameters *I/R* and *R* and the structural measures based on radiological imaging calculated for the proximal tibia specimens. Significance level: $p \leq 0.01$. Correlation coefficients with lower significance levels have been omitted.

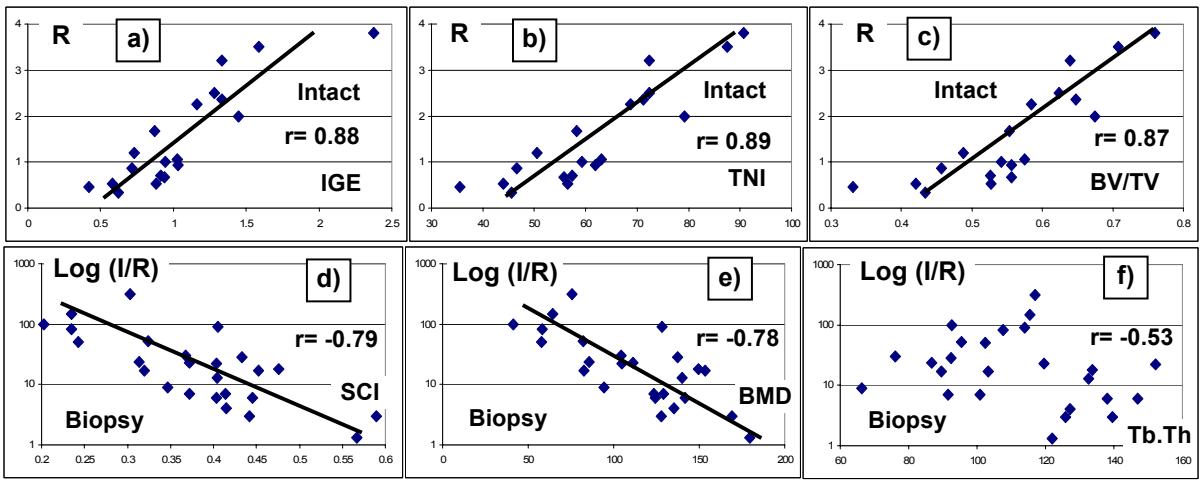

Figure 34. Selected relations between the ultrasonic parameters *R* and *I/R* and the 2D complexity measure IGE *(a)*, TNI *(b)*, SCI *(c)*, bone fraction BV/TV *(d)*, bone mineral density BMD (e) and trabecular thickness Tb.Th *(f)*, which were calculated from pQCT images in specimens with and without biopsy holes.

4.8.5 Pilot *in vivo* study

Both probes (Figures 28 and 30) were used to perform *in vivo* examination of the proximal tibia of five of the six healthy volunteers described in Sections 4.1.4 and 4.4.5. We found that:

- The developed method allows ultrasonic evaluation of proximal tibia *in vivo*. The results obtained with ultrasound provided similar ranking of the bone status as the radiological measures (see Section 4.4.5).
- Due to the acoustic properties of the subcutaneous tissue (soft tissue on the bone surface), the ultrasonic responses obtained *in vivo* were significantly different from those of the bone samples. Thus, the results obtained *in vivo* can not be directly compared with the results obtained from bone specimens.
- The intensity of the ultrasonic signal is strongly dependent on the pressure applied to the probe, which makes the measurements of I unstable. Consequently, the only currently available *in vivo* parameter is R.
- Therefore, it is necessary to further improve the accuracy and robustness of the system in order to make it suitable for routine examinations. Standardization of the probe application and an exclusion of the influence of soft tissue are required. These problems have partially been addressed with the second-generation probe (Figure 30) produced at the final stage of the project.

4.8.6 Conclusion about ultrasound evaluation of proximal tibiae

- An experimental system for ultrasonic evaluation of human tibial trabecular bone architecture was developed.
- The ability of the developed equipment and method for assessing structural differences of trabecular bone by the parameters derived from ultrasonic spectra and attenuations was established. Studies of bone specimens revealed good correlations between the proposed ultrasonic parameters and BMD and structural measures based on radiological imaging. It was demonstrated that it was possible to acquire adequate ultrasonic responses for *in vivo* evaluation of the bone status.
- The developed method and hardware operates in surface transmission mode and evaluates the frequency-dependent scattering properties of the trabecular bone. It provides quantitative measures which relate to the number of trabeculae within the propagation path and the trabecular spacing. No other currently available bone QUS device has such capabilities.
- The limitations, potential ultrasonic parameters, and a way for further improvement of the developed ultrasonic system for bone structure evaluation have been formulated.
- Future evolution of the developed ultrasonic method could focus on a development of a precise measurement system for *in vivo* examinations that minimizes the influence of soft tissues and standardizes the positioning and measurement procedures. It could also include a continuous assessment of ultrasound propagation signals as a function of the frequency in the low frequency band (0.05–0.15 MHz). However, further experiments of the physics of propagation of slow wave components in trabecular bone are needed. It will help to optimize the proposed ultrasound-based structural measures as well as to develop new parameters which provide structural information.

5. Future Studies

The results of this project can provide the foundation for quantitative monitoring, assessment of countermeasures, and evaluation of treatment results for structural changes in bone caused by metabolic diseases or exposure to microgravity. In particular, in the future the developed method will be used to evaluate 3D data of astronauts' extremities when these data become available. The trabecular structure of astronauts' bones is to be evaluated before and after spaceflight by use of a specially developed *in vivo* μCT scanner.

The project team has prepared a new project proposal "Assessing the Influence of Microarchitecture on the Mechanical Performance of Bone and its Changes in Microgravity from *in vivo* Measurements", which was approved by the independent review board and ESA MAP panel. The industry partners Scanco Medical AG and Siemens AG, Siemens Medical Solutions support the new study as well. This project will logically continue and substantially extend the current research bringing it to a new level of understanding of the relation between bone architecture and its mechanical properties.

Views and Recommendations from the Industrial Partners

Siemens AG

Siemens Medical Solutions has been participating in the project over the last five years and supported the research by several donations as well as by participation in regular meetings. The scientific interest by the Computed Tomography Division of Siemens is the characterization of bone structures which goes beyond the traditional Bone Mineral Density parameter used to quantify the extend of osteoporotic disease today.

The research work of the project on measures of complexity has led to the development of such parameters in two and three dimensional space. The application to various bone specimens has shown a definite relation between the measures of complexity and the anatomy of bones and thus is the basis of diagnostic interpretation for in vivo applications.

Most modern imaging technologies, like micro-CT, have been used to experimentally check underlying theoretical assumptions and algorithms. In vivo whole-body CT scans of the lumbar spines and the proximal tibiae of healthy volunteers have been performed.

We perceived the cooperation between the partners of the project as very productive and efficient. The individual tasks have been well defined and distributed among the partners. Corresponding results have been exchanged regularly and have been combined to form a complete picture. The regular team meetings between all partners have been an important element to achieve the present level of success.

The application of high resolution multislice CT to volunteers, patients, and astronauts as well as the assessment of the influence of microarchitecture on the mechanical performance of bone and is changes in microgravity condition are an interesting continuation of the previous research work to relate the measures of complexity to corresponding stages of disease in vivo.

Signed by Christian Asbeck
Siemens AG

Scanco Medical AG

I hereby want to express my thanks for working together in the MAP project AO-99-030 very successfully. The work done so far was very helpful for us in different aspects:

- Access to a larger number human biopsies / autopsies
- Comparison of our systems to others (image quality)
- Comparison of our software methods to others
- Comparison of our morphometry results with standard histology
- Fruitful discussions regarding CT-technology.

We therefore think that our work and manpower for this project was paid off by the above facts and we will definitely continue the project if possible.

Signed by Bruno Koller, PhD
General Manager
SCANCO Medical AG

Mercury Computer Systems GmbH

Mercury Computer Systems has been participating in the second phase of the ESA MAP Project AO-99-030 during 2003-2005.

The company supported the research by providing licences of the Amira software to all project teams as well as consulting service in software design questions. The research done so far was very helpful for us regarding the following aspects:

- the multifaceted analyses of large micro-CT data performed with Amira demonstrated well its capabilities
- the extension of Amira to an environment for analysis of trabecular bone represents a nice demonstration of the expandability and adaptability of Amira
- the comparison of Amira with software developed specifically for quantitative bone analysis provided insight into the potentials and limitations of Amira
- the partial extension of Amira for handling large image data by out-of-core algorithms or 64 bit addressing as well as for remote access to centrally stored data constitute good foundations for further developments
- the research results based on high resolution multislice CT provided us valuable hints about the status of alternative procedures for clinical bone disease diagnostics.

Considering all these results we consider our commitment for this project as worthwhile and we would like to see this research to be continued.

Signed by Malte Westerhoff, PhD
Mercury Computers Systems GmbH

Publications and Contribution to the Scientific Meetings

Scientific Publications

1. A. Zaikin, W. Gowin, S. Prohaska, J. Kurths. 2D Bone Modelling for Analysis of Changes in Bone Architecture and for Evaluation of Structural Measures, in: *Proc. of the 2nd European Congress Achievements In Space Medicine into health Care Practice and Industry, Berlin, 2003*, 100–106, 2003.
2. N. Marwan, P. Saparin, J. Kurths, W. Gowin. 3D measures of complexity for the assessment of complex trabecular bone structures. *Proc. Complexity in the Living. Rapporti ISTISAN*, **05/20**, 53–58, 2004.
3. S. Prohaska, A. Hutanu, R. Kähler, H.-C. Hege. Interactive Exploration of Large Remote Micro-CT Scans. *Proc. IEEE Visualization '04*, pp. 345–352, Austin, Texas, 2004.
4. R. Weinkamer, M.A. Hartmann, Y. Brechet and P. Fratzl. A stochastic lattice model for bone remodelling and aging. *Phys. Rev. Lett.* **93**, 228102, 2004.
5. P.I. Saparin, J.S. Thomsen, S. Prohaska, A. Zaikin, J. Kurths, H.-C. Hege, W. Gowin. Quantification of Spatial Structure of Human Proximal Tibial Bone Biopsies Using 3D Measures of Complexity. *Acta Astronautica* **56**, 820–830, 2005.
6. A. Zaikin, J. Kurths, P. Saparin, W. Gowin, S. Prohaska. Modelling Bone Resorption in 2D CT and 3D μCT Images. *International Journal of Bifurcation and Chaos* **15**, 2995–3009, 2005.
7. J.S. Thomsen, A. Laib., B. Koller, S. Prohaska, Li. Mosekilde, W. Gowin. Stereological Measures of Trabecular Bone Structure: Comparison of 3D Micro Computed Tomography with 2D Histological Sections in Human Proximal Tibial Bone Biopsies. *Journal of Microscopy* **218**, 171–179, 2005.
8. J.S. Thomsen, B.V. Morukov, L. Vico, C. Alexandre, P.I. Saparin, W. Gowin. Cancellous Bone Structure of Iliac Crest Biopsies Following 370 Days of Head-Down Bed Rest. *Aviation, Space, and Environmental Medicine* **76,** 915–922, 2005.
9. N. Marwan, J. Kurths. Line structures in recurrence plots. *Physics Letters A*, **336** (4-5), 2005, 349–357.
10. R. Weinkamer, M.A. Hartmann, Y. Brechet & P. Fratzl, Architectural changes of trabecular bone caused by the remodelling process. *Mat. Res. Soc. Symp. Proc.* **874**, L.1.9.1, 2005.
11. ESA MAP AO-99-030 Team. Assessment of Bone Structure and its Changes in Microgravity. *ESA SP-1290*, 282–305, 2005.
12. N. Marwan, P. Saparin, J.S Thomsen, J. Kurths. An Innovative Approach for the Assessment of 3D Structures in Trabecular Bone. *ESA SP-585* and *Journal of Gravitational Physiology* (in press).
13. N. Marwan, J. Kurths, P. Saparin, J.S. Thomsen. A New Quantitative Approach for Measuring Changes of 3D Structures in Trabecular Bone. *Proc. 3rd European Congress "Achievements in Space Medicine into Healthcare Practice and Industry", Berlin, 2005*, (in press).

14. N. Marwan, P. Saparin, J.S. Thomsen, J. Kurths. Generalisation of Recurrence Plot Analysis for Spatial Data. *Proc. NOLTA Conference, Bruges, 2005*, (in press).
15. P. Saparin, J.S. Thomsen, G. Beller, W. Gowin. Measures of Complexity to Quantify Bone Loss and Estimate Strength of Human Lumbar Vertebrae: Comparison of CT Image Analysis with Bone Histomorphometry and Biomechanical Tests. *ESA SP-585* and *Journal of Gravitational Physiology* (in press).
16. A. Tatarinov, W. Gowin, G. Beller, P. Saparin. A Perspective for Ultrasonic Assessment of Osteoporotic Changes of Bone Structure in Proximal Tibia. *ESA SP-585* and *Journal of Gravitational Physiology* (in press).
17. P. Saparin, J.S. Thomsen, J. Kurths, G. Beller, W. Gowin. Segmentation of bone CT-images and assessment of bone structure using measures of complexity. *Medical Physics*. (Revised manuscript resubmitted).

Oral Presentations at the Scientific Meetings

1. H.-C. Hege. Visualization in Biomedicine: Methods and Applications, *Summer School "Jacques Louis Lions" - Multidisciplinary Methods for Analysis, Optimization and Control of Complex Systems*, MACSI-net, Montecatini, Italy, March 17, 2003.
2. W. Gowin, P. Saparin, S. Prohaska, H.-C. Hege, S. Beller, D. Felsenberg. Architectural Reasons for the Femoral Neck Fracture Location. *2nd European Congress on Achievements in Space Medicine into Health Care Practice and Industry*, Berlin, Germany, March 27–29, 2003.
3. S. Prohaska, H.-C. Hege, M. Giehl, W. Gowin. Interactive Visualization to Support Quantification of Bone Biopsies. *2nd European Congress on Achievements in Space Medicine into Health Care Practice and Industry*, Berlin, Germany, March 27–29, 2003.
4. P. Saparin, W. Gowin, A. Zaikin, S. Prohaska. Quantification of changes in human bone structure at different skeletal locations using measures of complexity. *2nd European Congress on Achievements in Space Medicine into Health Care Practice and Industry*, Berlin, Germany, March 27–29, 2003.
5. J.S. Thomsen, B. Koller B, A. Laib, S. Prohaska, M. Giehl, W. Gowin. Comparison between static histomorphometric measures conducted by traditionally 2D histomorphometry and 3D μ-CT in human tibial biopsies. *2nd European Congress on Achievements in Space Medicine into Health Care Practice and Industry*, Berlin, Germany, March 27–29, 2003.
6. A. Zaikin, P. Saparin, S. Prohaska, J. Kurth, W. Gowin. 2D and 3D Bone Modelling for Analysis of Changes in Bone Architecture and for Evaluation of Structural Measures. *2nd European Congress on Achievements in Space Medicine into Health Care Practice and Industry*, Berlin, Germany, March 27–29, 2003.
7. H.-C. Hege: Creation and Visualization of 3D Anatomical Models, *3D Modelling 2003*, Paris, April 23, 2003.
8. W. Gowin, P. Saparin, M. Giehl. Skeletal Locations for the Examination of Bone Structure Alterations due to Microgravity Exposure. *14th IAA Humans in Space Symposium*, Banff, Alberta, Canada, May 18–22, 2003.

9. S. Prohaska, H.-C. Hege, M. Giehl, W. Gowin. A Virtual Laboratory for Assessment of Bone Biopsies. *14th IAA Humans in Space Symposium*, Banff, Alberta, Canada, May 18–22, 2003.
10. P. Saparin, J.S. Thomsen, S. Prohaska, A. Zaikin, J. Kurths, H.-C. Hege, W. Gowin. Quantification of Spatial Structure of Human Proximal Tibial Bone Biopsies Using 3D Measures of Complexity. *14th IAA Humans in Space Symposium*, Banff, Alberta, Canada, May 18–22, 2003.
11. H.-C. Hege. Perceptually Effective 3D Visualization of Complex Data. Keynote Lecture at *2003 Computer Graphics and Visualization Festa*, Nikkei Science, Tokyo, Japan, October 4, 2003.
12. P. Saparin on behalf of the project team. 2D and 3D Quantification of Bone Structure and its Changes in Microgravity Condition by Measures of Complexity. *DLR Human Physiology Workshop 2004*, Cologne, Germany, May 12–14, 2005.
13. S. Prohaska. Exploring High-Resolution Medical Image Data. *BIRS Workshop on Mathematical Foundations of Scientific Visualization, Computer Graphics, and Massive Data Exploration*, Banff, Alberta, Canada. May 22–27, 2004.
14. W. Gowin, P. Saparin, J.S. Thomsen, S. Prohaska, H.-C. Hege. The proximal tibia: a new site for bone status assessments. *25th Annual International Gravitational Physiological Meeting*, Moscow, Russia, June 6–11, 2004.
15. P. Saparin, J.S. Thomsen, S. Beller, G. Beller, W. Gowin. Comparison of pQCT image analysis and histomorphometry to quantify bone structural loss in the proximal tibia. *25th Annual International Gravitational Physiological Meeting*, Moscow, Russia, June 6–11, 2004.
16. J.S. Thomsen, B.V. Morukov, L. Vico, P.I. Saparin, W. Gowin. Static histomorphometry of the iliac crest after 360 days of antiorthostatic bed rest with and without countermeasures. *25th Annual International Gravitational Physiological Meeting*, Moscow, Russia, June 6–11, 2004.
17. J.S. Thomsen, B.V. Morukov, L. Vico, P.I. Saparin, W. Gowin. Static histomorphometry of the iliac crest after 360 days of antiorthostatic bed rest with and without countermeasures. *35th COSPAR (Committee on Space Research) Scientific Assembly*, Paris, France, July 18–25, 2004.
18. N. Marwan, P. Saparin, W. Gowin, J. Kurths. 3D measures of complexity for the assessment of trabecular bone structures. *2nd International Meeting "Complexity in the Living"*, Rome, Italy, September 28–30, 2004.
19. S. Prohaska, A. Hutanu, R. Kähler, H.-C. Hege. Interactive exploration of large remote micro-CT scans. *IEEE Visualization 2004*. Austin, Texas, USA. October 10–15, 2004.
20. J. Kurths, N. Marwan, P. Saparin, S. Prohaska, W. Gowin. Quantification of human bone measurements using measures of complexity. Invited presentation at *Ollendorff Minerva Center for Vision and Image Sciences German-Israeli Binational Workshop*, Haifa, October 20–21, 2004.
21. H.-C. Hege. Distributed Visualization and Data Analysis, *Visualization Workshop*, Kanazawa University, Kanazawa, Japan, Nov 15, 2004.
22. R. Weinkamer, M.A. Hartmann, Y. Brechet, P. Fratzl. A Stochastic Lattice Model for Bone Remodelling and Aging. *Materials Research Society (MRS) Spring Meeting "Structure and Mechanical Behaviour of Biological Materials"*, San Francisco, USA, March 28 – April 1, 2005.

23. P. Saparin, J.S. Thomsen, G. Beller, W. Gowin. Comparison of non-invasive pQCT image analysis by measures of complexity with bone histomorphometry and biomechanical tests to quantify bone loss and strength of lumbar vertebrae. *15th IAA Humans in Space Symposium*, Graz, Austria, May 22–26, 2005

24. P. Saparin, J.S. Thomsen, G. Beller, W. Gowin. Measures of Complexity to Quantify Bone Loss and Estimate Strength of Human Lumbar Vertebrae: Comparison of CT Image Analysis with Bone Histomorphometry and Biomechanical Tests. *ESA/ISGP Joint Life Science Conference "Life in Space for Life on Earth"*, Cologne, Germany, June 26 – July 1, 2005.

25. P. Saparin, J.S. Thomsen, G. Beller, W. Gowin. Processing of CT-images by Measures of Complexity to Quantify Bone Architecture and Predict its Strength. *13th International IEEE Workshop on Nonlinear Dynamics of Electronic Systems NDES 05*, Potsdam, Germany, September 20–25, 2005.

26. N. Marwan, P. Saparin, J. Kurths. Recurrence Plot Extension for 2D Spatial Data, *1st International Recurrence Plot Workshop*, Potsdam, Germany, September 23–25 2005.

27. N. Marwan, J. Kurths, P. Saparin, P., J. Thomsen. A New Quantitative Approach for Measuring Changes of 3D Structures in Trabecular Bone, *3rd European Congress "Achievements in Space Medicine into Healthcare Practice and Industry"*, Berlin, Germany, September 28–30, 2005.

28. N. Marwan, P. Saparin, J. Kurths. Generalisation of Recurrence Plot Analysis for Spatial Data. *International Symposium on Nonlinear Theory and its Applications NOLTA,* Bruges, Belgium, October 18–21, 2005.

29. P. Saparin, J.S. Thomsen, G. Beller, D. Felsenberg, P. Fratzl, W. Gowin. Measures of complexity to assess bone structure and estimate bone strength from pQCT- and CT-images of lumbar vertebrae and proximal tibiae. *3rd European Medical and Biological Engineering Conference EMBEC'05*, Prague, Czech Republic, November 20–25, 2005.

Poster Presentations at the Scientific Meetings

1. G. Beller, P. Saparin, W. Gowin. Structural measures of complexity in pQCT- and helical CT-imaging. *4th International Workshop on Musculoskeletal and Neuronal interactions*, Porto Carras, Greece, May 28-31, 2004.

2. N. Marwan, P. Saparin, W. Gowin, J. Kurths. On the way to new 3D measures of complexity for bone assessment. *8th Experimental Chaos Conference*, Florence, June 14–17, 2004.

3. N. Marwan, P. Saparin, J. Kurths. On the way to new 3D measures of complexity for bone assessment, *2nd International Meeting "Complexity in the Living"*, Rome, Italy, September 28–30, 2004.

4. J.S. Thomsen, P. Saparin, G. Beller, W. Gowin. Comparison of Measures of Complexity Derived From Peripheral Quantitative Computed Tomography Images with Static Histomorphometry and with Bone Strength Performed on Human Lumbar Vertebral Bodies. *Bone* **36** (Supplement 2), S328–S328, 2005. *2nd Joint Meeting of the European Calcified Tissue Society and the International Bone and Mineral Society*, Geneva, Switzerland, June 25–29, 2005.

5. R. Weinkamer, M.A. Hartmann, Y. Brechet, P. Fratzl. Simulation of trabecular bone remodelling and its regulation by mechanical and biological factors. *2nd Joint Meeting of the European Calcified Tissue Society and the International Bone and Mineral Society*, Geneva, Switzerland, June 25–29, 2005.
6. N. Marwan, P. Saparin, J.S. Thomsen, J. Kurths. An Innovative Approach for the Assessment of 3D Structures in Trabecular Bone. *ESA/ISGP Joint Life Science Conference "Life in Space for Life on Earth"*, Cologne, Germany, June 26 – July 1, 2005.
7. A. Tatarinov, W. Gowin, G. Beller, P. Saparin. A Perspective for Ultrasonic Assessment of Osteoporotic Changes of Bone Structure in Proximal Tibia. *ESA/ISGP Joint Life Science Conference "Life in Space for Life on Earth"*, Cologne, Germany, June 26 – July 1, 2005.
8. N. Marwan, P. Saparin, J. Kurths. An Innovative Approach for the Assessment of 3D Structures in Trabecular Bone, *13th International IEEE Workshop on Nonlinear Dynamics of Electronic Systems NDES 05*, Potsdam, Germany, September 20–25, 2005.

Other Scientific Work

Part of the projects travel funds provided by the ESA to the UoP was used to invite to the University of Potsdam leading specialists in the area of the recurrence plots. The idea of quantifying recurrences in the trabecular bone structure was studied in the project. Measuring recurrences in higher-dimensional spatial data is a very new field, where new solution has still to be developed. Therefore, the University of Potsdam organised a Recurrence Plot workshop (Potsdam, Germany, September, 22–24, 2005), where experts and applicants of recurrence plot based methods have met. A main topic of this workshop was to discuss recent developments especially in the analysis of spatial data using recurrence plot based methods.

Using financial support from the ESA project, it was possible to invite also Prof. J. Zbilut and Prof. Ch. Webber, the founders of the modern recurrence quantification analysis. The problems of application of recurrence plots to analyze 2D CT and 3D μCT bone images have been discussed and the results obtained during the project have been presented during the meeting. Some new ideas could be developed during the workshop, and new ways of cooperation were established for the further development of recurrence plot based methods. The attendees of the workshop were very satisfied; the workshop was a great success.

List of Intellectual Properties Rights

Max Planck Institute of Colloids and Interfaces

Claims of the Max Planck Institute of the Colloids and Interfaces with regards to the Intellectual Properties developed during the Second Phase of the Project:

1. The software and algorithms for preprocessing, symbol-encoding, and quantification of bone structure 2D measures of complexity from 2D CT- and pQCT-images acquired at different skeletal sites with. This includes:
    a. Algorithms for estimation of noise level (in Partnership with the CBF team) and noise reduction;
    b. Robust algorithm for standardized region of ROI for vertebral CT-and pQCT-images of different resolution acquired from bone specimens or *in vivo*.
    c. Approach to estimate an organization of soft tissue inside the bone which is based on symbol-encoding and 2D measures of complexity.

    The anteriority for the mentioned above Intellectual Properties which are documented in the project publications listed in this Report and in the publications (Saparin et. al., 2005a; Saparin et. al. 2005c). These items were developed by the Partners Peter Saparin (CBF, MPICI), Wolfgang Gowin, and Jürgen Kurths (UoP). The intellectual property items mentioned in the Background Information are excluded from this claim.
2. Software and algorithms for quantification of bone 3D bone architecture using symbolic encoding and 3D measures of complexity based on 3D symbol-encoding are claimed as joint Intellectual Properties of the Partners University of Potsdam, MPICI, and CBF as documented in the project publication (Saparin et. al., 2005b) and in this Report. The items were developed are Partners Peter Saparin (MPICI, CBF), Wolfgang Gowin, and the team University of Potsdam.
3. Algorithms and software to model the kinetics of remodelling in cancellous bone from 3D μCT images obtained from real bone or from simulated data as described in this report and documented in the publication listed in this report (Weinkamer et. al., 2004 and Weinkamer et. al., 2005).

University of Aarhus

Claims of University of Aarhus (represented by Jesper Skovhus Thomsen) with regards to the Intellectual Properties developed during the Second Phase of the Project:

1. The software and algorithms for analysis of 2D histomorphometric parameters from the histological bone sections as stated in the Background Information, in the Final Report Phase I, and documented in the publications listed in this Report.
2. The methods for biomechanical testing of the vertebral bodies using the interface material between the bone and compression plates which simulate the intervertebral disk as documented in the project publications listed in this Report.

Center of Muscle and Bone Research, Campus Benjamin Franklin, Charité – University Medicine Berlin

Claims of the CBF team with regards to the Intellectual Properties developed during the Second Phase of the Project include:

1. The procedures, positioning and acquisition parameters for high-resolution of CT-imaging of bone specimens, *in vivo* pQCT and CT-imaging of proximal tibia, and *in vivo* CT-imaging of lumbar vertebrae for the purpose of bone structural evaluation as it is documented in the present Report, publication listed therein, and Minutes of Meeting submitted to ESA in 2003–2005.
2. Calibration of CT-image calibration and assessment of noise level in the CT- and pQCT-images for the purpose of assessment of bone architecture.
3. The procedure of biopsy extraction and fixation.
4. The procedure of bone specimens preparations, air extraction, fixation, and packaging for the purpose of bone assessment of bone architecture.

Wolfgang Gowin who left CBF in September 2003, but continued working on the project until July 2004 contributed significantly to the development of all items mentioned above.

University of Potsdam

Claims of University of Potsdam with regards to the Intellectual Properties developed during the Second Phase of the Project:

1. Algorithms and software for symbol-encoding of the 3D μCT images and the corresponding measures of complexity, as described in the publications listed in this report are claimed as joint Intellectual Properties of the Partners University of Potsdam, MPICI, and CBF.
2. Definitions, algorithms and software for calculations of measures of complexity which are based on the Shape Index (in Partnership with MPICI), marching cubes, curvatures, appropriate entropies and mutual information, as well as Recurrence based measures of complexity, as described in this report and in publications (Marwan & Kurths, 2005) and (Marwan et. al., 2005).
3. The bone resorption models for 2D based on virtual slicing and for 3D based on the stochastic approach, as described in the publication (Zaikin et. al., 2005).

Wolfgang Gowin who left CBF in September 2003, but continue working on the project until July 2004 contributed to the development of items 1 and 3.

Zuse Institute Berlin (ZIB)

In addition to the achievements of the first phase of the project, during the second phase the following Intellectual Property was gained by ZIB and claimed as its Intellectual Properties: a complete working environment to analyze large micro-CT scans of trabecular bone. The environment was developed as an extension package to the visualization system Amira. It comprises:

1. Software interfaces to handle image data larger than main memory (out-of-core data);
2. Integration of the HDF5 library as a out-of-core storage format;

3. Integration of Globus' GridFTP to allow remote access to centrally stored data via the Internet;
4. Extensions of some parts of Amira to 64 bit addressing of image data, which allows to load data larger than 2 GB completely into main memory (if enough RAM is available);
5. All structural measures are implemented as Amira modules.

Remarks:

Items 1–3 are described in detail in the publication (Prohaska et. al, 2004).

Items 1–4 were developed in collaboration with Mercury Computer Systems GmbH.

Items 2–3 were gained in collaboration with the Gridlab Project at ZIB, http://www.zib.de/visual/projects/gridlab/.

Based upon the working environment a workflow was established to locate micro fractures in human vertebral bodies after compression load testing. The procedure includes the following steps:

- scanning the vertebral body prior to and after compression testing in a micro-CT;
- manually selecting corresponding points (landmarks) on both scans;
- using the landmarks to place the image data in a common coordinate system;
- calculating Euclidean distance between trabecular bone surfaces;
- highlighting regions that contain changes;
- manually inspecting the data to locate micro-fractures;

The Intellectual Properties Rights for this procedure which details are described in the present Report are claimed in Partnership with University of Aarhus (Jesper Skovhus Thomsen).

Kamri SIA and Max Planck Institute of Colloids and Interfaces

Claims of the Partners Kamri SIA and Max Planck Institute of Colloids and Interfaces with regards to the Intellectual Properties developed during the period March–September 2005 accordingly to the Research Agreement include:

- Software algorithms for data acquisition and processing related to ultrasonic testing of proximal tibia using unilateral access and applying broadband frequency range.
- Specifications for ultrasonic transducers and probe design comprising frequency range, contacting interfaces, standardization of positioning and application conditions.
- Ultrasonic parameters sensitive to the trabecular bone architecture and its differences in the proximal tibia.

Claimed items are described in the present Final Report and in the publication (Tatarinov 2005). The partners appreciate the supports received from Wolfgang Gowin and the CBF team.

Inventory List of Items Purchased under the Contract

Equipment Item[1]	Price, Euro	Acquired by	Location
pQCT Scanner Stratec XCT-3000 including control PC, peripheral devices, and fixating set	**46 400,00**	**CBF**	**CBF**
RAM Extension, 14 GB for HP Visualize J6000 workstation	**5 521,60**	**CBF**	**CBF** Transferred to **MPICI** in September 2004 together with the workstation.
NAS Fileserver Transtec Zaratustra ZA4NAS1000A rack-mount, 1 TB storage	**4 367,00**	**CBF**	**ZIB** Installed in ZIB in order to serve all project teams and provide backup of all the project data
HP workstation zx6000 2 × 1.3 GHz Itanium 2 CPU, RAM: 10 GB, Hard disk: 73 GB	**12 029,20**	**UoP**	**UoP**
Sun workstation W2100Z 2 × 2.4 GHz Opteron CPU, RAM: 16 GB, Hard disk: 120 GB.	**10 2046,00** Co-funded by ZIB**,** **9 744,00 Euro** funded by Project	**ZIB**	**ZIB**

[1] Accordingly to the Article 5 of The Contract only items which price is above 2800 Euro are included.

References

Allison, N. & Brooks, B. (1921). Bone Atrophy. An Experimental and Clinical Study of the Changes in Bone Which Result from Non-Use. *Surg Gynecol Obstet* **33,** 250–260.

Bell, G.H., Dunbar, O., Beck, J.S. & Gibb, A. (1967). Variations in Strength of Vertebrae with Age and Their Relation to Osteoporosis. *Calcif Tissue Res* **1**, 75–86.

Benhamou, C. L., Poupon, S., Lespessailles, E., Loiseau, S., Jennane, R., Siroux, V., Ohley, W. & Pothuaud, L. (2001). Fractal Analysis of Radiographic Trabecular Bone Texture and Bone Mineral Density: Two Complementary Parameters Related to Osteoporotic Fractures. *J Bone Miner Res* **16**, 697–704.

Bergeron, R.D., Rhodes, P.J., Sparr, T.M., & Tang, X. (2005). Out of Core Visualization Using Iterator Aware Multidimensional Prefetching. *Proc. SPIE, Visualization and Data Analysis* **5669**. 295–306.

Bordier, P., Matrajt, H., Miravet, L. & Hioco, D. (1964). Mesure histologique de la masse et de la résorption des travées osseuses. *Pathol Biol* **12**:1238–1243.

Brodlie, K.W., Duce, D.A., Gallop, J.R., Walton, J.P.R.B . & Wood, J.D. (2004). Distributed and Collaborative Visualization. Computer Graphics Forum, 23, 223–251.

Chen, T.-J., Chuang, K.-S., Wu, J., Chen, S. C., Hwang, I.-M. & Jan, M.-L. (2003). A Novel Image Quality Index using Moran I Statistics. *J Dig Imag* **16**, 210–215.

Chen, P.J. & Chen, T. (2005). Measurements of acoustic dispersion on calcaneus using spilt spectrum processing technique. *Med Eng Phy,* (n press).

Cox, M. & Ellsworth, D. (1997). Application-Controlled Demand Paging for Out-of-Core Visualization. *IEEE Visualization '97*, 235–244.

Dougherty, G. & Henebry, G.M. (2001a). Fractal Signature and Lacunarity in the Measurement of the Texture of Trabecular Bone in Clinical CT Images. *Med Eng Phys* **23**, 369–380.

Ebbesen, E.N., Thomsen, J.S., Beck-Nielsen, H., Nepper-Rasmussen, H.J. & Mosekilde, Li. (1999). Lumbar Vertebral Body Compressive Strength Evaluated by Dual-Energy X-Ray Absorptiometry, Quantitative Computed Tomography, and Ashing. *Bone* **25**, 713–724.

Ellis, H.A. & Peart K.M. (1972). Quantitative Observations on Mineralized and Non-Mineralized Bone in the Iliac Crest. *J Clin Pathol* **25**, 277–286.

Feldkamp, L.A., Goldstein, S.A., Parfitt, A.M., Jesion, G. & Kleerekoper, M. (1989). The Direct Examination of Three-Dimensional Bone Architecture in Vitro by Computed Tomography. *J Bone Miner Res* **4**, 3–11.

Fratzl, P. (2004). Hierarchical Structure and Mechanical Adaptation of Biological Materials. In *Lecture notes NATO-ASI on Learning from Nature how to design new implantable Biomaterials.* (Eds. Reis, R.L., Weiner, S.) 15–34.

Garrahan, N.J., Mellish, R.W.E. & Compston, J.E. (1986). A New Method for the Two-Dimensional Analysis of Bone Structure in Human Iliac Crest Biopsies. *J Microsc* **142**, 341–349.

Gowin W., Saparin, P., Kurths, J. & Felsenberg, D. (2001). Bone Architecture Assessment with Measures of Complexity. *Acta Astronaut* **49**, 171–178.

Gregg, E.W., Kriska, A.M., Salamone, L.M., Roberts, M.M., Anderson, S.J., Ferrell, R.E., Kuller, L.H. & Cauley, J.A. (1997). The Epidemiology of Quantitative Ultrasound: A Review of the Relationships With Bone Mass, Osteoporosis and Fracture Risk. *Osteoporos Int*, **7**, 89–99.

Grigoriev, A.I., Morukov, B.V., Oganov, V.S., Rakhmanov, A.S. & Buravkova, L.B. (1992). Effects of Exercise and Bisphosphonate on Mineral Balance and Bone Density During 360 Day Antiorthostatic Hypokinesia. *J Bone Miner Res* **7**, S449–S455.

Gundersen, H.J.G., Boyce, R.W., Nyengaard, J.R. & Odgaard A. (1993). The ConnEulor: Unbiased Estimation of Connectivity Using Physical Disector Under Projection. *Bone* **14**, 217–222.

Hahn, M., Vogel, M., Pompesius-Kempa, M. & Delling, G. (1992). Trabecular Bone Pattern Factor – A New Parameter for Simple Quantification of Bone Microarchitecture. *Bone* **13**, 327–330.

Hans, D., Fan, B. & Fuerst, T. (1999). Non-Heel Quantitative Ultrasound Devices. In *Quantitative Ultrasound: Assessment of Osteoporosis and Bone Status.* (Eds. Njeh, C.F., Hans, D., Fuerst, T., Glüer C.C. & Genant, H.K.). Martin Dunitz Ltd., 145–162.

Hansen, C.D. & Johnson, C.R. (2005). *The Visualization Handbook*, Elsevier.

Hansson, T.H., Roos, B.O. & Nachemson, A. (1975). Development of Osteopenia in the Fourth Lumbar Vertebra during Prolonged Bed Rest after Operation for Scoliosis. *Acta Orthop Scand* **46**, 621–630.

Hart, R. T. (2001). Bone Modelling and Remodelling: Theories and Computation. In *Bone Mechanics Handbook* (Ed. Cowin, S.C.), CRC Press, Chapter 31, 1–42.

Heaney, R.P. (2003). Remodeling and Skeletal Fragility. *Osteoporos Int* **14**, S12–S15.

Hildebrand, T. & Rüegsegger, P. (1997a) A New Method for the Modelindependent Assessment of Thickness in Three-dimensional Images. *J Microsc* **185**, 67–75.

Hildebrand, T. & Rüegsegger, P. (1997b) Quantification of Bone Microarchitecture with the Structure Model Index. *Comput Meth Biomech Biomed Engin* **1**, 15–23.

Ito, M., Nakamura, T., Matsumoto, T., Tsurusaki, K. & Hayashi, K. (1998). Analysis of Trabecular Microarchitecture of Human Iliac Bone Using Microcomputed Tomography in Patients With Hip Arthrosis With or Without Vertebral Fracture. *Bone* **23**, 163−169.

Jinnai, H., Watashiba, T., Kajihara, Y., Nishikawa, M., Takahashi, M. & Ito, M. (2002). Surface Curvatures of Trabecular Bone Microarchitecture. *Bone* **30**, 191–194.

Kakurin, L.I., Kuzmin, M.P., Matsnev, E.I. & Mikhailov, V.M. (1976a). Physiological Effects Induced by Antiorthostatic Hypokinesia. *Life Sci Space Res* **14**, 101–108.

Kakurin, L.I., Lobachik, V.I., Mikhailov, V.M. & Senkevich, Y.A. (1976b). Antiorthostatic Hypokinesia as a Method of Weightlessness Simulation. *Aviat Space Environ Med* **47**, 1083–1086.

Kleerekoper, M., Villanueva, A.R., Stanciu, J., Sudhaker Rao, D. & Parfitt, A.M. (1985). The Role of Three-Dimensional Trabecular Microstructure in the Pathogenesis of Vertebral Compression Fractures. *Calcif Tissue Int* **37**, 594–597.

Krupina, T.N., Fyodorov, B.M., Filatova, L.M., Tsyganova, N.I. & Matsnev, E.I. (1976). Effect of Antiorthostatic Bed Rest on the Human Body. *Life Sci Space Res* **14**, 285–287.

Krølner, B. & Toft, B. (1983). Vertebral Bone Loss: An Unheeded Side Effect of Therapeutic Bed Rest. *Clin Sci* **64**, 537–540.

Lafage-Proust, M.H., Collet, P., Dubost, J.M., Laroche, N., Alexandre, C. & Vico, L. (1998). Space Related Bone Mineral Redistribution and Lack of Bone Mass Recovery after Reambulation in Young Rats. *Am J Physiol* **274**, 324–334.

Lang, C., Ohser, J. & Hilfer, R. (2001). On the Analysis of Spatial Binary Images. *J Microsc* **203**, 303–313.

Lang, T., LeBlanc, A., Evans, H., Lu, Y., Genant, H. & Yu A. (2004). Cortical and Trabecular Bone Mineral Loss from the Spine and Hip in Long-Duration Spaceflight. *J Bone Miner Res* **19**, 1006–1012.

Langton, C.M., Whitehead, M.A., Langton, D.K., Langley, G. (1997). Development of a cancellous bone structural model by stereolithography for ultrasound characterisation of the calcaneus. *Med Eng Phys*, **19**(7), 599–604.

Laval-Jeantet, A.-M., Bergot, C., Carroll, R., & Garcia-Schaefer, F. (1983). Cortical Bone Senescence and Mineral Bone Density of the Humerus. *Calcif. Tissue Int.* **35**, 268–272.

Law, C., Schroeder, W.J., Martin, K.M. & Temkin, J. (1999). A Multi-Threaded Streaming Pipeline Architecture for Large Structured Data Sets. *Proc. IEEE Visualization '99*, 225–232.

LeBlanc, A., Schneider, V., Krebs, J., Evans, H., Jhingran, S. & Johnson, P. (1987). Spinal Bone Mineral After 5 Weeks of Bed Rest. *Calcif Tissue Int* **41**, 259–261.

LeBlanc, A., Schneider, V., Shackelford, L., West, S., Oganov, V., Bakulin, A. & Voronin, L. (2000). Bone Mineral and Lean Tissue Loss after Long Duration Space Flight. *J Musculoskel. Neuron. Interact.* **1**, 157–160.

LeBlanc, A.D., Schneider, V.S., Evans, H.J., Engelbretson, D.A. & Krebs, J.M. (1990). Bone Mineral Loss and Recovery After 17 Weeks of Bed Rest. *J Bone Miner Res* **5**, 843–850.

Lorensen, W.E. & Cline, H.E. (1987). Marching Cubes: A High Resolution 3D Surface Construction Algorithm. *SIGGRAPH Comput Graph* **21**, 163−169

Luke, E. J. & Hansen, C. D. (2002). Semotus Visum: A Flexible Remote Visualization Framework. *IEEE Visualization '02*, 61–68.

Majumdar, S., Lin, J., Link, T., Millard, J., Augat, P., Ouyang, X., Newitt, D., Gould, R., Kothari, M., Genant, H. (1999). Fractal Analysis of Radiographs: Assessment of Trabecular Bone Structure and Prediction of Elastic Modulus and Strength. *Med Phys* **26**, 1330–1340.

Marwan, N. & Kurths, J. (2005). Line Structures in Recurrence Plots. *Phys Lett A* **336**, 349–357.

Marwan, N., Saparin, P., Thomsen, J.S., Kurths, J. (2005). An Innovative Approach for the Assessment of 3D Structures in Trabecular Bone. *J Grav Physiol* (in press).

Marx, J. (2004). Coming to Grips with Bone Loss. *Science* **305**, 1420–1422.

Melsen, F., Melsen, B. & Mosekilde, Le. (1978). An Evaluation of the Quantitative Parameters Applied in bone Histology. *Acta Pathol Microbiol Scand A* **86**, 63–69.

Modlesky, C.M., Majumdar, S., Narasimhan, A. & Dudley, G.A. (2004). Trabecular Bone Microarchitecture is Deteriorated in Men With Spinal Cord Injury. *J Bone Miner Res* **19**, 48–55.

Moore, R.J., Durbridge, T.C., Woods, A.E. & Vernon-Roberts, B. (1989). Variation in Histomorphometric Estimates across Different Sites of the Iliac Crest. *J Clin Pathol* **42**, 814–816.

Mosekilde, Li., Mosekilde, Le. & Danielsen, C.C. (1987). Biomechanical Competence of Vertebral Trabecular Bone in Relation to Ash Density and Age in Normal Individuals. *Bone* **8**, 79–85.

Muller, M., Moilanen, P., Bossy, E., Nicholson, P., Kilappa, V., Timonen, J., Talmant, M., Cheng, S., & Laugier, P. (2005) Comparison of three ultrasonic axial transmission methods for bone assessment. *Ultrasound Med Biol* **31**(5), 633–42.

Nature Insight (2001). Complex Systems. *Nature* **410**, 241–284.

Njeh, C.F., Nicholson, P.H.F. & Langton, C.M. (1999). The Physics of Ultrasound Applied to Bone. In *Quantitative Ultrasound: Assessment of Osteoporosis and Bone Status*. (Eds. Njeh, C.F., Hans, D., Fuerst, T., Glüer, C.C. & Genant, H.K.). Martin Dunitz Ltd., 67–76.

Njeh, C.F., Fuerst, T., Diessel, E. & Genant, H.K. (2001). Is Quantitative Ultrasound Dependent on Bone Structure? A Reflection. *Osteoporos Int*, **12**, 1–15.

Olson, G. B. (1997). Computational Design of Hierarchically Structured Materials. *Science* **277**, 1237–1242.

Padilla, F. & Laugier P. (2005). Recent developments in trabecular bone characterization using ultrasound. *Curr Osteoporos Rep* **3** (2), 64–69.

Palle, S., Vico, L., Bourrin, S. & Alexandre, C. (1992). Bone Tissue Response to Four-Month Antiorthostatic Bedrest: A Bone Histomorphometric Study. *Calcif Tissue Int* **51**, 189–194.

Parfitt, A.M., Mathews, C.H.E, Villanueva, A.R., Kleerekoper, M., Frame, B. & Rao, D.S. (1983). Relationships between Surface, Volume, and Thickness of Iliac Trabecular Bone in Aging and Osteoporosis: Implications for the Microanatomic and Cellular Mechanisms of Bone Loss. *J Clin Invest* **72**, 1396–1409.

Parfitt, A.M. (1987). Trabecular Bone Architecture in the Pathogenesis and Prevention of Fracture. *Am J Med* **82**, 68–72.

Prohaska, S., & Hege, H.-C. (2002). Fast Visualization of Plane-Like Structures in Voxel Data. *Proc. IEEE Visualization '02*, 29–36.

Prohaska S., Hutanu, A., Kähler, R., & Hege, H.-C. (2004). Interactive Exploration of Large Remote Micro-CT Scans. *Proc. IEEE Visualization '04*, 345–352.

Romano, M., Thiel, M., Kurths, J. & von Bloh, W. (2004). Multivariate Recurrence Plots. *Phys Let A* 330, 214-223.

Ross P.D. (1998) Epidemiology of osteoporosis. In *Bone densitometry and osteoporosis* (Eds. Genant H.K., Guglielmi G. & Jergas M.) Springer, 21-42.

Roux, W. (1896). Ueber die Dicke der statischen Elementartheile und die Maschenweite der Substantia spongiosa der Knochen. *Z Orthop Chir* **4**, 284–306.

Rüegsegger, P., Koller, B. & Müller, R. (1996). A Microtomographic System for the Nondestructive Evaluation of Bone Architecture. *Calcif Tissue Int* **58**, 24–29.

Ruimerman, R., Hilbers, P., van Rietbergen, B. & Huiskes, R. (2005). A Theoretical Framework for Strain-Related Trabecular Bone Maintenance and Adaptation. *J Biomech* **38**, 931–941.

Saparin, P., Gowin, W., Kurths, J. & Felsenberg, D. (1998). Quantification of Cancellous Bone Structure Using Symbolic Dynamics and Measures of Complexity. *Phys Rev E* **58**, 6449–6459.

Saparin P., Gowin W. & Felsenberg D. (2002). Comparison of Bone Loss with Changes of Bone Architecture at Six Different Skeletal Sites Using Measures of Complexity. *J Gravit Physiol* **9**, 177–178.

Saparin P., Thomsen J.S., Beller, G. & Gowin W. (2005a). Measures of Complexity to Quantify Bone Loss and Estimate Strength of Human Lumbar Vertebrae: Comparison of CT Image Analysis with Bone Histomorphometry and Biomechanical Tests. *J Gravit Physiol* (in press).

Saparin, P., Thomsen J.S., Prohaska, S., Kurths, J., Zaikin, A., Hege, H.-C., Gowin, W. (2005b). Quantification of Spatial Structure of Human Proximal Tibial Bone Biopsies Using 3D Measures of Complexity, *Acta Astronautica* **56,** 820−830.

Saparin, P., Thomsen, J.S., Kurths, J., Beller, G. & Gowin W. (2005c). Segmentation of bone CT-images and assessment of bone structure using measures of complexity, *Medical Physics* (revised manuscript submitted).

Stalling D., Westerhoff M. & Hege H.-C. (2005). Amira: A Highly Interactive System for Visual Data Analysis. In *The Visualization Handbook* (Eds. Hansen, C.D. & Johnson, C.R.), Elsevier, 749–767.

Tatarinov, A. Pontaga, I., Vilks, U. (1999) Modeling the influence of mineral content and porosity on ultrasound parameters in bone by using synthetic phantoms. *Mechanics Composite Materials* **35**, 147−154.

Tatarinov, A. & Sarvazyan, A. (2003). Dual-Fequency Method for Ultrasonic Assessment of Bones: Model Study. *Proc World Congr Ultrasonics, Paris*, CDROM, 895–898.

Tatarinov, A., Gowin, W., Beller, G. & Saparin, P. (2005). A Perspective for Ultrasonic Assessment of Osteoporotic Changes of Bone Structure in Proximal Tibia. *J Gravit Physiol* (in press).

Thomsen, J.S., Ebbesen, E.N. & Mosekilde, Li. (2000). A New Method of Comprehensive Static Histomorphometry Applied on Human Lumbar Vertebral Cancellous Bone. *Bone* **27**, 129–138.

Thomsen, J.S., Ebbesen, E.N. & Mosekilde, Li. (1998). Relationships between Static Histomorphometry and Bone Strength Measurements in Human Iliac Crest Bone Biopsies. *Bone* **22**, 153–163.

Thomsen, J.S., Laib, A., Koller, B., Prohaska, S., Mosekilde, Li. & Gowin, W. (2005a). Stereological Measures of Trabecular Bone Structure: Comparison of 3D Micro Computed Tomography with 2D Histological Sections in Human Proximal Tibial Bone Biopsies. *J Microsc* **218**, 171–179.

Thomsen, J.S., Morukov, B.V., Vico, L., Alexandre, C., Saparin, P.I. & Gowin, W. (2005b). Cancellous Bone Structure of Iliac Crest Biopsies following 370 Days of Head-Down Bed Rest. *Aviat Space Environ Med*. **76**, 915– 922.

Vesterby, A., Mosekilde, Li., Gundersen, H.J.G., Melsen, F., Mosekilde, Le., Holme, K. & Sørensen, S. (1991). Biological Meaningful Determinants of the in Vitro Strength of Lumbar Vertebrae. *Bone* **12**, 219–224.

Vico, L., Chappard, D., Alexandre, C., Palle, S., Minaire, P., Riffat, G., Morukov, B. & Rakhmanov, S. (1987). Effects of a 120 Day Period of Bed-Rest on Bone Mass and Bone Cell Activities in Man: Attempts at Countermeasure. *Bone Miner* **2**, 383–394.

Vico, L., Collet, P., Guignandon, A., Lafage-Proust, M.-H., Thomas, T., Rehailia, M. & Alexandre, C. (2000). Effects of Long-Term Microgravity Exposure on Cancellous and Cortical Weight-Bearing Bones of Cosmonauts. *Lancet* **355**, 1607–1611.

Viktorov, I.A. (1967). Rayleigh and Lamb Waves, Physical Theory and Applications. Plenum Press, New York.

Vitter, J. S. (2001). External Memory Algorithms and Data Structures: Dealing with Massive Data. *ACM Computing Surveys* **33**, 209–271.

Wear, K.A. & Laib A. (2003). The dependence of ultrasonic backscatter on trabecular thickness in human calcaneus: theoretical and experimental results. *IEEE Trans Ultrason. Ferroelectr. Freq. Control* **50** (8), 979–986.

Wehrli, F.W., Saha, P.K., Gomberg, B.R., Song, H.K., Snyder, P.J., Benito, M., Wright, A. & Weening, R. (2002). Role of Magnetic Resonance for Assessing Structure and Function of Trabecular Bone. *Top Magn Reson Imaging* **13**, 335–355.

Weinkamer, R., Hartmann, M. A., Brechet, Y. & Fratzl, P. (2004). Stochastic Lattice Model for Bone Remodeling and Aging. *Phys Rev Lett* **93**, 228102.

Weinkamer, R., Hartmann, M. A., Brechet, Y. & Fratzl, P. (2005). Architectural Changes of Trabecular Bone Caused by the Remodeling Process. *Mater Res Soc Symp Proc* **874**, L1.9.

Zaikin, A., Gowin, W., Prohaska, S., & Kurths, J. (2003) 2D Bone Modelling for Analysis of Changes in Bone Architecture and for Evaluation of Structural Measures, in: *Proc. of the 2nd European Congress Achievements In Space Medicine into health Care Practice and Industry*, Berlin, Germany, March 27–29, 2003, 100–106.

Zaikin, A., Saparin, P., Kurths, J., Prohaska, S. & Gowin, W. (2005) Modelling Bone Resorption in 2D CT and 3D μCT Images, *Int J Bifurcat Chaos* **15** (9), 2995–3009.

Zimmerman, M.C., Vuono-Hawkins, M., Parsons, J.R., Carter, F.M., Gutteling, E., Lee, C.K. & Langrana, N.A. (1992). The Mechanical Properties of the Canine Lumbar Disc and Motion Segment. *Spine* **17**, 213–220.

Zerath, E., Godet, D., Holy, X., Andre, C., Renault, S., Hott, M. & Marie, P.J. (1996). Effects of Spaceflight and Recovery on Rat Humeri and Vertebrae: Histological and Cell Culture Studies. *J Appl Physiol* **81**, 164–171.

Zurek W.H., editor (1990), *Complexity, Entropy and the Physics of Information (Santa Fe Institute studies in the sciences of complexity)*. Addison Wesley Publishing.